5-1-2013

Surface modification of a proton exchange membrane and hydrogen storage in a metal hydride for fuel cells

Lisa Andrews

SURFACE MODIFICATION OF A PROTON EXCHANGE MEMBRANE AND HYDROGEN STORAGE IN A METAL HYDRIDE FOR FUEL CELLS

A thesis presented to the

School of Chemistry and Materials Science

College of Science

At Rochester Institute of Technology

Rochester, NY 14623

In Partial Fulfillment of the Requirement for the

Degree of Master of Science

In Materials Science and Engineering

By:

Lisa Andrews

May 2013

CERTIFICATION OF APPROVAL

SURFACE MODIFICATION OF A PROTON EXCHANGE MEMBRANE AND HYDROGEN STORAGE IN A METAL HYDRIDE FOR FUEL CELLS

By:

Lisa Andrews

_____ _____

Research Advisor Date

Dr. Gerald Takacs

_____ _____

Director Date

Dr. KSV Santhanam

COPYRIGHT RELEASE FORM

SURFACE MODIFICATION OF A PROTON EXCHANGE MEMBRANE AND HYDROGEN STORAGE IN A METAL HYDRIDE FOR FUEL CELLS

_____ _____

Lisa Andrews Date

ACKNOWLEDGEMENT

I would like to thank those who have helped me succeed in completing this thesis. First, I would like to express appreciation to my research advisor, Dr. Gerald Takacs for giving me the opportunity to work in his laboratory as well as his guidance, support and encouragement throughout my graduate education. I am grateful for his help, patience, and mentoring with my lab work and writing of this thesis.

Furthermore, I would like to thank my committee members Dr. Alla Bailey and Dr. Alan Entenberg for their time and suggestions. I am sincerely thankful to Dr. Bailey for her extra assistance and effort toward our hydrogen storage and grafting research.

I would also like to thank Dr. K.S.V. Santhanam for giving me the opportunity to study at the Rochester Institute of Technology along with his advisement throughout my Master's education. My appreciation goes to Autumn, Brenda, and the School of Chemistry and Materials Science for support and always answering my questions. I am grateful to Tom Allston for his help with instrumentation and the stock room staff for their assistance with glassware and equipment.

A special thank you to Dr. Brian Landi and Dr. Reginald Rogers for providing single-walled carbon nanotube samples and to Michael Mehan, Dr. Tom Debies, and Dr. Greg Thompson for the time they devoted to the valuable XPS and SEM analysis.

Finally, I would like to thank my family, friends, and research colleagues: Andrew Morgan, Ryan Divens, and Entesar Al Abdulal for their motivation and support.

TABLE OF CONTENTS

PAGE

LIST OF FIGURES

PAGE

LIST OF TABLES

PAGES

ABSTRACT

Interest in fuel cell technology is rising as a result of the need for more affordable and available fuel sources. Proton exchange membrane fuel cells involve the catalysis of a fuel to release protons and electrons. It requires the use of a polymer electrolyte membrane to transfer protons through the cell, while the electrons pass through an external circuit, producing electricity. The surface modification of the polymer, Nafion®, commonly researched as a proton exchange membrane, may improve efficiency of a fuel cell.

Surface modification can change the chemistry of the surface of a polymer while maintaining bulk properties. Plasma modification techniques such as microwave discharge of an argon and oxygen gas mixture as well as vacuum-ultraviolet (VUV) photolysis may cause favorable chemical and physical changes on the surface of Nafion for improved fuel cell function. A possible increase in hydrophilicity as a result of microwave discharge experiments may increase proton conductivity. Grafting of acrylic acid from the surface of modified Nafion may decrease the permeation of methanol in a direct methanol fuel cell, a process which can decrease efficiency. Modification of the surface of Nafion samples were carried out using:

1) An indirect Ar/O_2 gas mixture plasma investigating the reaction of oxygen radicals with the surface,

2) A direct Ar/O_2 gas mixture plasma investigating the reaction of oxygen radicals and VUV radiation with the surface and,

3) VUV photolysis investigating exclusively the interaction of VUV radiation with the surface and any possible oxidation upon exposure to air.

Acrylic acid was grafted from the VUV photolysed Nafion samples. All treated surfaces were analyzed using X-ray photoelectron spectroscopy (XPS). Fourier transform infrared spectroscopy (FTIR) was used to analyze the grafted Nafion samples. Scanning electron microscopy (SEM) and contact angle measurements were used to analyze experiments 2 and 3.

Using hydrogen as fuel is a promising option. Effective hydrogen storage methods must be used as sources of available hydrogen. One possibility is to use hydrogen stored in a solid chemical compound such as magnesium hydride. The kinetics of hydrogen release from the hydrolysis of magnesium hydride with 2 wt% acetic acid was examined. The hydrogen produced was supplied to a fuel cell and the amount of hydrogen consumed by the fuel cell was determined.

Carbon nanotubes also can play a role in energy sources and as components in fuel cells. VUV photo-oxidized single walled carbon nanotubes (SWNT) paper was grafted with polyacrylic acid and analyzed using XPS.

Part 1

Introduction

The present necessity for the energy needed for every day life poses problems when fuels are scarce. Dependence on oil between countries causes an increase in the cost of fuels. In addition, fuel emissions are polluting the atmosphere releasing chemicals including carbon dioxide, carbon monoxide, formaldehyde, benzene, and nitrogen dioxide that are produced from car engines [1, 2]. These chemicals can be harmful to both the environment as well as human health as greenhouse gases and carcinogens. Advancements in fuel cell technology are being made that will work toward reducing these problems. Hydrogen fuel cells for automobiles exemplify this innovative technology. The fuel cell takes in hydrogen to produce electricity, only to release heat and water [3].

Fuel cells were developed by W. Grove in 1839 and were first constructed using two platinum electrodes immersed in sulfuric acid with hydrogen being supplied to one electrode, oxygen to the other to produce current [4]. Over the years the fuel cell has advanced in structure and there are now several different types. Categories of fuel cells include: alkali, phosphoric acid, molten carbonate, solid oxide, and proton exchange [5]. Proton exchange membrane fuel cells or polymer electrolyte membrane fuel cells (PEMFC) have been under much investigation. In this type, protons produced at the anode transport through a polymeric electrolyte membrane (PEM) to reach the cathode. Hydrogen fuel cells are examples of PEMFCs. A fuel cell is an electrochemical device involving an anode, where oxidation occurs, and a cathode, where reduction occurs. In a

hydrogen fuel cell, hydrogen is used as fuel and is released to the anode. The electrode catalyzes the reaction of molecular hydrogen into protons and electrons:

$$H_2 \rightarrow 2H^+ + 2e^- \quad (1)$$

The protons produced travel through the membrane to reach the cathode. Oxygen is taken from the air at the cathode where another catalyst electrode initiates the reaction of:

$$\tfrac{1}{2}O_2 + 2H^+ + 2e^- \rightarrow H_2O \quad (2)$$

The electrons formed at the anode pass through an external circuit to conduct electricity. The electrons then meet with the protons and oxygen at the cathode to produce water [6].

An important part of the PEMFC is the polymer electrolyte membrane that is used. This membrane must be able to effectively transport protons. In addition, the PEM should possess good mechanical strength so as to not break or deform during use, have high thermal stability to withstand the working temperature of the fuel cell, 90-110°C, and be resistant to chemical attack and degradation [6].

Perfluorinated sulfonic acid polymers can be used as proton exchange membranes. They are fluorocarbons that contain sulfonic acid groups. The fluorocarbon backbone provides excellent stability to the polymer and the sulfonic acid groups are responsible for absorption of water and proton transport.

Nafion (Fig. 1), which is a highly researched PEM, was first created at Du Pont in the 1960s by Dr. Walther Grot [7]. The synthesis involves a copolymerization of tetrafluoroethylene, commercially known as Teflon®, and perfluoro-3,6-dioxa-4-methyl-7-octene-sulfonic acid [7].

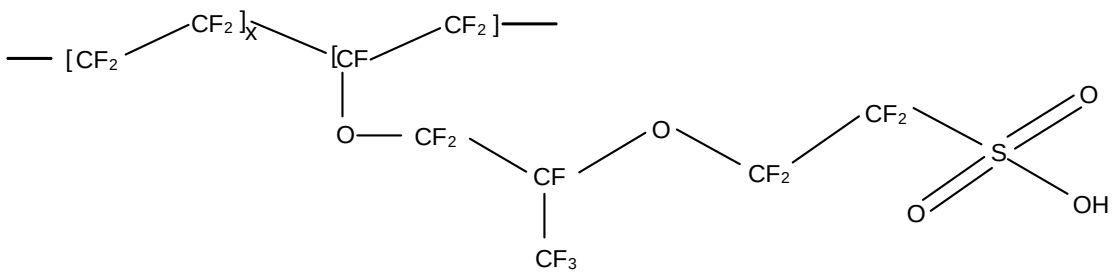

Figure 1. Structure of Nafion with x = ~5 to 11 [6].

Nafion contains about five to eleven repeat units of fluorocarbon (CF_2-CF_2) followed by a repeat unit with a pendent chain including a sulfonic acid group [6]. Nafion is the first of its class as an ionomer, which are polymers that contain less than fifteen percent ionized species [8]. For Nafion, the ionized species are sulfonic acid anions.

Due to its fluorocarbon structure and sulfonic acid groups, Nafion contains several key properties that make it desirable as a PEM to be used in fuel cells. Its stable fluorocarbon backbone makes chemical attack from surrounding species difficult [7]. Nafion is resistant to any radicals that may be produced within a fuel cell such as hydroxyl or peroxy radicals [6]. The resistance to chemical attack ensures long lifetime and low degradation. As a result, Nafion does not fragment and release byproducts [7]. The highly electronegative fluorine atoms that are prominent in the structure of Nafion and the stability of the backbone contribute to the strong acidity of the sulfonic acid proton, making Nafion a super-acid catalyst [6, 7]. Additionally, Nafion has the ability to absorb a large amount of water. The difference in hydrophilicity of the sulfonic acid and the fluorocarbon backbone allows for the separation of Nafion into hydrophilic and hydrophobic domains. The hydrophilic sulfonic acid groups absorb water and are

sequestered toward the center, creating the hydrophilic domain, while the fluorocarbon backbone pushes itself away, creating the hydrophobic domain [6]. The hydrophilic domain is responsible for proton transport while the hydrophobic domain maintains stability.

The protons, which are produced at the anode are able to exchange with hydrogen atoms from the absorbed water molecules and sulfonic acid groups within the hydrophilic domain of the Nafion membrane to reach the cathode in the following manner:

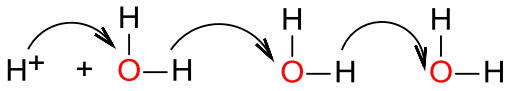

(3)

Figure 2. Proton transport by water molecules [9].

Hydration of the Nafion membrane is important within a fuel cell in order to conduct protons as shown in Fig. 2 [9].

The use of Nafion as a proton exchange membrane in fuel cells can be effective, although, there are some obstacles, including low proton conductivity at low levels of humidity, fuel crossover, and high cost, which need to be overcome.

The improvement of Nafion for fuel cell applications is being highly researched. Surface modification allows for a change in surface chemistry and morphology while maintaining bulk properties. Surface modification techniques of the membrane are being investigated as methods to help solve some of the problems associated with its use in fuel cells. Using

plasmas to modify the surface of Nafion have been employed as means of overcoming its limitations.

Low energy plasma sources have been used to alter the surface of various polymeric membranes. Polyether ether ketone (PEEK) showed an increase in oxygen concentration under treatment with air plasma [10]. Low density polyethylene (LDPE), biaxially oriented polypropylene (BOPP), polystyrene (PS), and poly(methyl methacrylate) (PMMA) were also exposed to plasmas of several noble gases to give rise to cross-links, bond cleavage, or double bond formation [11]. A remote oxygen plasma causes significant change in surface roughness and hydrophobicity for fluorinated ethylene polypropylene (FEP) [12], a polymer with a structure similar to Nafion.

There has been extensive research into the plasma treatment of polytetrafluoroethylene (PTFE). PTFE in an argon plasma implemented oxygen containing functional groups onto its surface resulting in an increased oxygen to carbon ratio and an increase in hydrophilicity [13] and PTFE exposed to ammonia or nitrogen/hydrogen plasmas have shown an increase in amino groups as well as unsaturation [14]. Another research group treated PTFE with an ammonia plasma and discovered the presence of carbonyl and amido groups following treatment as well as the increased ability of the polymer to adhere to nitril rubber [15]. Golub et al studied the modification of PTFE with oxygen [16] and nitrogen plasmas [17] and recorded an increase in O/C ratio with a corresponding decrease in the F/C ratio in the first few minutes of exposure followed by a decrease in the O/C ratio and an increase in the F/C ratio for the remainder of the experiments. Another study exposed both PTFE and PFA (perfluoroalkoxyvinyl ether copolymer) to an argon plasma followed by air which resulted in the formation of peroxy

radicals [18]. Microwave plasma treatments of PTFE with ammonia gas increased wettability by the incorporation of polar groups as well as defluorination [19].

Previous studies have used plasmas to modify the surface of Nafion. The treatment of Nafion with an argon plasma over varying treatments times and varying power settings showed a decrease in the F/C ratio from 2.1 to 1.7 with increasing power and XPS analysis determined the formation of carbonyl and hydroxyl groups [20]. A helium/hydrogen gas mixture radio frequency (RF) powered plasma was used to etch the surface of Nafion for increased electrochemical surface area, leading to increased current density of a membrane electrode assembly (MEA) along with an increase in hydrophilicity [21]. Similarly, ion beam bombardment of Nafion with positive argon ions resulted in changes in surface roughness that increased the interfacial surface area between polymer and catalyst for enhanced fuel cell power [22]. Yong-Hun Cho and group plasma etched Nafion with the use of argon and oxygen gases to improve the performance of the MEA by 19% [23]. An argon RF powered plasma led to defluorination and an increase in hydrophilicity at the surface of Nafion samples, however, there was also a decrease in sulfur atom concentration and proton conductivity [24]. Changes in surface chemistry while maintaining sulfonic acid groups is ideal for Nafion surface modification since the sulfonic acid groups are critical to proton conduction.

Sputtering techniques have been used to modify the surface of Nafion [25-28]. Palladium was sputtered onto Nafion [25] and initially argon plasma-etched Nafion [26] to show a decrease in methanol permeability. Along with this decrease in fuel crossover, however, the proton conductivity was decreased in the Nafion/Pd composite [25]. Sputtering

platinum on Nafion membranes [27, 28] has also been studied. Platinum of 5-10 nm in thickness improved the performance of a fuel cell with an increase in generated power over other thicknesses of the Pt layer [27]. Oxygen sputtering onto Nafion increased the selectivity of proton transfer through the membrane [29].

Similarly, anionic exchange layers: from 4-vinylpyridine momomer [29], containing ammonium ion [30], and from ethylene and ammonia [31] were plasma polymerized onto Nafion surfaces to increase proton permeability selectivity.

Several methods have been used to reduce methanol crossover in direct methanol fuel cells. Barrier films have been plasma polymerized onto the surface of Nafion [32, 33] while Nafion grafted with poly(glycidyl methacrylate), has also been shown to decrease methanol permeation [34]. Electrochemical modification of Nafion with the conductive polymer, polyaniline [35] and electrodeposition of polypyrrole [36] were shown to be effective in lowering diffusion of methanol as well. The addition of basic material including polyethylenimine, poly(4-vinylpyridine), and polyaniline into the acidic Nafion polymer can reduce the pull of methanol through the membrane by decreasing the size of ion clusters that form within Nafion [37].

In this thesis, VUV photolysis using a microwave powered argon plasma, and a direct and an indirect argon/oxygen microwave discharge were used to modify the surface of Nafion 117 samples. Following these experiments, some treated samples were grafted with acrylic acid. XPS and FTIR were used to determine changes in surface chemistry, contact angle analysis to look at changes in wettability, and SEM to observe changes in surface morphology and roughness.

Carbon nanotubes are materials that have use in a wide variety of applications including alternative energy. Carbon nanotubes were first discovered by Sumio Iijima in 1991 and were described as helical structures of graphite with diameters of 4 to 30 nm containing 2 to 50 individual graphite sheets [38]. These structures were to become known as multi-walled carbon nanotubes (MWNTs). Single-walled carbon nanotubes (SWNTs), discovered in 1993, also by Iijima and group, contain a single tubule of about 1 nm in diameter [39].

There are many properties that SWNTs possess as a result of their distinctive structure including: good mechanical strengths, thermal conductivity and electrical conductivity [40]. These properties among others allow for carbon nanotubes to be useful in a variety of applications including polymer electrolyte membrane fuel cells [41, 46], hydrogen storage [42], biosensors [43], electronics, [44] and lithium ion batteries [45].

A drawback to the use of carbon nanotubes is that they have low solubility and form aggregates in many solvents [47]. To overcome this problem, researchers have functionalized carbon nanotubes with long polymer chains to enhance their solubility, often by grafting methods. Polystyrene-grafted MWNT was produced by atom transfer radical polymerization (ATRP) with a CuBr/bipy catalyst [47], polyacrylic acid-grafted MWNT was synthesized by gamma radiation of the MWNT in ethanol to produce radical species, then in acrylic acid for grafting [48]. Polyacrylonitrile grafted SWNTs have been prepared by polymerization in micelles after the SWNTs were exfoliated with sodium dodecylbenzene sulfonate and made dispersible in water [49]. The use of radiation induced graft polymerization (RIGP) of several vinyl monomers has produced

MWNTs grafted with acrylic acid, methacrylic acid, glycidal methacrylate, maleic anhydride, and 4-vinylphenylboronic acid [50]. Another method of attaching polyacrylic acid to carbon nanotubes was to covalently bond it to MWNTs functionalized with formaldehyde [51].

This thesis focused on the graft polymerization of acrylic acid onto VUV photo-oxidized single-walled carbon nanotubes using an iron sulfate heptahydrate and ascorbic acid initiating system under argon gas. XPS was performed to confirm the presence of polyacrylic acid on the surface of the SWNTs.

Optimum fuel storage is critical for the use of fuel cells as an effective form of energy. Hydrogen is being explored as a clean energy carrier which avoids harming the environment when used as fuel, releasing only water and heat as byproducts. One of the obstacles to using hydrogen fuel cells is to find an effective method of storing hydrogen. There are three main methods to store hydrogen: as a compressed gas, as a cooled liquid, and in a solid compound. Metal hydrides are advantageous for storage of hydrogen in a solid compound because they hold high volumes of hydrogen at small masses of metal hydride [4]. Magnesium hydride is a good candidate for hydrogen storage in a solid with a capacity up to 7.7 wt% [52]. The affordability of magnesium and its reversible hydrogen storage add to the qualifications of magnesium hydride as an attractive option for storage in a metal hydride [52].

By comparison, for an internal combustion engine vehicle performing at 25 miles per gallon of gasoline to travel 300 miles, a hydrogen fuel cell vehicle would need to be

equipped with about 85 kg of MgH_2 (79 kg Mg metal) according to the energy equivalent 1 gallon of gasoline to 1.09 kg hydrogen [4]. A car could contain a block of Mg for hydrogen to be pumped into to create MgH_2. The same block of magnesium could be reused once the hydrogen is released and new hydrogen could be pumped in as needed.

The thermal decomposition of magnesium hydride into magnesium and hydrogen as well as the hydrolysis into magnesium hydroxide and hydrogen both present methods of releasing H_2 gas. Drawbacks to these methods are that the decomposition of magnesium hydride occurs at high temperatures over 320°C and that the hydrolysis of magnesium hydride is a very slow reaction [53].

Hydrogen sorption studies have been carried out [54-57] to improve the hydrogen absorption and desorption of metal hydrides. Ball-milling magnesium hydride decreases crystal size, increases surface area and creates defects in structure that allow for hydrogen desorption at lower temperatures [54]. Furthermore, the addition of Raney nickel to ball-milled MgH_2 [55], the use of nanoconfined $2LiBH_4$-MgH_2 [56], and alloying Mg and MgH_2 with iron [57] have also shown improved hydrogen sorption behavior.

It has been shown that the formation of the water-insoluble magnesium hydroxide $Mg(OH)_2$ acts as a passive layer which blocks water access to MgH_2, thus reducing the rate of hydrolysis [58-62].

One method to overcome this problem is to ball-mill magnesium hydride to increase its surface area to water plus the addition of chloride ions to deteriorate the passive $Mg(OH)_2$ layer [61, 62]. Another solution is the use of ultrasonic irradiation to generate large shear forces to break off the $Mg(OH)_2$ and expose new MgH_2 to the water [59]. A

third is to carry out the hydrolysis in organic acids such as malonic, glycolic, and citric, in which salts formed as a byproduct are soluble so they do not prevent water from reaching MgH_2 [60].

A recent study performed the hydrolysis of magnesium hydride in 2 wt% acetic acid as described by the reaction (4) [53].

$$2MgH_{2\,(s)} + 2H_2O_{\,(l)} + 2CH_3COOH_{\,(aq)} \rightarrow Mg(OH)_{2\,(s)} + Mg(CH_3COO)_{2\,(aq)} + 4H_{2\,(g)} \quad (4)$$

The use of 2 wt% acetic acid for hydrolysis significantly increased the percent yield of hydrogen from 4% for MgH_2 in just water to 75% in acetic acid at 60 minutes of reaction [53]. However, in depth kinetic analysis of this reaction was not carried out.

This thesis presents the kinetics of the hydrolysis of magnesium hydride using 2 wt% acetic acid in an original way with the use of ideal gas law equipment. The hydrogen released by the hydrolysis reaction was directly supplied to a fuel cell. Parameters were measured to calculate the amount and rate of hydrogen consumption powering the fuel cell. Aspects of these studies were modified and used for an undergraduate laboratory assignment on hydrogen technology.

Part 2

Experimental

2.1 Nafion Preparation

Nafion® 117, with a 1100 g/mol sulfonic acid equivalent weight and a thickness of 0.007 in., was purchased from SIGMA-ALDRICH, Co. in St. Louis, MO. All Nafion samples were washed before surface modification. Samples were cut into pieces of about 1.5 cm x 1.5 cm or 1.5 cm x 2 cm and then washed by the following method: heating at 80-100°C in either 0.9% or 3% hydrogen peroxide (H_2O_2) for one hour to remove absorbed organic impurities followed by heating at 80-100°C in either 5 x 10^{-3}M or 1M sulfuric acid (H_2SO_4) for one hour to replace any cations associated with the sulfonic acid groups with protons [63], and lastly heating in deionized water at 80-100°C for one hour [24, 63, 64]. Regardless of the concentration of hydrogen peroxide and sulfuric acid used, all samples were clean with no or very few contaminants as analyzed by XPS. The cleaned samples were placed in a desiccator for two to three days to completely dry.

2.2 Control: Nafion in the Presence of Indirect Ar MW Discharge

An argon gas microwave discharge plasma was maintained with a frequency of 2.45 GHz and a working power of 24 Watts. The pressure in the reaction chamber was about 0.150 Torr. The plasma was located horizontally to the location of the Nafion membrane so that the membrane was not in the presence of VUV radiation. This was performed as a control experiment to show that no oxygen is present in the Ar MW discharge and its results can be compared with results of other surface modification or oxidation experiments. The setup as shown in Fig. 3 was used for this experiment.

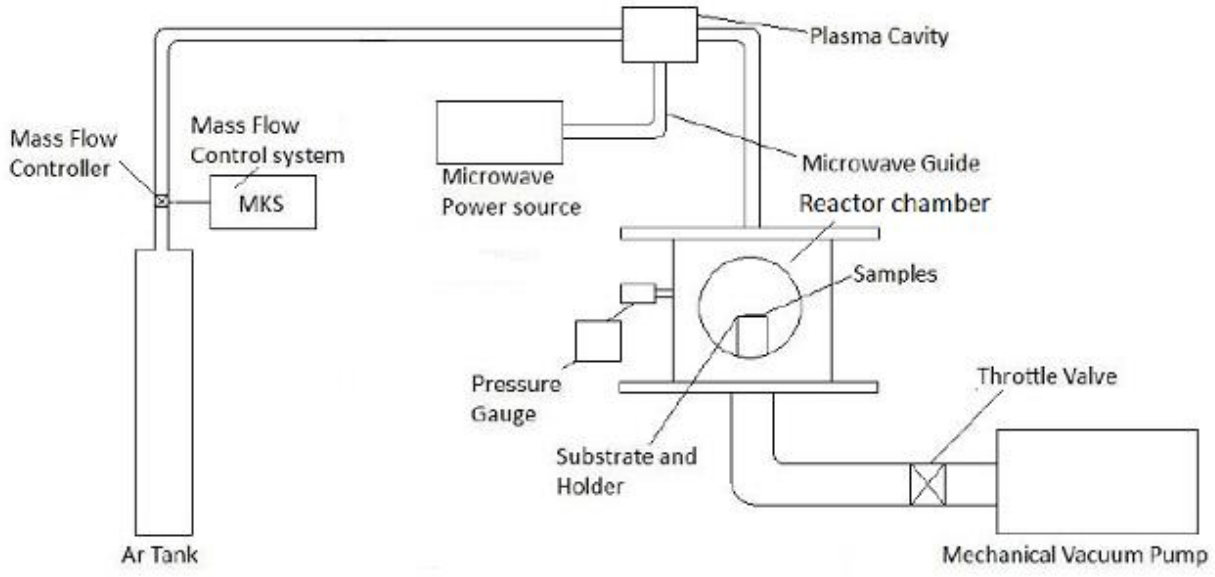

Figure 3. Setup for the indirect Ar MW discharge experiment.

Argon gas was flown into the plasma cavity at a rate of 50 standard cubic centimeters per minute (sccm) with the use of the MKS mass flow control system. A microwave powered plasma was initiated with a spark from a Tesla coil. The Tesla coil created excited argon atoms that, upon relaxation, emitted VUV radiation of wavelengths 104.8 and 106.7 nm. These VUV photons did not reach the sample due to its orientation with respect to the sample. The sample was placed inside of the reaction chamber and the system was under a vacuum in order to provide an inert atmosphere.

2.3 Reaction of Nafion with Oxygen Atoms

An argon and oxygen gas mixture plasma was maintained with a frequency of 2.45 GHz and a power ranging from 21 to 34 Watts and a low pressure of about 0.150-0.170 Torr.

The plasma was oriented horizontally to the Nafion sample so that the sample was in the presence of only oxygen atoms and no VUV radiation as displayed in Fig. 4 [64]:

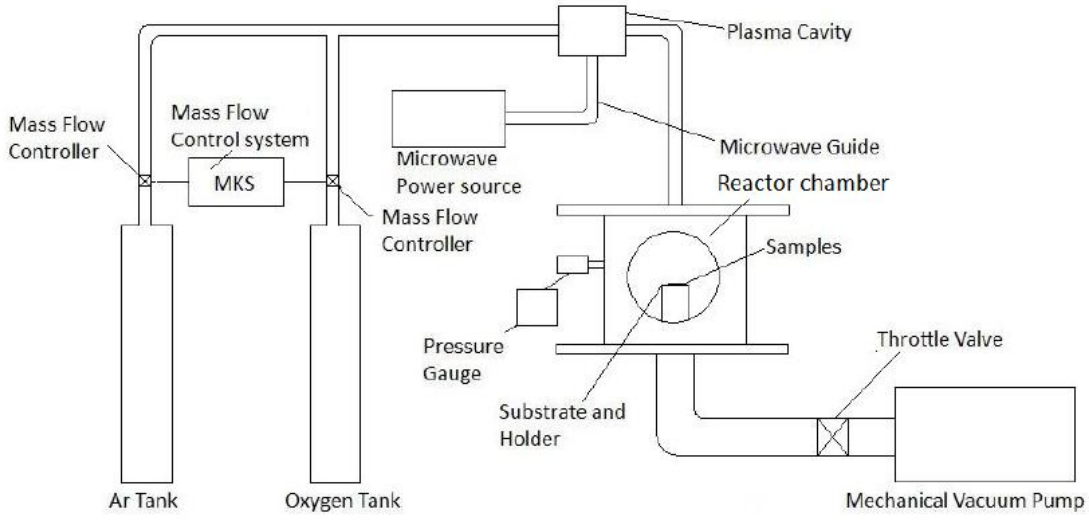

Figure 4. Setup for the indirect Ar/O_2 MW discharge experiment.

The argon was flown in at a rate of 50 sccm and oxygen at a rate of 10 sccm. All other parameters are identical to the setup in section 2.2.

2.4 Nafion in the Presence of a Direct Ar/O_2 MW Discharge

An argon and oxygen gas mixture plasma was maintained with a frequency of 2.45GHz, an average working power of 25 Watts and a low pressure of about 0.150-0.170 Torr. The plasma was oriented vertically to the location of the sample so that the VUV radiation emitted from the excited argon and oxygen could reach the Nafion sample and interact with its surface. In this experiment, both VUV radiation and excited oxygen atoms were able to react with the surface of the sample as shown in Fig. 5.

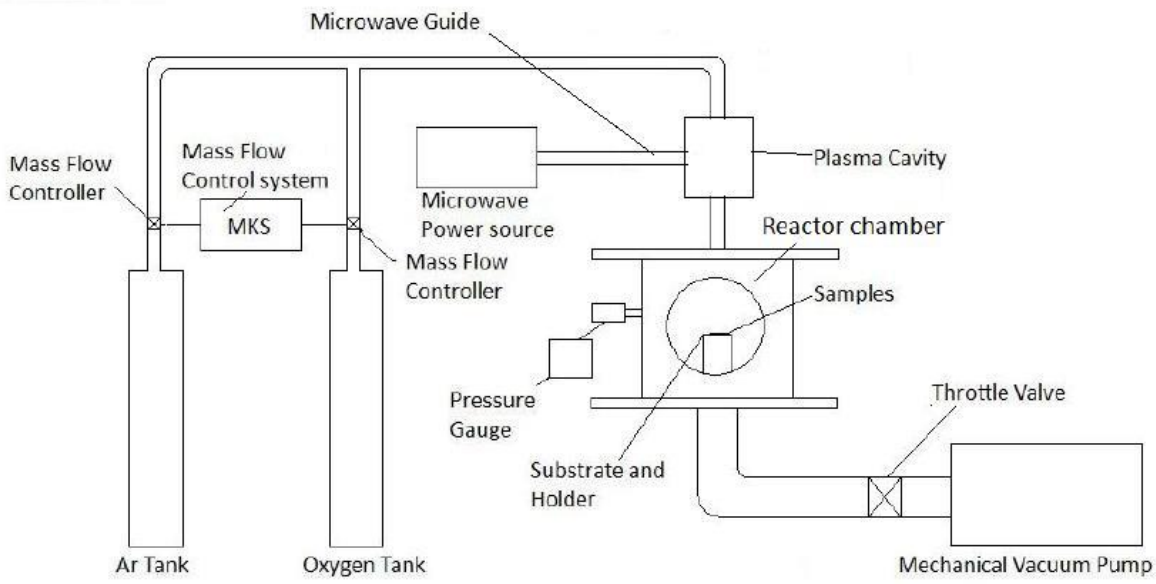

Figure 5. Setup for the direct Ar/O_2 MW discharge experiment.

The argon was flown in at a rate of 50 sccm and oxygen at a rate of 10 sccm. All other parameters are identical to the setup in section 2.2.

2.5 VUV Photolysis of Nafion

An argon microwave discharge plasma was maintained with a frequency of 2.45 GHz, an average working power of 24 Watts, and a low pressure of about 0.140-0.160 Torr. The plasma was oriented vertically to the Nafion sample so that the sample was in the direct presence of the emitted VUV radiation (Fig. 6).

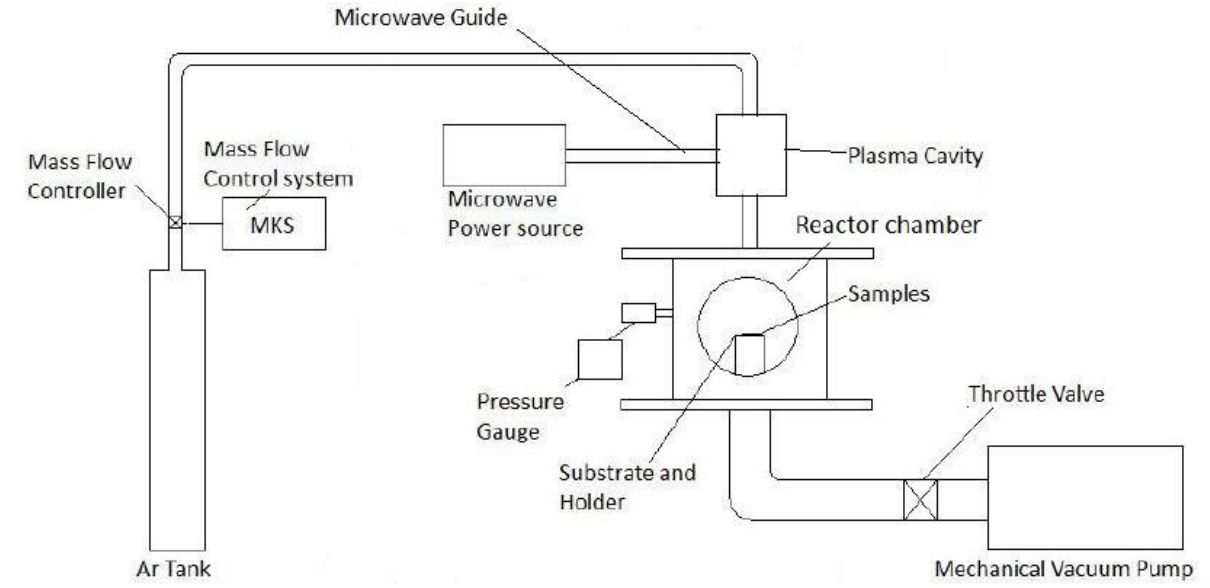

Figure 6. Setup for the VUV photolysis experiment.

The same flow rate of 50 sccm for argon gas was maintained with the MKS control system. All other parameters are identical to the setup in section 2.2.

2.6 Graft Polymerization of Nafion and Single-Walled Carbon Nanotubes (SWNTs)

2.6.1 VUV Photo-Oxidation of SWNT Paper

VUV photo-oxidation was carried out in a low pressure argon microwave plasma with a frequency of 2.45 GHz and a power of 10 Watts. Argon gas was flowing to the plasma cavity at a rate of 50 sccm and oxygen was flown to the reaction chamber about 2 mm above the SWNT sample at a rate of 10 sccm. The plasma cavity containing the argon microwave discharge was located about 23.8 cm directly above the sample and was oriented vertically to the reaction chamber so that the sample was in the direct presence

of the photons emitted by excited argon species. The oxygen flowing over the sample absorbed the emitted photons, creating oxygen radicals which were then able to oxidize the surface of the SWNT sample. The pressure within the reaction chamber remained in the range of 0.505 and 0.535 Torr throughout the reactions. VUV photo-oxidation treatment to SWNT samples was carried out for 0, 15, 30, 60, and 120 minutes [64]. The setup for the VUV photo-oxidation experiment is shown in Fig. 7.

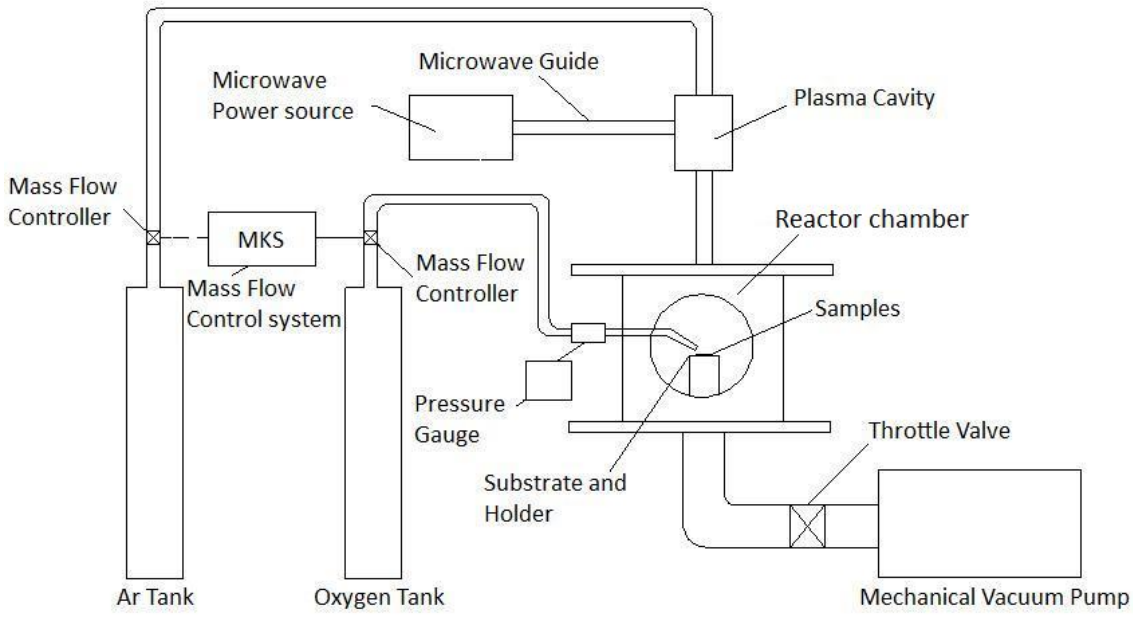

Figure 7. Setup for VUV photo-oxidation treatment of SWNT [64].

2.6.2 Grafting of VUV Photo-Oxidized SWNTs with Poly(Acrylic Acid)

The previously VUV photo-oxidized SWNTs were cut into shapes to distinguish each photo-oxidation treatment time sample from one another. The samples were previously

treated with 0, 15, 30, 60, and 120 minutes of VUV photo-oxidation and subsequently XPS analyzed to determine surface atomic percentages and functional groups.

Graft polymerization occurred in a 500 ml 3-neck round bottom flask with attached condenser, thermometer, and porous fritted disc with Ar gas running through it. An aqueous solution of iron sulfate heptahydrate and L-ascorbic acid with concentrations of 2.0×10^{-3} M and 3.6×10^{-3} M, respectively was prepared and added to the round bottom flask at 65°C. The control, the 15 min, and the 30 min treated samples were added to the solution. Acrylic acid was added to the flask to give a concentration of 10 M for a total solution of 100 ml. The ratio of acrylic acid to deionized water was 2.2 (68 ml acrylic acid and 32 ml water). The ferrous ions from the iron sulfate served to reduce oxygen containing functional groups on VUV photo-oxidized SWNT samples creating a radical. The radical would then initiate polymerization of acrylic acid. Ferrous ions also reduced radicals in the bulk solution to prevent bulk polymerization and the L-ascorbic acid reduced ferric ions back to ferrous ions to maintain constant concentration of ferrous ions [63]. The reaction was carried out at 65° C for one hour. The acrylic acid solution was decanted and the flask containing the samples was rinsed with deionized water several times followed by the heating of the samples in deionized water at 65-80°C for 2 hours to remove excess acrylic acid. After the 2 hours were complete, the samples were dried in a desiccator for several days. The same procedure was performed with the remaining 60 min and 120 min samples plus another control sample. A control experiment was carried out using the same grafting procedure as just described with 0, 15, 30, 60, and 120 min VUV photo-oxidized samples in the absence of acrylic acid to observe any changes that might be caused by the heated aqueous solution containing the initiators.

2.6.3 Control Experiment: Grafting Reaction of SWNTs in the Absence of Acrylic Acid

VUV photo-oxidized SWNTs (0, 15, 30, 60, and 120 min treatments) were exposed to a solution (100 ml) of iron sulfate heptahydrate (2.0×10^{-3}M) and L-ascorbic acid (3.6×10^{-3}M) at 65°C in the absence of acrylic acid. The reaction was run for 1 hour at 65°C followed by 2 hours of heating in deionized water at 65-80°C in a 500 ml flask with condenser, thermometer, and Pasteur pipette with argon flow (Fig. 8). The samples were then dried in a desiccator. This reaction served as a control to observe how the oxidized SWNTs behaved in the presence of initiators without acrylic acid.

Figure 8. Experimental setup for the grafting of carbon nanotubes with polyacrylic acid.

2.6.4 Grafting of VUV Photolysis Treated Nafion with Poly(Acrylic Acid)

Grafting was performed in a 500 ml 3-neck round bottom flask with condenser, thermometer, and a Pasteur pipette as an argon gas outlet. A solution of 1 x 10^{-2} M iron sulfate heptahydrate and 1.4 x 10^{-2} M L-ascorbic acid added to the flask along with acrylic acid to give the final solution (100 ml) a concentration of 6.8M acrylic acid. The solution was purged for 15 min with argon at 65°C. VUV photolysis treated Nafion

samples (0, 5, 15, 30, 60, and 90 min) were cut into distinct shapes and added to the solution. The reaction was run for 1.5 hours at 65°C. The samples were rinsed with hot deionized water and then heated in deionized water at 65-80°C to remove excess acrylic acid. Following grafting, the samples were dried in a desiccator.

2.6.5 Control Experiment: Grafting Reaction of VUV Photolysis Treated Nafion in the Absence of Acrylic Acid

Nafion samples treated with VUV photolysis (0, 5, 15, 30, 60, 90 min) were cut into shapes to distinguish the samples from one another. A 100 ml aqueous solution of 1.0 x 10^{-2} M iron sulfate heptahydrate and 1.4 x 10^{-2} M L-ascorbic acid was added to a 500 ml flask with condenser, thermometer, and Pasteur pipette with argon flow at 65°C. The solution was purged with argon for 15 min followed by the addition of the Nafion samples. The reaction was run for 1.5 hours. The samples were heated in deionized water for another 2 hours at 65-80°C and then dried in a desiccator. This reaction investigated any interaction of modified Nafion with the initiators in the heated solution.

2.7 Methods of Analysis

2.7.1 X-Ray Photoelectron Spectroscopy

XPS analysis was used as a surface characterization technique to examine the top 2-5 nm from the surface of Nafion and SWNT samples. About an 800 μm sample was placed under a molybdenum sample mask to be exposed to the X-Ray beam using a Physical

Electronics model 5800 XPS instrument. The angle between the sample and the analyzer was 45°. Samples were attached to a stainless steel sample holder with the use of double backed conductive copper tape underneath the molybdenum mask [66, 67]. Samples were irradiated with an Al kα X-Ray radiation source with an energy of 1486 eV and electrons from a BaO field emission charge neutralizer neutralized the samples which served to limit radiation damage [67]. With the irradiation of the sample with the X-Ray beam, one photon displaces an inner core electron from the sample plus a kinetic energy [68]. The kinetic energy (KE), described in equation (5), equals the energy of the X-Ray photon (hν) minus a binding energy (BE) and a work function (w), which is a correction factor taking into account the electrostatic environment [68]:

$$KE = h\nu - BE - w \quad (5)$$

The binding energy is characteristic to each element and allows for the determination of the elemental concentrations on the surface of the samples. Each Nafion (VUV photolysis, direct and indirect Ar/O_2 MW discharge, PAA grafting, and control grafting) and SWNT (PAA grafting and control grafting) experiment was analyzed by XPS. All XPS experiments were carried out by Dr. Tom Debies and Michael Mehan of Xerox Analytical Services at Xerox Research Center in Webster, NY.

2.7.2 Scanning Electron Microscopy

SEM was used to examine the physical surface structure and morphology of Nafion. Samples with an area of about 1 cm^2 were analyzed. The samples were adhered to a conductive pad and covered with gold of 20 nm thickness in preparation for the analyses.

A Hitachi S-4800 FESEM instrument was used for all samples. Images were produced and magnified by 500, 1000, and 5000 times [69]. In scanning electron microscopy, a focused electron beam bombards the sample and is scanned over the area under analysis. In response to this electron beam, the sample produces signals from backscattered and secondary electrons. The signals are detected and used to produce an image of physical characteristics of the material [68]. In this work, SEM images were produced from secondary electrons accelerating at 5 kV and all SEM analysis was performed by Dr. Greg Thompson of Xerox Analytical Services at Xerox Research Center in Webster, NY [69]. SEM images were produced for VUV photolysis treated Nafion and direct Ar/O_2 MW discharge treated Nafion.

2.7.3 Contact Angle Analysis

As a measure of wettability, contact analysis was performed for clean Nafion, VUV photolysis treated Nafion, Ar/O_2 direct MW discharge treated Nafion, polyacrylic acid grafted Nafion, as well as control grafted Nafion. A Rame Hart Standard Goniometer Model No. 250-F1 with computer software program DROPimage Advanced was used for contact angle measurements. A static sessile drop method was used to measure the contact angle for all samples. In the static sessile drop method, a small deionized water droplet is placed onto the sample with the use of a microsyringe and contact angles are measured quickly after placement of the drop. Nafion samples absorbed water rapidly soon after the droplet was placed and time (about 1 min) was allowed for the sample to become more stable before the contact angle was measured. Advancing and receding

contact angle measurements were recorded for a clean untreated Nafion sample to observe its hydrophobic and hydrophilic behavior.

2.7.4 Fourier Transform Infrared Spectroscopy

To examine any changes in functional groups on the surface of Nafion following modifications, FTIR analysis was performed. A Shimadzu IR Prestige-21 was used in all measurements and plots of percent transmittance vs. wavenumber (cm^{-1}) were created. A resolution of 16 cm^{-1} was used and either 150 or 200 scans were run in each measurement. FTIR measures the wavenumber, which is directly proportional to energy and frequency, of the absorption of infrared radiation by bonds containing a dipole moment [65]. Each bond type absorbs infrared radiation within a specific range of frequencies and observation of an FTIR spectrum can suggest information about the structure of a molecule. FTIR analysis was used to compare structural differences between polyacrylic acid grafted Nafion and control grafted Nafion.

2.8 Hydrogen Storage of Magnesium Hydride

2.8.1 Kinetics of Hydrolysis of Magnesium Hydride with Acetic Acid

A PASPORT Absolute Pressure/Temperature Sensor, PASPORT Interface USB Link, and an Ideal Gas Law Syringe were purchased from PASCO and a Dr. Fuel Cell Dismantlable Fuel Cell – Extension Kit and a Dr. Fuel Cell Load Measurement Box were purchased from Fuel Cell Store. The fuel cell was connected to the measurement box and

set up to observe voltage and current measurements. The measurement box incorporates a resistance setting for a motor. Using a plastic 3-way adapter, the pressure/temperature sensor was connected through tubing to both the fuel cell and the ideal gas syringe. Another plastic 3-way adapter was used to connect the fuel cell to a 100 ml round bottom flask and to the pressure sensor. A pinch clamp was used to shut off the pathway to the fuel cell so that all of the hydrogen being produced in the hydrolysis would be directed toward the pressure sensor. The magnesium hydride (150 mg, VWR International) was placed inside the flask and capped with a septum stopper. The 5 ml of 2 wt% acetic acid was added using a syringe and needle through the septum stopper to ensure that hydrogen produced was not released to the surroundings. The Interface USB Link was plugged into a computer and the DataStudio program was used to display the pressure vs. time data. The setup is shown in Fig. 9 and described in Fig. 10:

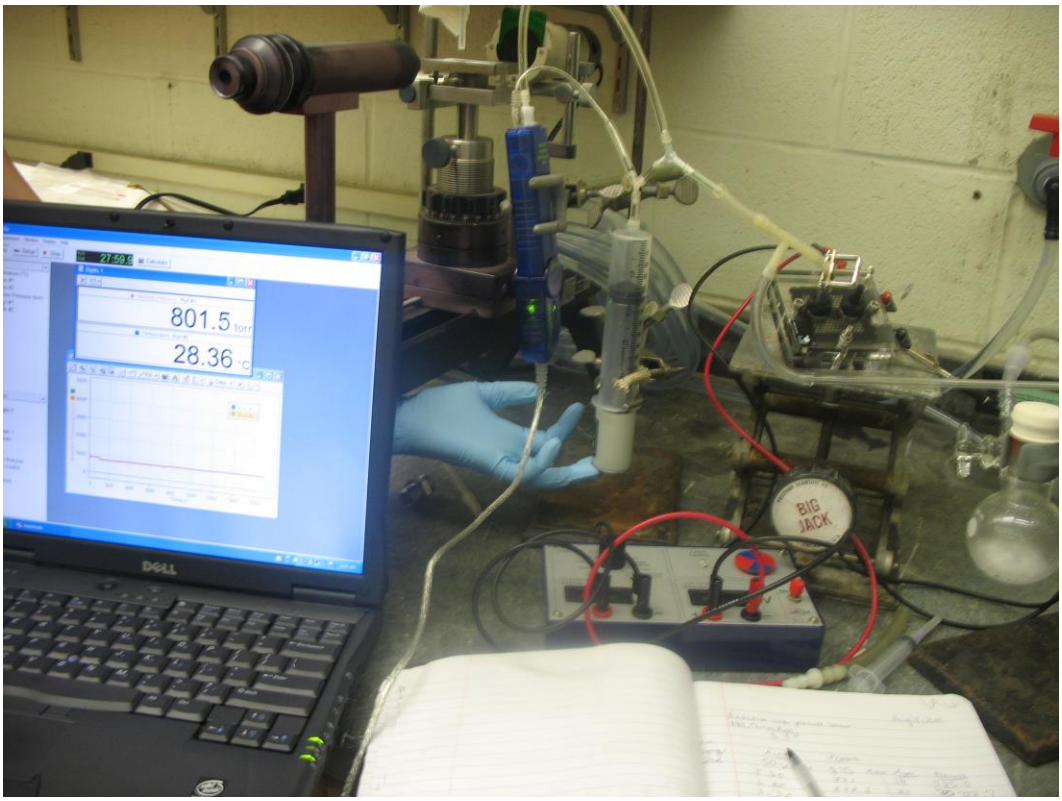

Figure 9. PASPORT Absolute Pressure/Temperature Sensor, USB Link, and Ideal Gas Law Syringe setup with fuel cell, flask, and DataStudio program.

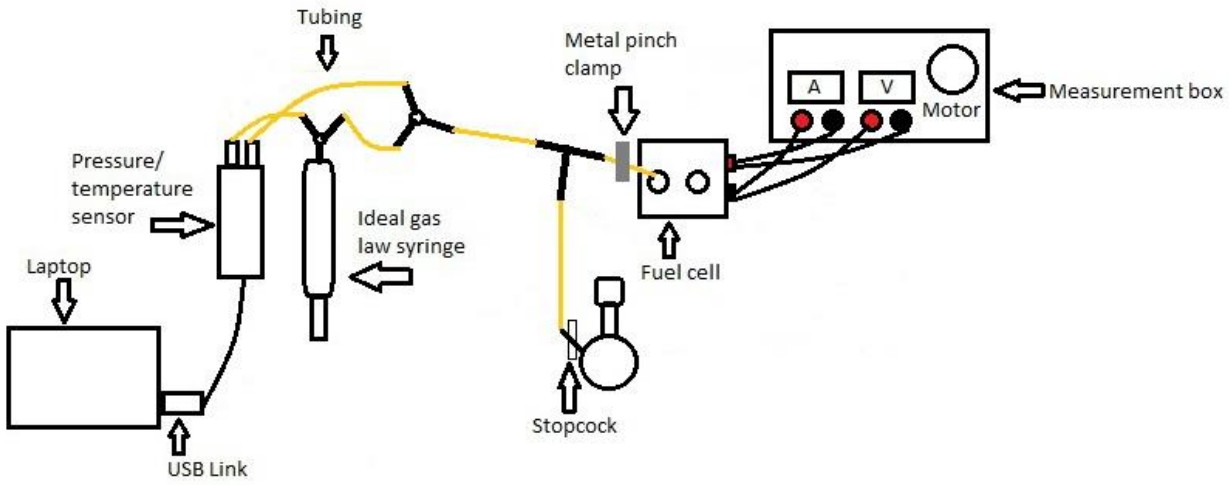

Figure 10. Description of the kinetics of hydrolysis experiment with fuel cell, motor, ideal gas law equipment, and laptop.

The gas law syringe was kept at a constant volume of 20 ml throughout the whole experiment. The pathway to the pressure sensor remained open during the addition of the acetic acid and throughout the rest of the hydrolysis. A plot of pressure vs. time in Torr and minutes was created with DataStudio for the hydrolysis reaction. The hydrolysis was carried out for 80 minutes and was stopped before reaching completion.

The total volume of the system was calculated by moving the gas law syringe a fixed amount and measuring the pressure at each point. The volume of the system was calculated using Boyle's law (6):

$$P_1 (V_1 + X) = P_2 (V_2 + X) \quad (6)$$

Where P_1 is the pressure at the volume V_1, P_2 is the pressure at the volume V_2, and X is the volume of the system minus 5 ml acetic acid.

2.8.2 Fuel Cell Consumption of Hydrogen

After the 80 minute hydrolysis described in section 2.8.1 was complete, the pinch clamp, which had been previously shut to the fuel cell, was opened to allow the hydrogen to reach the fuel cell and measurements of current, voltage, and the motor run time were recorded.

Another setup was created where the fuel cell was connected to both the measurement box and the round bottom flask through tubing (Figs. 11 and 12). The magnesium hydride (100 mg, 150mg) was placed inside the flask and capped with a septum stopper. The 5 ml of 2 wt% acetic acid was added using a syringe and needle through the septum stopper in the same manner as in section 2.8.1. A metal pinch clamp was placed on the tubing connecting the flask to the fuel cell in order to build up pressure for hydrogen gas to overcome the atmospheric pressure and the pathway to the fuel cell.

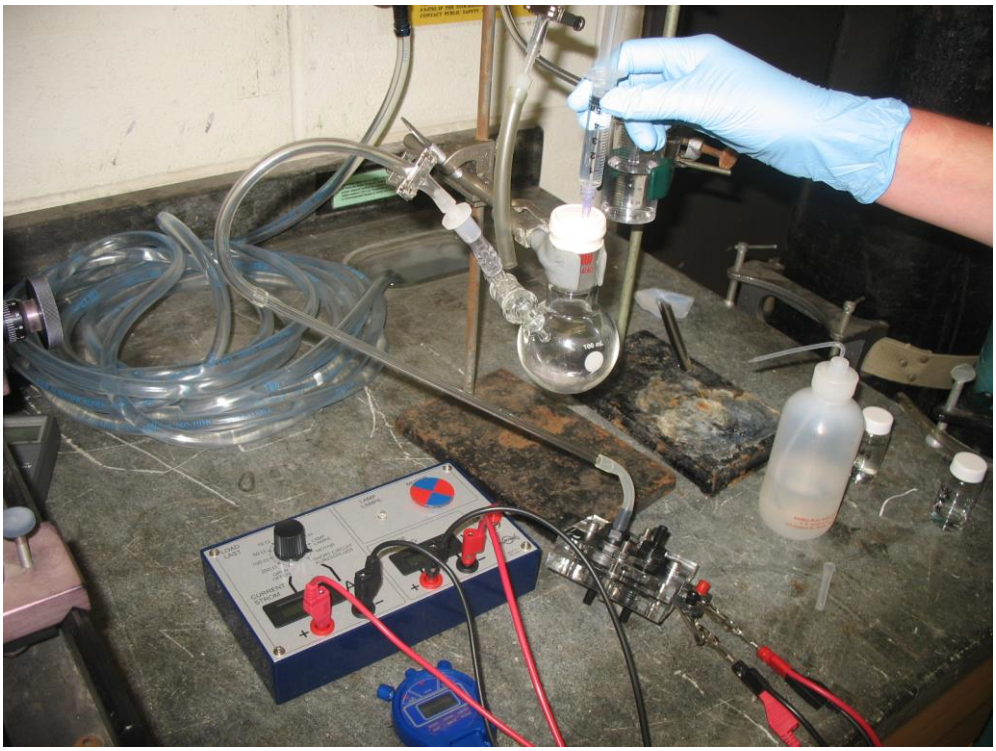

Figure 11. Addition of acetic acid to the reaction flask connected to the fuel cell with load measurement box.

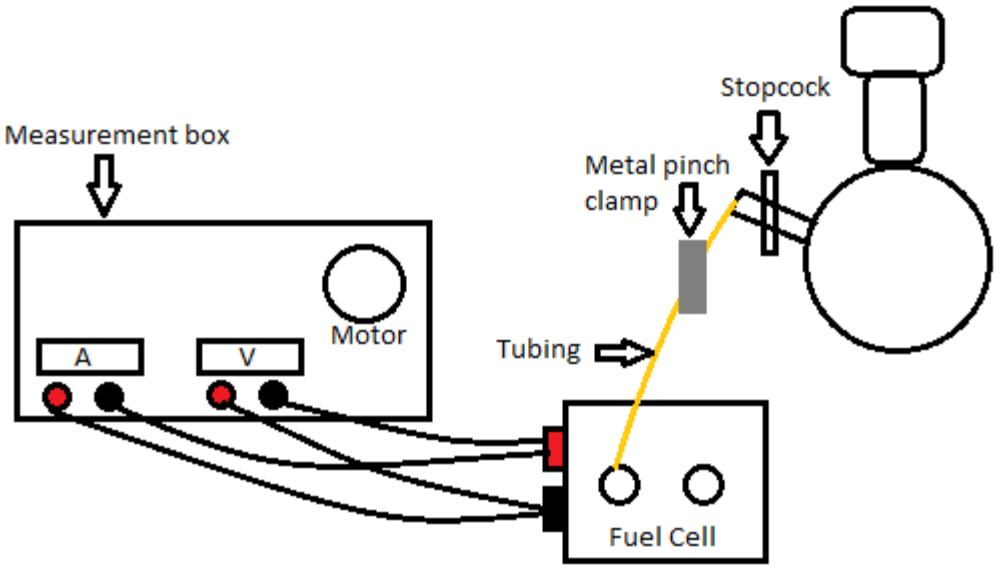

Figure 12. Experimental setup for fuel cell consumption of hydrogen released from the hydrolysis.

After several minutes of reaction, the pinch clamp was opened and the working motor on the measurement box was observed. The time the motor had run, the voltage, and the current values were recorded. The pinch clamp was then shut for a period of time to once again build up pressure. The clamp was reopened and the same parameters were measured for several of these steps. This procedure was repeated for two trials (100 mg and 150 mg MgH_2) for 78 min of reaction for the 100 mg sample and for 47 min of reaction for the 150 mg sample. The reactions were both stopped before reaching completion.

2.8.3 Hydrogen Storage Capacity of Magnesium Hydride Determination with TGA

Thermogravimetric analysis (TGA) was used to determine the weight loss of the magnesium hydride sample under thermal decomposition. Magnesium hydride that had been stored in an inert Ar atmosphere was used. A TGA TA 2050 instrument (TA Instrument) was used and the furnace was kept under nitrogen to maintain an inert atmosphere. The TGA was run with a ramp of 20 ºC/min up to 800ºC and held at an isothermal for 2 min.

Part 3

Results

3.1 X-ray Photoelectron Spectroscopy

3.1.1 Indirect Plasmas: Ar Control and Ar/O_2: Reaction of Oxygen Atoms with Nafion

Nafion in the presence of indirect argon plasma was performed as a control experiment. In the indirect experiment, the plasma is oriented horizontally so that no VUV photons are able to reach the sample. Indirect argon and oxygen mixture plasma served to react Nafion samples with oxygen atoms only. Oxygen atoms from the plasma are able to enter the reaction chamber to react with the samples while VUV photons stay in the horizontally oriented plasma. Quantitative XPS analysis for two clean Nafion samples labeled as Control 1 and Control 2 is compared with Nafion samples exposed to indirect Ar plasma and indirect Ar/O_2 plasma in Table 1.

Table 1
Quantitative XPS analysis for Nafion treated with indirect Ar and Ar/O_2 plasmas

Sample	At% Carbon	At% Oxygen	At% Fluorine	At% Sulfur
Control (1)	32.09	8.06	58.70	1.15
Control (2)	31.81	7.96	59.17	1.06
Ar: 30 min.	31.21	8.11	59.64	1.04
Ar: 60 min.	32.00	7.74	59.23	1.03
Ar/O_2: 5 min.	30.01	8.70	59.89	1.40
Ar/O_2: 10 min.	32.09	8.34	58.30	1.27
Ar/O_2: 30 min.	31.78	8.36	58.52	1.34
Ar/O_2: 60 min.	32.64	7.76	58.58	1.03
Ar/O_2: 90 min.	30.74	8.66	59.85	0.76

Nafion samples were washed prior to their modification. The Control (1), Ar: 30 min, Ar/O_2: 5 min, Ar/O_2: 10 min, and Ar/O_2: 30 min samples are compared with one

another because they were washed in the same batch and analyzed at the same time following modification. The rest of the samples (Control (2), Ar 60 min, Ar/O_2: 60 min, and Ar/O_2: 90 min) are compared because they were washed and analyzed together as well. Very little change is seen in the atomic percentages of each atom comparing Control (1) with Ar: 30min. and Control (2) with Ar: 60 min. There is minimal change comparing Control (1) with the 5, 10, and 30 min Ar/O_2 treated samples and the Control (2) with Ar/O_2 60 min sample. However, there is a slight change between the Control (2) and the Ar/O_2 90 min. sample: There is a 0.70% increase in oxygen and a 0.30% decrease in sulfur. This change is also supported in the overlapped O 1s spectra (Fig. 13)

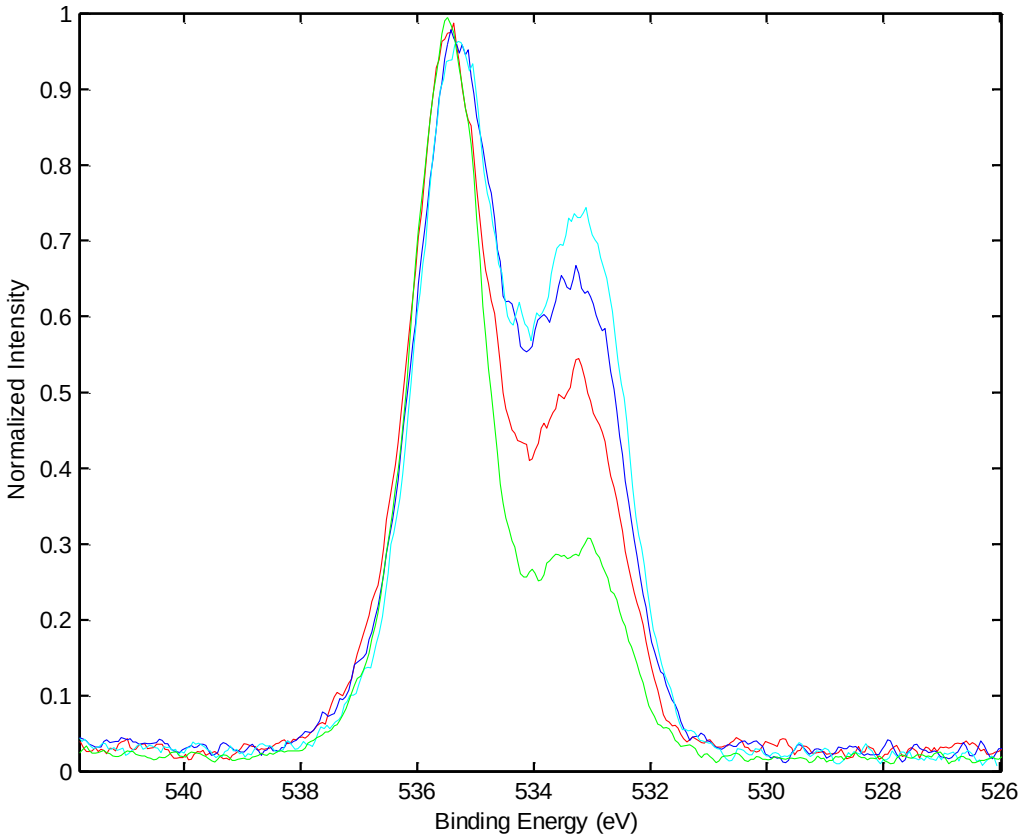

Figure 13. Overlapped O 1s spectra for Control (2) (red), Ar: 60 min (blue), Ar/O_2: 60 min (light blue), and Ar/O_2: 90 min (green).

The O 1s characteristic binding energies for Nafion are displayed in Table 2.

Table 2
O 1s characteristic binding energies for Nafion [66]

Species	Binding Energy (eV)
O-C=O (Composite)	532.7
Sulfonic acid	533.4
CF-O*-CF_2	535.1

The intensity of Ar/O_2: 90 min. sample peak is significantly lower at 533.4 eV, corresponding to the sulfonic acid groups than the Control (2) peak. The long treatment time of 90 minutes might have allowed enough time for the oxygen atoms from the plasma to begin breaking C-S bonds (bond energy of 2.72 eV [21]), the weakest bond in the Nafion structure, and remove sulfonic acid groups. The Ar: 60 min. sample and the Ar/O_2 60 minute sample peaks are higher at 533.4 eV than the Control (2), in the O 1s spectrum, however it is not indicated in the elemental analysis (Table 1) that there is an increase in sulfur percentage.

The C 1s characteristic binding energies for Nafion are listed in Table 3. The overlapped C 1s spectrum (Fig. 14) shows an increase in CF_3 groups for the Ar/O_2: 90 min sample and a slight decrease for the Ar: 60 min and the Ar/O_2: 60 min samples, however a change in fluorine was not shown in the elemental analysis for any of these samples (Table 1).

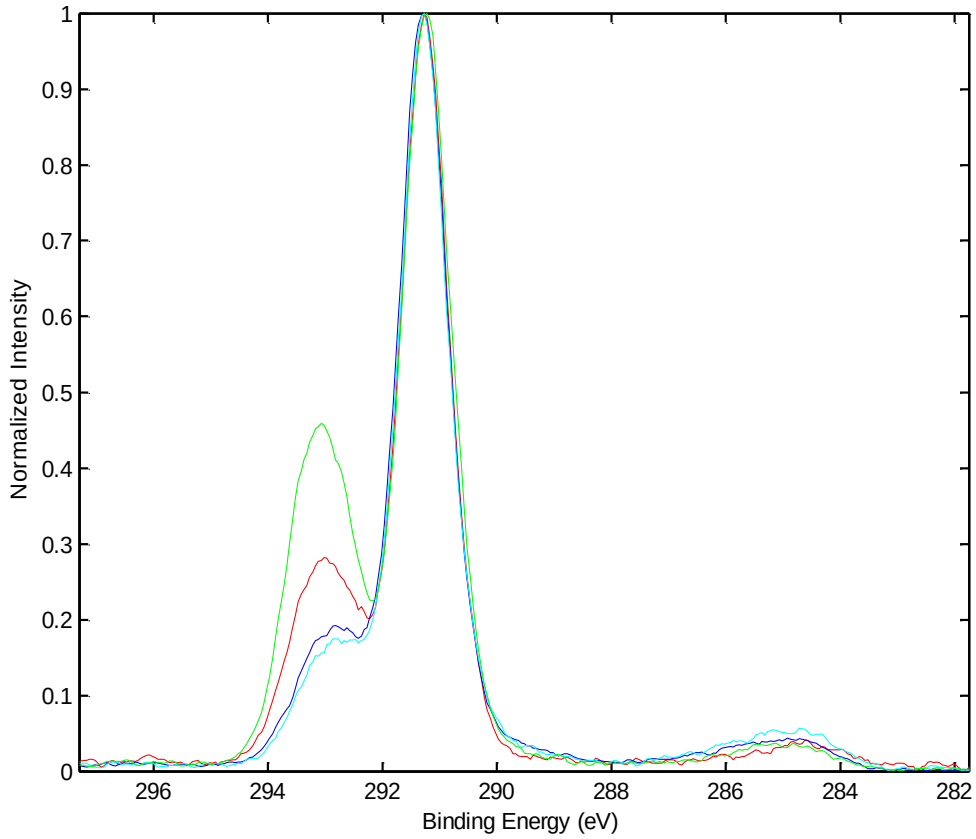

Figure 14. Overlapped C 1s spectra for Control (2) (red), Ar: 60 min (blue), Ar/O_2: 60 min (light blue), and Ar/O_2: 90 min (green).

Table 3
C 1s characteristic binding energies for Nafion [66]

Species	Binding Energy (eV)
C-C	284.7
O-C-C* ‖ O	285.4
C*-O-C=O	286.2
O=C-O	289.3
CF	289.2
CF_2	291.8
CF_3	293.0

3.1.2 Nafion in the Presence of a Direct Ar/O_2 MW Discharge

Nafion was reacted with both VUV radiation and oxygen atoms in the direct Ar/O_2 MW discharge experiment. The quantitative XPS analysis is summarized in Table 4.

Table 4
Quantitative XPS analysis for Nafion treated with direct Ar/O_2 plasma

Treatment Time	At% Carbon	At% Nitrogen	At% Oxygen	At% Fluorine	At% Sulfur
Control	30.52	0.00	8.78	59.22	1.47
5 min	31.33	0.39	7.50	60.09	0.69
15 min	31.28	0.32	6.83	61.38	0.19
30 min	31.21	0.35	5.77	62.61	0.06
60 min	31.26	0.22	5.05	63.41	0.06
90 min	31.49	0.30	5.08	63.05	0.08

The percentage of sulfur quickly diminishes with treatment time. The percent carbon increases very slightly from the control to the 5 min treatment time then levels to roughly the same value for the 5-90 min samples. There is a decrease in oxygen concentration and an increase in fluorine concentration. A small increase in nitrogen concentration is also observed. The sharp decrease in sulfur and the decrease in oxygen indicate that sulfonic acid groups are being removed. Since percent sulfur and oxygen are decreased, fluorine is taking up more percentage of the polymer. The overlapped O 1s spectra (Fig. 15) support a decrease in sulfonic acid groups.

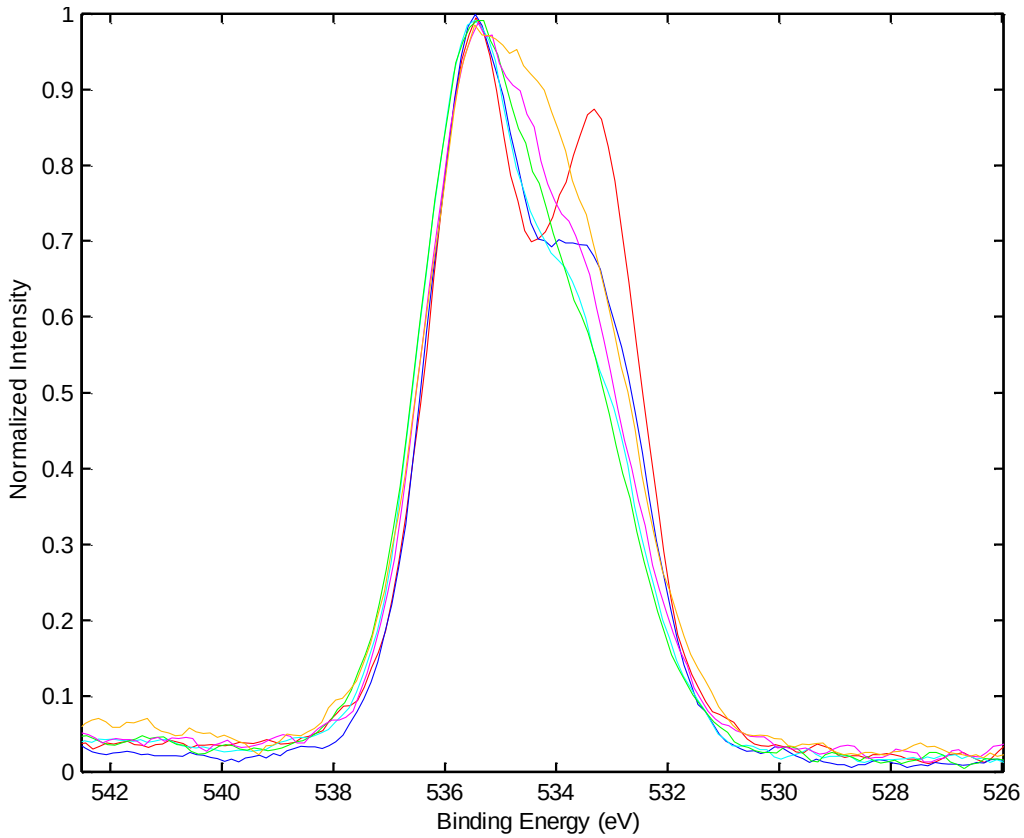

Figure 15. Overlapped O 1s spectra for Nafion samples treated with direct Ar/O_2 plasma. Control (red), 5 min (blue), 15 min (light blue), 30 min (green), 60 min (pink), and 90 min (yellow).

The decrease in the peak at 533.4 eV indicates a decrease in the sulfonic acid group (Table 2). Since the plasma contains both argon and oxygen gases, some of the VUV photons are being absorbed by oxygen in the plasma. With a loss of VUV photons to the oxygen, there are less photons available that can be interacted with the Nafion samples. Oxygen atoms may react to break C-S bonds and remove sulfonic acid groups.

The overlapped C 1s spectra (Fig. 16) show a decrease in CF_3 groups at 293.0 eV.

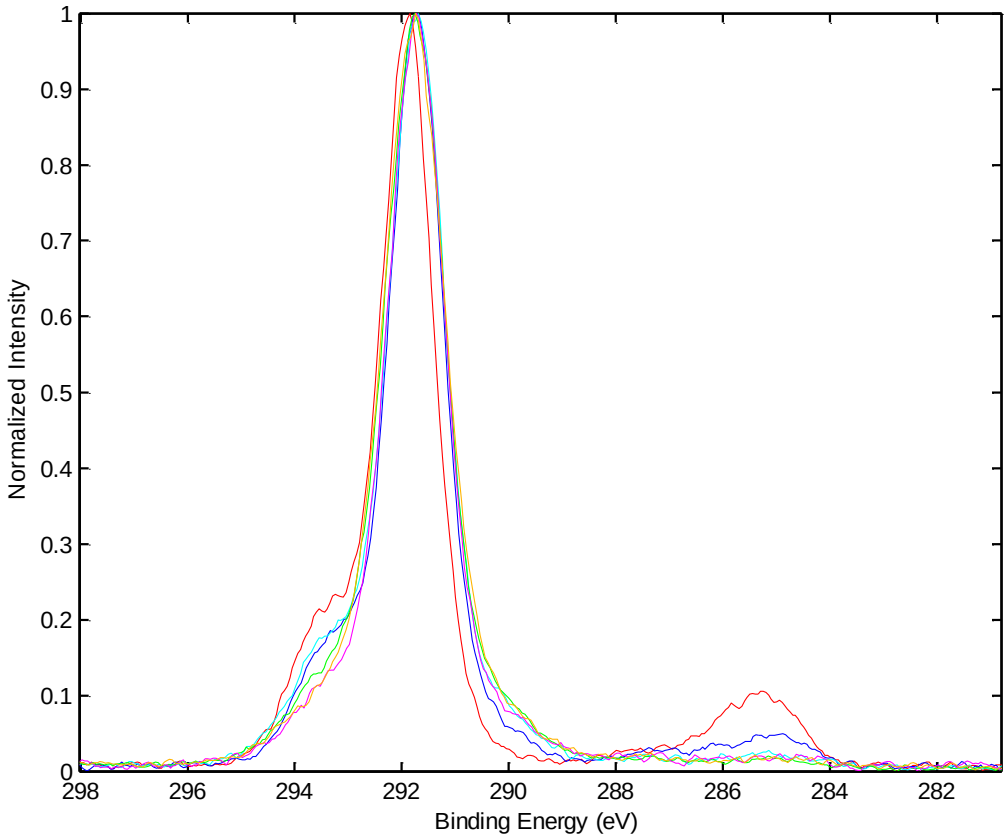

Figure 16. Overlapped C 1s spectra for Nafion samples treated with direct Ar/O_2 plasma. Control (red), 5 min (blue), 15 min (light blue), 30 min (green), 60 min (pink), and 90 min (yellow).

The VUV photons (104.8 nm and 106.7 nm) that are emitted from the argon in the plasma have energies of 11.63 eV and 11.84 eV. The photons that are not absorbed by oxygen may interact with bonds on the surface of Nafion. The C-F bond strength (4.86 eV), as well as, C-C (3.86 eV), C-O (3.58 eV), S-O (3.64 eV), and C-S (2.72 eV) [21] can be broken by the absorbed photons. The decrease in CF_3 groups may be caused by photons breaking C-F bonds on these groups. In support of this, the results of the C 1s

curve fittings (Table 5, spectra not shown), which give the percent area under the curve for various functional groups, show a decrease in CF_3 groups as well as an increase in CF_2 groups. With one fluorine atom being removed from a CF_3 group, CF_2 groups are formed. A radical formed on a carbon atom from a newly formed CF_2 group may react with O_2 in the system or when taken out of the vacuum reaction chamber and exposed to air. The C 1s curve fittings results show an increase in O=C-O functional groups. C-C bonding is also decreased as indicated in both the C 1s spectra (Fig. 16) at 284.7 eV and in the results of the C 1s curve fittings (Table 5). The VUV photons can also break C-C bonds and new functional groups may be formed from radicals on carbon atoms that were previously bonded to other carbon atoms. The small increase in nitrogen percentages from the quantitative XPS analysis (Table 4) may be a result of radicals on the surface of Nafion reacting with N_2 from air.

Table 5
Results of the C 1s curve fittings spectra for direct Ar/O_2 treatment of Nafion

Species	Control	5 min.	15 min.	30 min.	60 min.	90 min.
C-C	6.7	3.2	1.6	0.8	0.8	0.9
O-C-C* ‖ O	3.3	1.5	0.0	0.0	0.0	0.0
C*-O-C=O	0.8	1.1	0.7	1.0	0.7	0.6
O=C-O	1.0	4.1	4.2	5.7	5.4	5.1
CF	0.0	0.0	0.0	0.0	0.0	0.0
CF_2	73.5	75.1	81.5	84.0	85.4	87.7
CF_3	14.8	15.0	12.0	8.6	7.8	5.7

3.1.3 VUV Photolysis of Nafion

Nafion was reacted with VUV photons emitted by argon plasma in the VUV photolysis experiment. The experiment was carried out in 4 different trials. The quantitative XPS analysis of each trial is overviewed in Tables 6(a-d).

Table 6a
Quantitative XPS analysis for VUV photolysis of Nafion, Trial 1

Treatment Time	At% Carbon	At% Nitrogen	At% Oxygen	At% Fluorine	At% Sulfur
Control (1)	33.58	0.22	8.31	56.45	1.44
Control (2)	31.55	0.19	8.62	58.38	1.27
5 min.	31.87	0.75	7.5	59.3	0.58
15 min.	33	1.98	11.34	52.22	1.47
30 min.	33.16	2.96	12.93	49.21	1.74
60 min.	36	3.4	12.67	46.47	1.46
90 min.	40.86	3.81	14.15	39.84	1.34

Table 6b
Quantitative XPS analysis for VUV photolysis of Nafion, Trial 2

Treatment Time	At% Carbon	At% Nitrogen	At% Oxygen	At% Fluorine	At% Sulfur
Control	31.15	0	8.44	59.03	1.38
5 min.	31.71	0.67	7.12	59.87	0.62
15 min.	31	2.04	9.77	56.03	1.16
30 min.	32.7	2.38	9.36	54.62	0.93
60 min.	34.29	3.04	9.84	51.84	0.98
90 min.	34.85	3.22	10.32	50.65	0.96

Table 6c
Quantitative XPS analysis for VUV photolysis of Nafion, Trial 3

Treatment Time	At% Carbon	At% Nitrogen	At% Oxygen	At% Fluorine	At% Sulfur
Control	30.29	0	8.41	59.92	1.38
5 min.	31.59	0.64	7.01	60.08	0.68
15 min.	30.64	2.07	9.49	56.66	1.15
30 min.	31.88	2.41	9.63	55.01	1.07
60 min.	34.98	2.75	10.33	50.85	1.08
90 min.	36.8	3.3	11.63	47.02	1.25

Table 6d
Quantitative XPS analysis for VUV photolysis of Nafion, Trial 4

Treatment Time	At% Carbon	At% Nitrogen	At% Oxygen	At% Fluorine	At% Sulfur
Control	32.91	0	8.08	57.65	1.36
5 min.	32.8	0.41	6.35	59.74	0.71
15 min.	31.86	2.13	9.53	55.15	1.33
30 min.	34.89	2.73	9.9	51.28	1.2
60 min.	36	3.59	9.86	49.32	1.22
90 min.	37.21	4.96	11.91	44.61	1.32

In all trials, the percentage of oxygen, carbon, and nitrogen increased, and the percentage of fluorine decreased with treatment time. Since there is no oxygen present in the plasma, all of the VUV photons emitted can react with Nafion and have the ability to break C-F, C-O, C-C, C-S, and S-O bonds, leaving more radicals on the surface than in the Ar/O_2 direct plasma experiment. The free radicals may react with oxygen and nitrogen when exposed to air. There is a more significant increase in nitrogen for the VUV photolysis experiment than for the direct Ar/O_2 MW discharge experiment. There is an increase in oxygen with VUV photolysis contrary to the decrease in oxygen for direct Ar/O_2 MW discharge. The decrease in fluorine indicates the breakage of C-F bonds. In all four trials, there is a consistent decrease in sulfur percentage for the 5 min sample. An explanation could be that for this short time period, the photons are breaking the weakest C-S bonds first. When more time is allowed, as with the other treatment times, the photons have more time to break the stronger bonds. Since the sulfur percentages increase again for the rest of the treatment times, the longer time periods may allow for the reformation of the C-S bonds while other bonds are being broken.

The VUV photolysis experiment that led to the most surface oxidation was Trial 1 (Table 6a). The overlapped C 1s spectra (Fig.17) shows a large increase in C*-O-C=O at 286.2 eV and O=C-O at 289.3 eV.

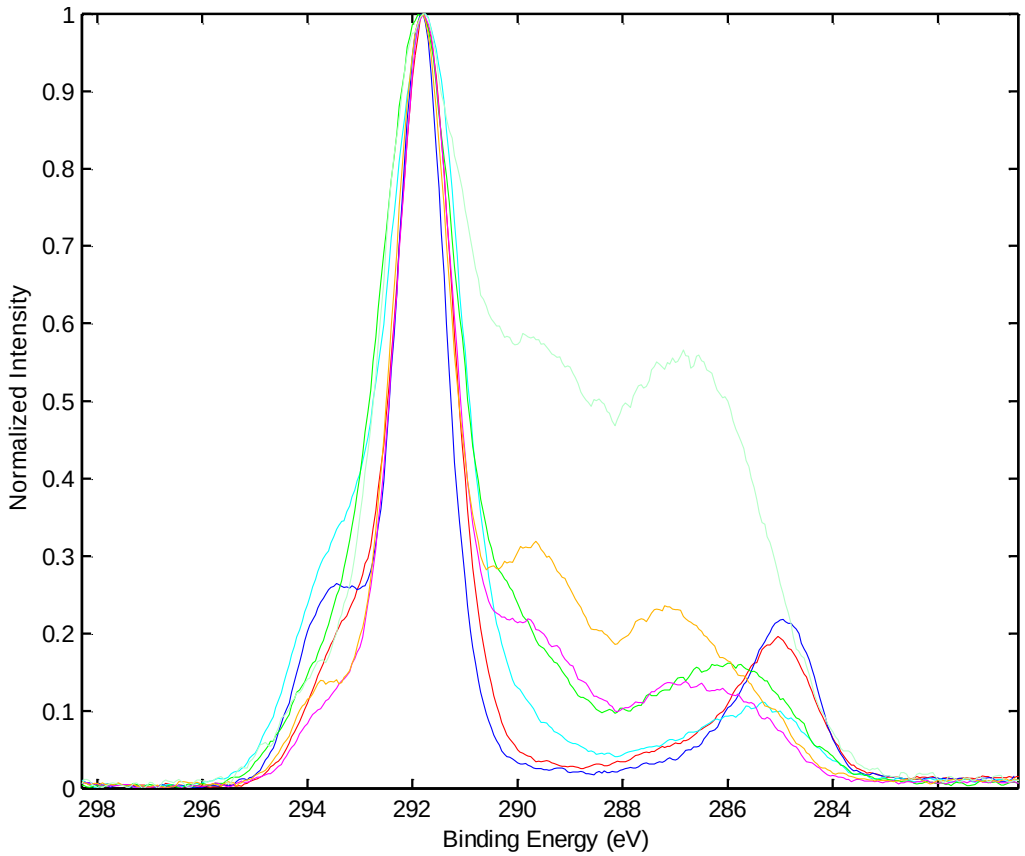

Figure 17. Overlapped C 1s spectra for Trial 1 VUV photolysis. Control (1) (red), Control (2) (blue), 5 min (light blue), 15 min (green), 30 min (pink), 60 min (yellow) and 90 min (light green).

More evidence for the increase in oxygen-containing functional groups is shown in the results of the C 1s curve fittings (Table 7).

Table 7
Results of the C 1s curve fittings spectra for VUV photolysis of Nafion Trial 1

Species	Control (1)	Control (2)	5 min.	15 min.	30 min.	60 min.	90 min.
C-C	11.0	14.4	4.0	1.9	0.0	0.6	0.0
O-C-C* ‖ O	2.8	2.6	2.5	2.2	2.5	3.1	7.0
C*-O-C=O	4.6	1.9	3.3	13.0	11.1	12.3	23.3
O=C-O	0.0	0.0	0.0	8.1	16.0	20.1	22.4
CF	2.6	1.8	4.8	2.0	3.1	8.1	4.5
CF_2	65.0	60.2	67.8	65.2	61.3	49.9	38.9
CF_3	14.1	19.1	17.6	7.5	5.9	5.9	3.9

The carbon under examination in the C*-O-C=O group could be a carbon atom from a C-O within Nafion. The VUV photons could break C-F bonds from a CF-O-CF_2 group and leave a radical on one of the carbon atoms, which could then react to form a ketone. The C*-O-C=O could also be due to the formation of an ester group. The CF_2 and CF_3 groups decrease and the CF groups increase. Losing a fluorine atom from a CF_2 or CF_3 groups could result in an increase in CF groups, where the carbon is now bonded to other substituents.

The overlapped O 1s spectra (Fig. 18) and the results of the curve fittings for the O 1s spectra (Table 8) suggest that there is a removal of sulfonic acid groups for the 5 minute treatment time.

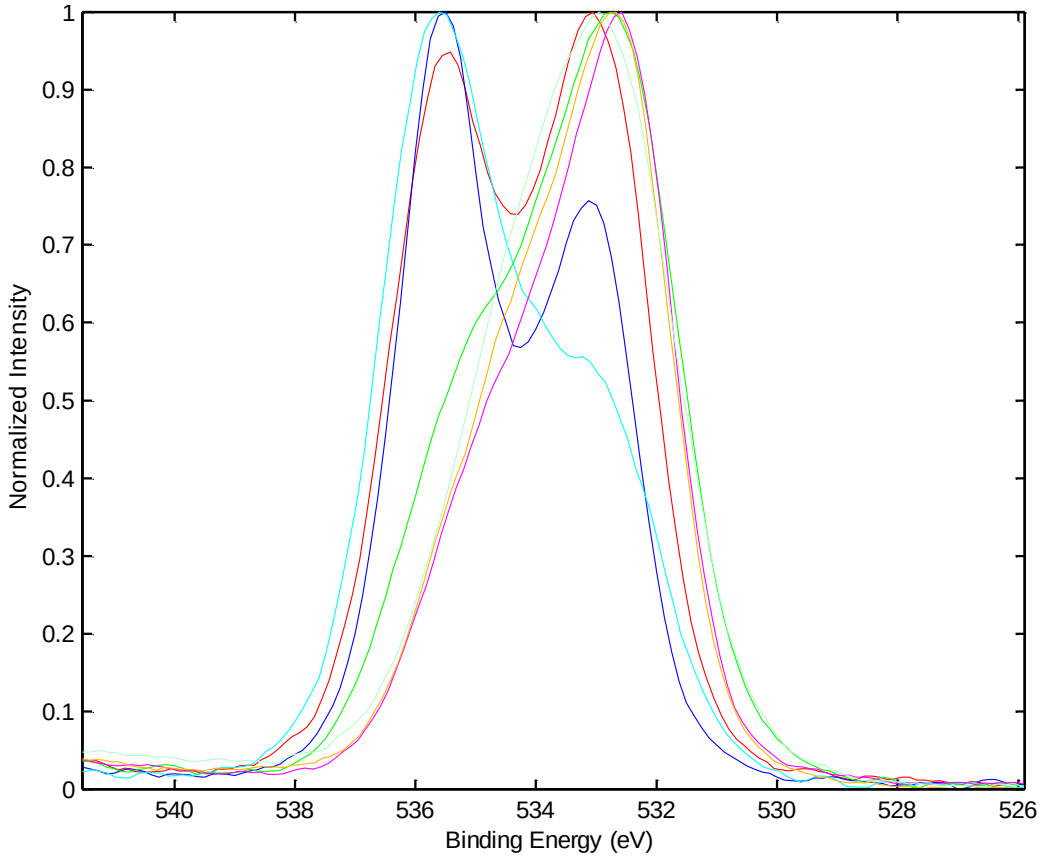

Figure 18. Overlapped O 1s spectra for Trial 1 VUV photolysis. Control (1) (red), Control (2) (blue), 5 min (light blue), 15 min (green), 30 min (pink), 60 min (yellow) and 90 min (light green).

Table 8
Results of the O 1s curve fitting for VUV photolysis of Nafion Trial 1

Species	Control (1)	Control (2)	5 min.	15 min.	30 min.	60 min.	90 min.
C-O composite + acid	51.0	44.8	33.9	66.9	65.4	63.8	63.6
CF-O*-CF_2	48.9	55.2	66.1	33.1	34.6	36.2	36.4

The intensity of the 5 min sample peak at 533.4 eV, corresponding to sulfonic acid, is significantly less intense than the peaks for the other samples. The C-O composite + acid group decreases only for the 5 min treatment time.

3.1.4 Grafting of VUV Photolysis Treated Nafion

The Trial 3 VUV photolysis samples were grafted with polyacrylic acid. The quantitative XPS analysis for Trial 3 VUV photolysis samples is shown in Table 9.

Table 9
Quantitative XPS analysis for Trial 3 VUV photolysis treated Nafion grafted with polyacrylic acid

Sample	At% C	At% N	At% O	At% F	At% S
Control	33.58	0.22	8.31	56.45	1.44
Control, PAA grafted	36.24	0.28	13.10	49.17	1.21
5 min. VUV, PAA grafted	46.57	0.42	19.40	33.22	0.40
15 min. VUV, PAA grafted	47.37	0.45	19.11	32.98	0.09
30 min. VUV, PAA grafted	46.77	0.85	17.32	34.96	0.10
60 min. VUV, PAA grafted	48.84	0.90	18.58	31.60	0.08
90 min VUV, PAA Grafted	47.65	0.68	16.16	35.37	0.13

Compared with Table 6c, there is an increase in oxygen and carbon and a decrease in fluorine, nitrogen, and sulfur at each treatment time from VUV treatment to PAA grafting. The increase in carbon could be attributed to the added carbon chain from polyacrylic acid. The increase in oxygen results from the added carboxylic acid that is present in every repeat unit in polyacrylic acid. The decrease in sulfur, nitrogen, and fluorine percentages indicates that these atoms are now hidden because of the added bulk of the polyacrylic acid chains, and XPS does not detect them as strongly. The large decrease in fluorine is most indicative of grafting because fluorine is so prominent in untreated Nafion.

The decrease in CF_2 groups and the increase in acid groups (285.4 eV) from VUV treatment to PAA grafting are shown in the results of the C 1s curve fittings (Table 10).

Table 10
Results of the C 1s curve fittings for Trial 3 VUV photolysis Nafion grafted with polyacrylic acid

Species	Control	Control, PAA grafted	5 min. VUV, PAA grafted	15 min. VUV, PAA grafted	30 min. VUV, PAA grafted	60 min. VUV, PAA grafted	90 min. VUV, PAA grafted
C-C	9.9	11.0	2.7	3.9	0.0	0.0	0.0
O-C-C* ‖ O	3.6	0.0	16.1	17.4	10.3	6.5	13.8
C*-O-C=O	4.9	13.5	24.9	23.6	34.4	39.4	23.7
O=C-O	0.3	6.4	8.3	8.9	9.6	9.3	17.6
CF	2.4	24.3	12.6	11.8	9.3	17.4	13.8
CF_2	64.6	37.9	20.7	17.4	14.2	14.2	17.9
CF_3	14.3	7.1	14.7	17.0	22.3	13.2	13.2

There is a significant increase in the C*-O-C=O group as compared to the Trial 3 VUV photolysis experiment (Table 11). This might occur if a growing polyacrylic acid chain in the solution was terminated on a carboxylic acid group on the VUV treated surface of Nafion. The increase in oxygen and decrease in fluorine is observed even for the control sample that was not treated with VUV photolysis and was PAA grafted. This suggests that pre-treatment with VUV photolysis may not be necessary for grafting. However, there is an overall general increase in oxygen groups and decrease in fluorine groups,

only with minor discrepancies, with VUV treatment time for the PAA grafted samples which indicates that grafting is enhanced with VUV photolysis treatment.

Table 11
Results of the C 1s curve fittings for Trial 3 VUV photolysis treated Nafion

Species	Control	5 min	15 min	30 min	60 min	90 min
C-C	9.2	4.2	0.6	0.0	0.0	0.0
O-C-C* ‖ O	0	1.5	2.3	2.1	5.3	4.7
C*-O-C=O	0.5	0.0	3.3	5.6	12.9	17.2
O=C-O	0.1	1.0	6.9	9.8	22.3	24.7
CF	2.2	3.2	2.2	3.5	1.2	0.3
CF_2	67.4	73.0	76.6	71.3	51.0	47.1
CF_3	20.6	17.1	8.3	7.8	7.2	6.1

The overlapped C 1s spectra (Fig. 19) shows a sharp increase for PAA grafted VUV treated samples at 285.4 eV which corresponds to carboxylic acid groups. Compared to the overlapped C 1s spectra for the Trial 3 VUV photolysis experiment (Fig. 20), there is a more intense increase in this peak for the PAA grafted samples than for the VUV only treated samples.

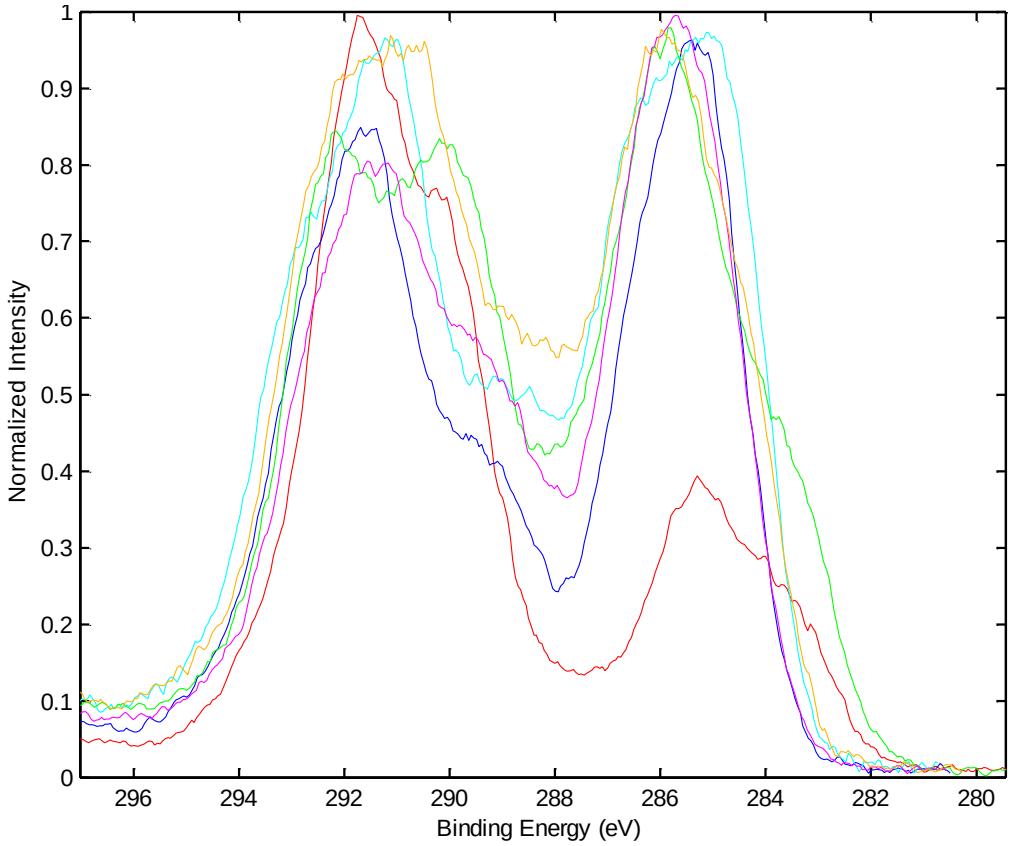

Figure 19. Overlapped C 1s spectra for Trial 3 VUV photolysis grafted Nafion with polyacrylic acid. Control, PAA grafted (red); 5 min VUV treatment, PAA grafted (blue); 15 min VUV, PAA grafted (light blue); 30 min VUV, PAA grafted (green); 60 min VUV, PAA grafted (pink); and 90 min VUV, PAA grafted (yellow).

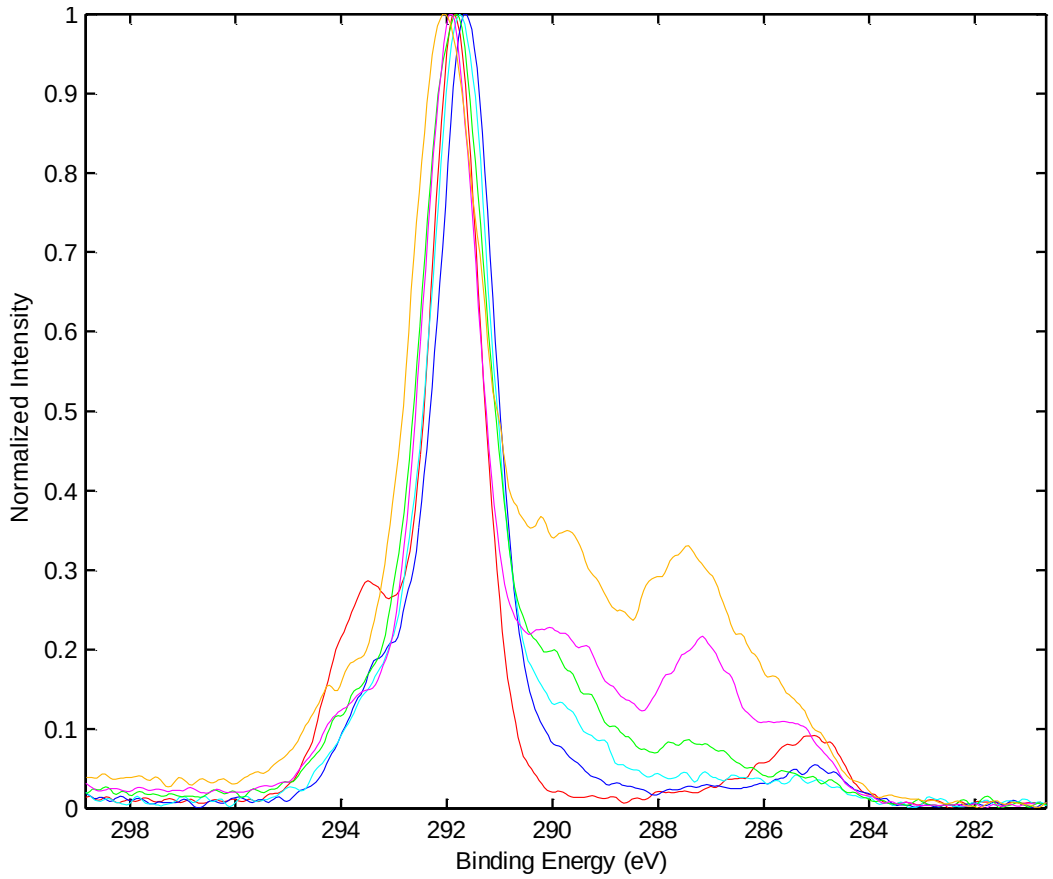

Figure 20. Overlapped C 1s spectra for Trial 3 VUV photolysis Nafion. Control (red), 5 min (blue), 15 min (light blue), 30 min (green), 60 min (pink) and 90 min (yellow).

The increase in intensity of the 285.4 eV peak in Fig. 19 for the 5-90 minute samples as compared to the control grafted sample also gives evidence that VUV photolysis pre-treatment enhances PAA grafting.

3.1.5 Grafting of VUV Photo-Oxidized Single-Walled Carbon Nanotube Paper

VUV photo-oxidized SWNT paper was grafted with polyacrylic acid. The quantitative XPS analysis for VUV photo-oxidized SWNTs are given in Table 12.

Table 12
Quantitative XPS analysis for VUV photo-oxidized single-walled carbon nanotube paper

Sample	At% Carbon	At% Oxygen
Control	96.45	3.55
15 min.	93.75	6.25
30 min.	90.91	9.09
60 min.	89.03	10.97
120 min.	85.80	14.20

With treatment time, there is an increase in oxygen concentration and a decrease in carbon concentration. Table 13 gives characteristic binding energies for each functional group present on the control SWNT sample. The results of the C 1s curve fittings for the control and VUV photo-oxidized samples are shown in Table 14.

Table 13
C 1s characteristic binding energies for single-walled carbon nanotube paper [67]

Binding Energy	Assignment
284.7	C-C sp^2
285.2	C-C sp^3
285.9	ether, glycol
286.6	Energy Loss, alcohol
287.1	Epoxide ring C
287.9	C=O, O-C-O, Energy loss
288.6	O-C=O
289.2	COOH
291.4	Energy Loss

Table 14
Results of the C 1s curve fittings for VUV photo-oxidized single-walled carbon nanotube paper samples

Binding Energy	Control 0 min	15 min.	30 min.	60 min.	120 min.
284.7	42.2	40.2	39.7	38.8	38.5
285.2	26.4	27.6	25.0	25.0	24.5
285.9	12.0	13.2	13.3	12.5	12.7
286.6	2.9	3.5	4.2	5.1	4.5
287.1	3.4	0.8	0.7	1.4	1.3
287.9	1.2	3.7	4.5	4.8	6.7
288.6	2.4	3.2	4.4	4.4	4.7
289.2	4.5	3.8	4.0	4.1	4.0
291.4	4.9	4.2	4.1	3.9	3.2

The functional groups with the greatest increase from VUV photo-oxidation were ether, glycol, alcohol, C=O, O-C-O, and O-C=O. A more detailed discussion of the VUV photo-oxidation of SWNTs is given in reference 64.

A control grafting experiment where VUV photo-oxidized SWNT samples were exposed to the solution of $FeSO_4 \cdot 7H_2O$ and L-ascorbic acid in the absence of acrylic acid was performed. The quantitative XPS analysis is shown in Table 15.

Table 15
Quantitative XPS analysis for control grafting experiment of single-walled carbon nanotube paper in the absence of acrylic acid

Sample	At% Carbon	At% Oxygen	At% Iron
Control	97.41	2.59	0.00
0 min VUV, exposed to solution	85.77	13.84	0.39
15 min VUV, exposed to solution	85.67	14.19	0.14
30 min VUV, exposed to solution	83.95	15.54	0.51
60 min VUV, exposed to solution	83.61	15.97	0.42
120 min VUV, exposed solution	82.92	16.56	0.52

There is a significant increase in the oxygen concentration from VUV photo-oxidation to control grafting with VUV treatment time. The samples exposed to the solution also contain a small amount of iron. The results of the curve fittings of the C 1s spectra for the control and the samples exposed to the aqueous solution are given in Table 16.

Table 16
Results of the C 1s curve fittings for the single-walled carbon nanotube paper samples exposed to the solution in absence of acrylic acid

Binding Energy	Control 0 min VUV, not exposed to solution	Control 0 min VUV, exposed to solution	15 min VUV, exposed to solution	30 min VUV, exposed to solution	60 min VUV, exposed to solution	120 min VUV, exposed to solution
284.7	42.8	45.1	35.9	38.4	36.1	31.8
285.2	30.5	23.6	27.7	26.3	26.9	29.5
285.9	10.2	11.7	12.7	10.2	9.8	10.2
286.6	2.8	2.3	7.9	9.4	10.4	11.6
287.1	0.7	0.0	0.0	0.0	0.0	0.0
287.9	1.3	2.2	2.7	2.2	2.4	2.5
288.6	0.5	3.8	1.8	3.7	4.3	4.5
289.2	3.8	6.6	7.4	6.2	6.1	6.1
291.4	7.5	4.6	4.0	3.6	4.0	3.8

Changes that occur as a result of this experiment include a decrease in ether or glycol groups at 285.9 eV, an increase in energy loss or alcohols at 286.6 eV, the elimination of epoxides at 287.1 eV, a decrease in C=O, O-C-O, or energy loss at 287.9 eV, and an increase in COOH at 289.2 eV. There was most likely a decrease in the energy loss as opposed to an increase because a decrease was seen in VUV photo-oxidation as a result of loss of aromaticity from exposure to VUV radiation [70]. There is a decrease in sp^2 hybridized C-C bonding which indicates that double bonds are broken to form new

functional groups. The VUV photo-oxidized SWNTs reacted with the initiators under heat to form the new groups. This type of experiment can also be considered a surface modification technique based on these results. There is a small increase in the sp^3 hybridized C-C bonding for these samples. A larger percentage of sp^3 hybridized C-C bonding is present in the polyacrylic acid grafted samples (Tables 18a and 18b) indicating the added polymer chain.

The quantitative XPS analysis for two trials of polyacrylic acid grafted samples is shown in Tables 17a-b.

Table 17a
Quantitative XPS analysis for polyacrylic acid grafted VUV photo-oxidized single-walled carbon nanotube paper, Trial 1

Sample	At% Carbon	At% Nitrogen	At% Oxygen
control	95.61	0.00	4.39
Control, PAA grafted	89.35	0.00	10.65
15 min VUV, PAA grafted	81.16	1.11	17.72
30 min VUV, PAA grafted *	88.19	0.00	11.81
60 min VUV, PAA grafted	81.29	1.00	17.71
120 min VUV, PAA grafted	81.53	0.93	17.54

*There was a problem with the 30 min VUV, PAA grafted sample and its data is not used

Table 17b
Quantitative XPS analysis for polyacrylic acid grafted VUV photo-oxidized single-walled carbon nanotube paper, Trial 2

Sample	At% Carbon	At% Nitrogen	At% Oxygen	At% Iron
control	95.61	0.00	4.39	0.00
Control, PAA grafted	89.21	0.31	10.48	0.00
15 min VUV, PAA grafted	88.27	0.39	11.34	0.00
30 min VUV, PAA grafted	81.88	0.75	17.37	0.00
60 min VUV, PAA grafted	80.42	0.48	18.63	0.47
120 min VUV, PAA grafted *	85.50	0.60	13.90	0.00

*There was a problem with the 120 min VUV, PAA grafted sample and its data is not used

The concentration of oxygen is higher for many of the polyacrylic acid grafted samples (Tables 17a and 17b) than for the samples exposed to the initiator solution (Table 15) with the exception of the Control, PAA grafted samples for both trials and the 15 min VUV, PAA grafted sample for Trial 2. There is a small amount of nitrogen present on the grafted samples. This could be a result of a minor contamination in the argon gas that is used during the grafting experiment. The 60 min VUV photo-oxidized polyacrylic acid grafted sample from Trial 2 contained the highest percentage of oxygen. The sample also contains a small percentage of iron from the iron sulfate heptahydrate initiator.

The overlapped C 1s spectra are shown in Fig. 21 and the results of the C 1s curve fittings are given in Tables 18a-b.

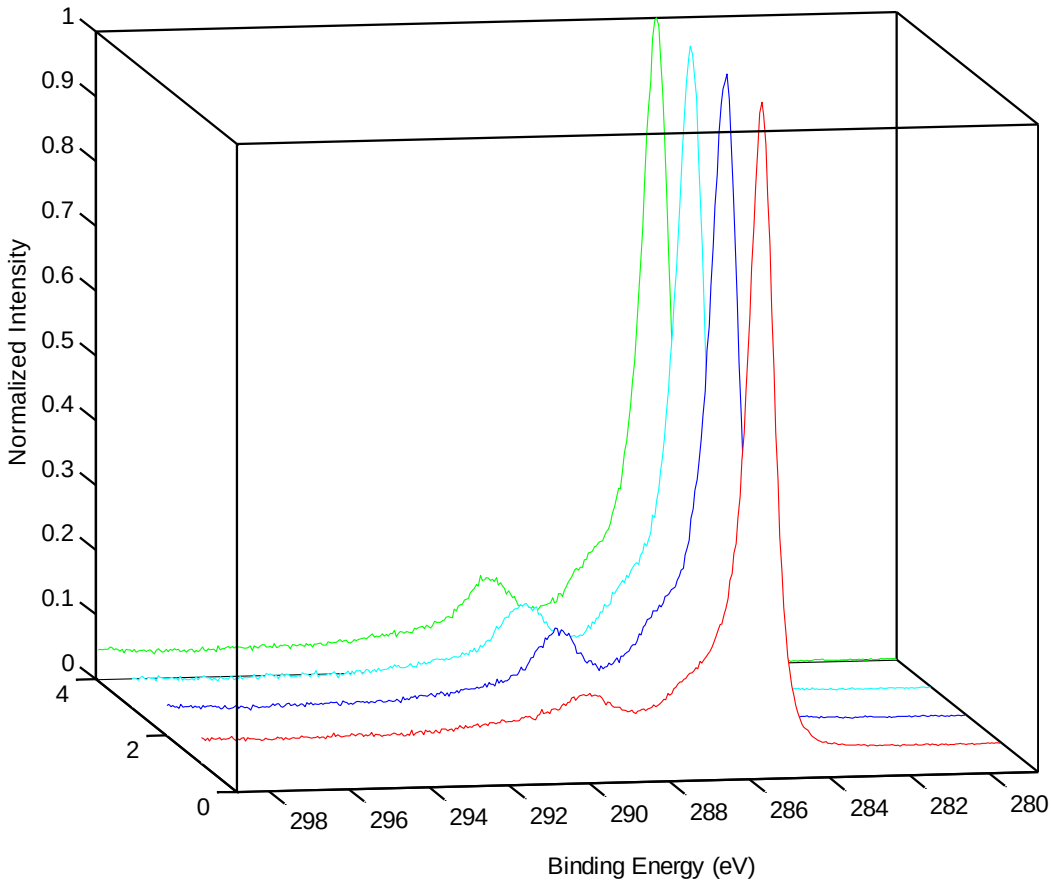

Figure 21. Overlapped C 1s spectra for polyacrylic acid grafted VUV photo-oxidized single-walled carbon nanotube paper, Trial 1. 0 min VUV, PAA grafted (red); 15 min VUV, PAA grafted (blue); 60 min VUV, PAA grafted (light blue); 120 min VUV, PAA grafted (green).

Table 18a
Results of the C 1s curve fittings for the polyacrylic acid grafted VUV photo-oxidized grafted single-walled carbon nanotube paper, Trial 1

Binding Energy	Control 0 min VUV, not PAA grafted	Control 0 min VUV, PAA grafted	15 min VUV, PAA grafted	60 min VUV, PAA grafted	120 min VUV, PAA grafted
284.7	45.7	36.3	25.3	24.9	28.3
285.2	30.1	37.5	40.9	40.8	39.8
285.9	10.7	12.7	17.0	17.0	16.9
286.6	3.4	0.0	0.0	0.0	0.0
287.1	2.7	0.0	0.0	0.0	0.0
287.9	3.6	0.0	0.0	0.0	0.0
288.6	2.7	5.3	9.5	10.1	10.3
289.2	0.0	5.0	5.2	4.6	3.3
291.4	1.1	3.3	2.2	2.6	1.5

Table 18b
Results of the C 1s curve fittings for the polyacrylic acid grafted VUV photo-oxidized single-walled carbon nanotube paper, Trial 2

Binding Energy	Control 0 min VUV, not PAA grafted	Control 0 min VUV, PAA grafted	15 min VUV, PAA grafted	30 min VUV, PAA grafted	60 min VUV, PAA grafted
284.7	45.7	42.7	42.5	33.0	34.7
285.2	30.1	33.4	34.5	37.9	41.0
285.9	10.7	9.4	8.9	10.9	7.9
286.6	3.4	0.0	0.0	0.0	0.0
287.1	2.7	0.0	0.0	0.0	0.0
287.9	3.6	2.0	1.8	2.6	1.7
288.6	2.7	3.7	3.3	7.2	5.6
289.2	0.0	5.1	5.4	4.9	6.5
291.4	1.1	3.8	3.7	3.4	2.5

There is a significant increase in the sp^3 hybridized C-C bonding (285.2 eV) in both trials of the grafted samples from the samples exposed to the initiator solution. This shows evidence of an added polymer chain containing large amounts sp^3 hybridized C-C bonding which is present in polyacrylic acid. There is a decrease in the sp^2 hybridized C-C bonding (284.7 eV) in Trial 1 indicating that more double bonds are broken and can react with the acrylic acid monomer. There is a considerable increase in O-C=O at 288.6 eV, a group prominent in polyacrylic acid, in the Trial 1 grafted samples compared to the control grafted samples. There is an increase at 288.6 eV in the Trial 2 grafted samples

as well, however, to a lesser degree. The XPS data indicate that polyacrylic acid grafting occurred on both Trial 1 and Trial 2 samples by the increase in sp^3 hybridized C-C bonding and the increase in the O-C=O group. The larger increase in both of these groups in the Trial 1 (Table 18a) samples gives evidence that polyacrylic acid is present in a greater extent in Trial 1 than in Trial 2. The overlapped C 1s spectra (Fig. 21) and the overlapped O 1s spectra (Fig. 22) for Trial 1 show further that there is an increase in O-C=O groups. The O 1s characteristic binding energies for SWNTs are given in Table 19.

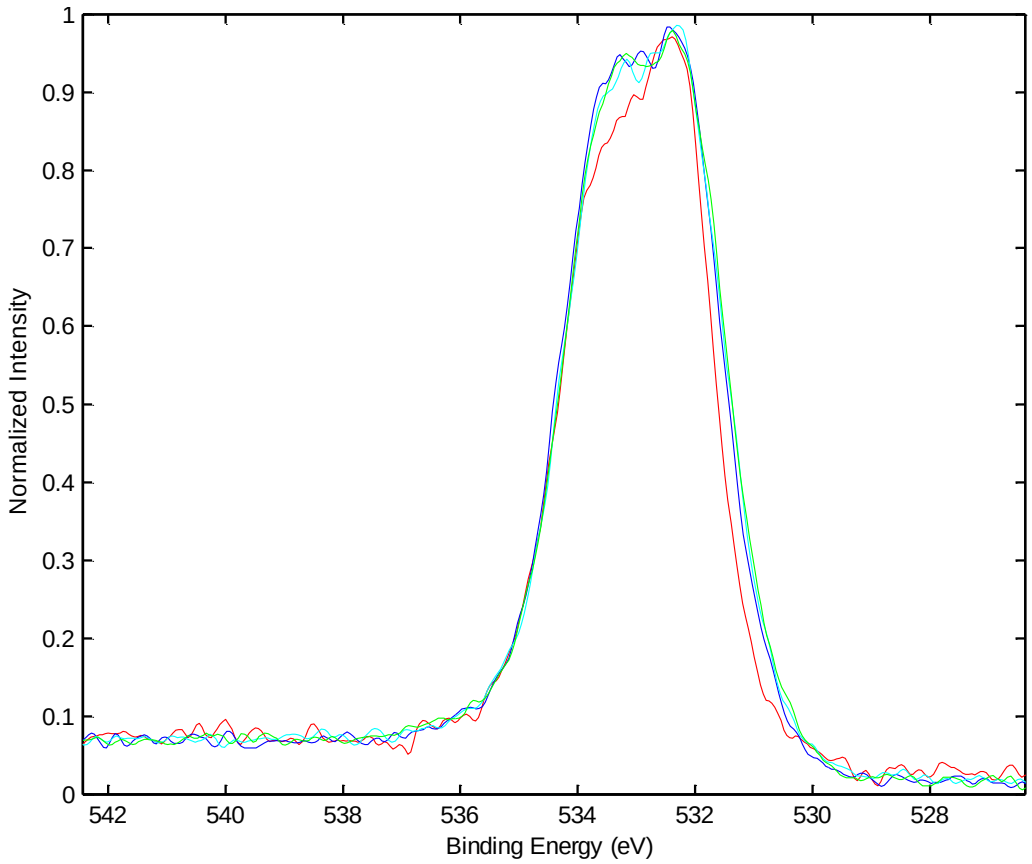

Figure 22. Overlapped O 1s spectra for polyacrylic acid grafted VUV photo-oxidized single-walled carbon nanotube paper, Trial 1. 0 min VUV, PAA grafted (red); 15 min

VUV, PAA grafted (blue); 60 min VUV; PAA grafted (light blue); 120 min VUV, PAA grafted (green).

Table 19
O 1s characteristic binding energies for single-walled carbon nanotubes [67]

C-O Group	O 1s Binding Energies
C-OH	532.7 eV
C=O	532.4 eV
O-C=O	532.2 eV, 533.6 eV
COOH	532.2 eV, 533.5 eV

The broad increase from 537.5 eV to 533.6 eV from the 0 min VUV, PAA grafted sample to the VUV treated grafted samples indicates the increase in C-OH, C=O, O-C=O, and COOH groups from the perspective of the O 1s electron.

3.2 Scanning Electron Microscopy

3.2.1 SEM Images of VUV Photolysis Treated Nafion

Very little change is seen between the control and the VUV photolysis treated samples. The 1000X magnified SEM images are shown in Fig. 23.

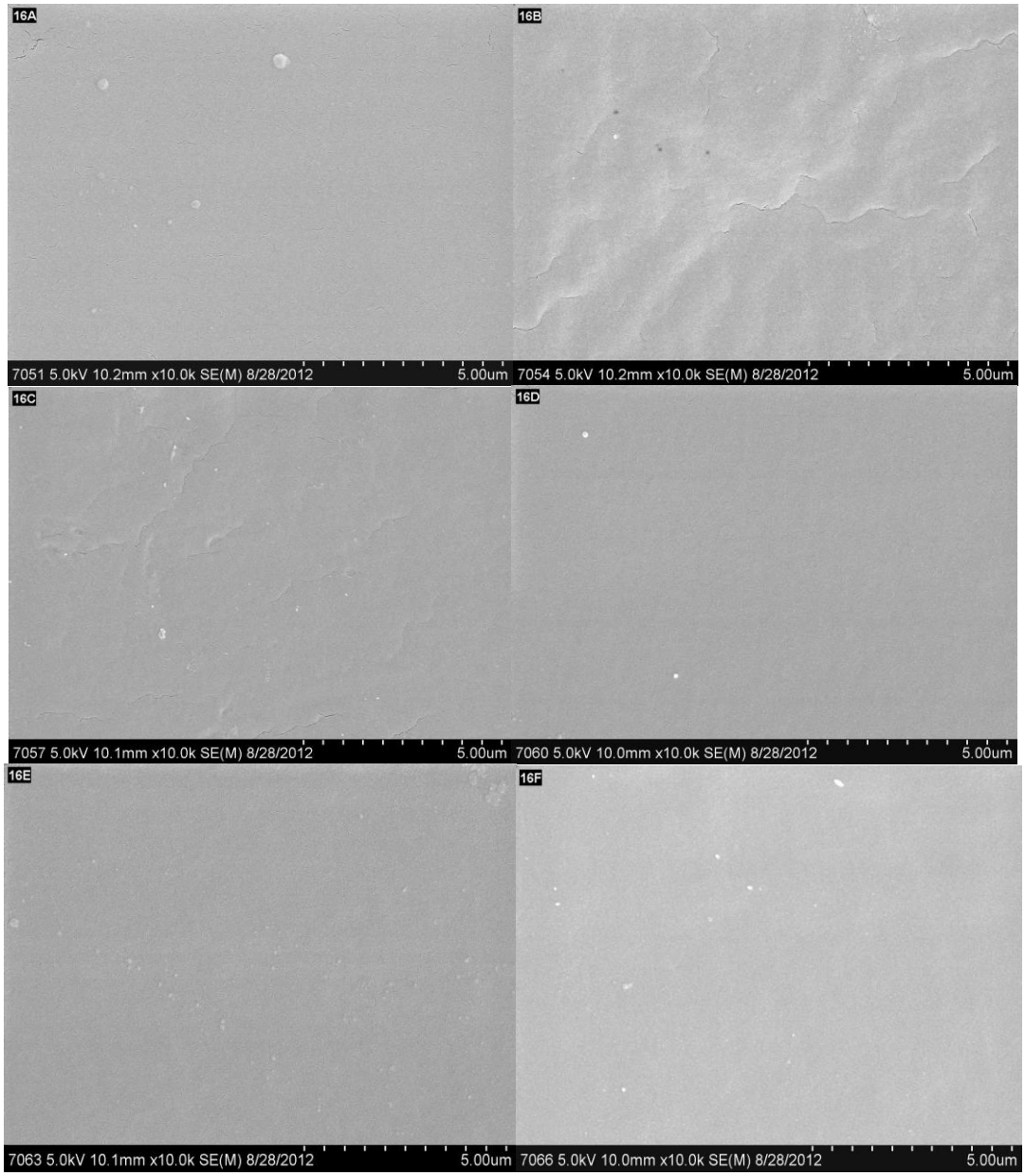

Figure 23. 1000X magnified SEM images of untreated control (top left), 5 min (top right), 15 min (middle left), 30 min (middle right), 60 min (bottom left), and 90 min (bottom right) VUV photolysis treated Nafion samples.

The main difference between these samples is that the 5 min sample has a more rippled appearance than the others. The 15 min sample also appears slightly rippled. The 60 and

90 min samples contain the most bumps as shown in the 5000X magnified SEM images for these samples (Fig. 24).

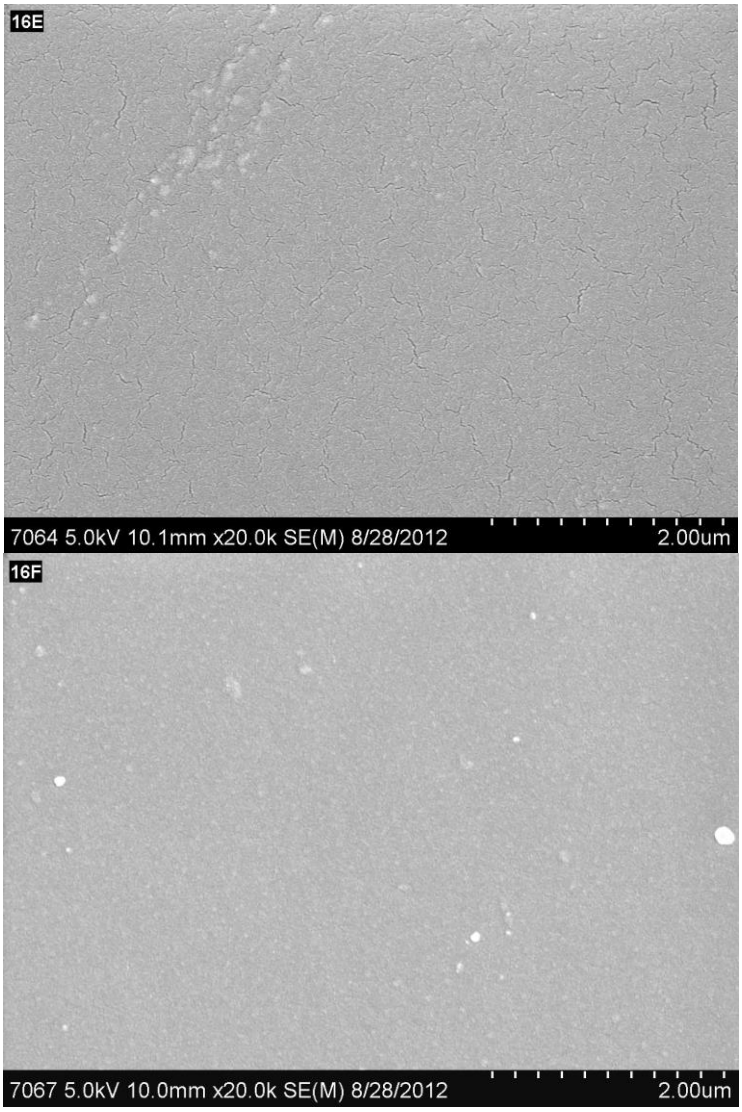

Figure 24. 5000X magnified SEM images of 60 min (top) and 90 min (bottom) VUV photolysis treated Nafion samples.

3.2.2 SEM Images of Direct Ar/O_2 MW Discharge Treated Nafion

The 1000X magnified SEM images of a control sample and direct Ar/O_2 MW discharge treated Nafion samples are displayed in Fig. 25.

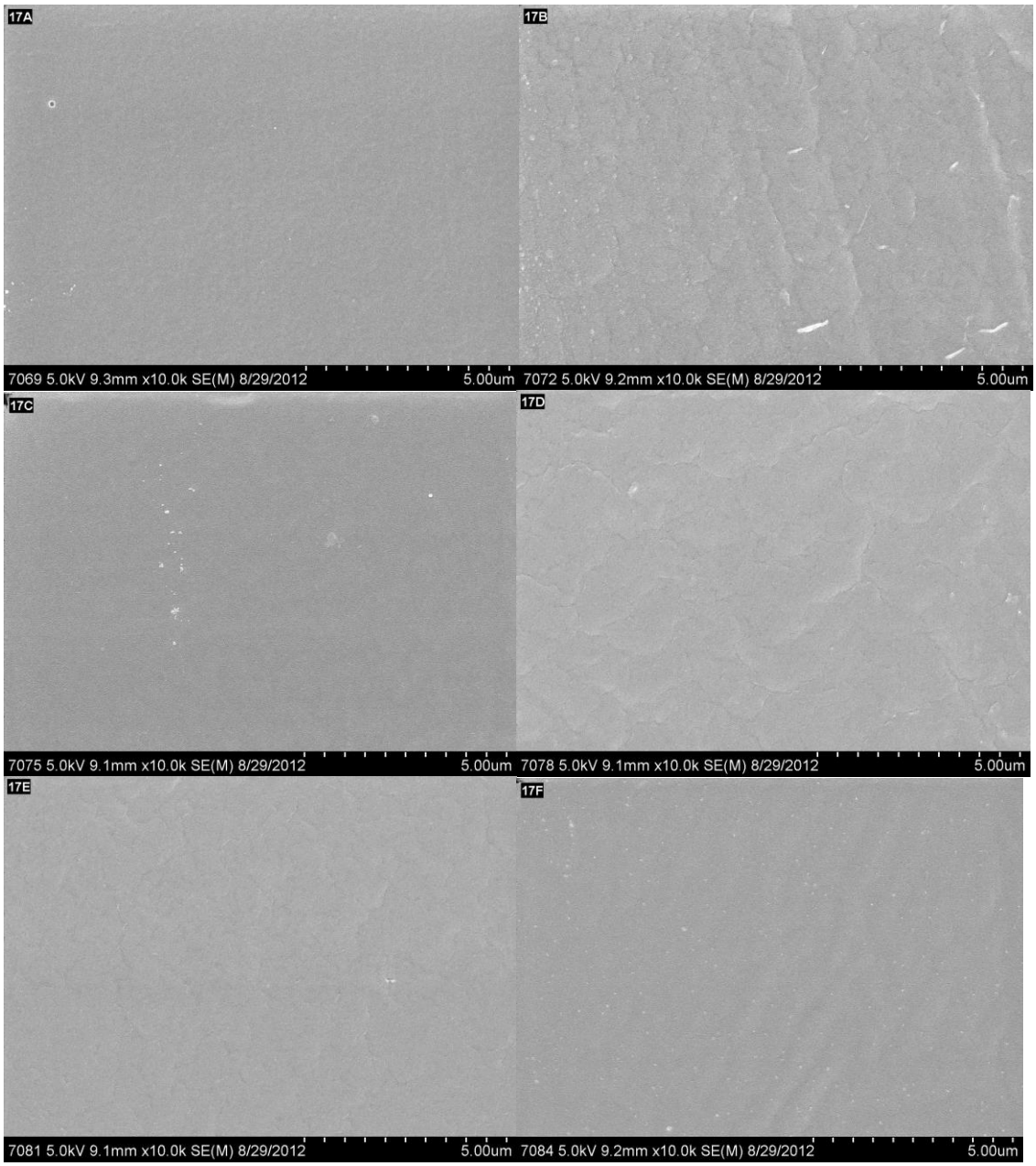

Figure 25. 1000X magnified SEM images of untreated control (top left), 5 min (top right), 15 min (middle left), 30 min (middle right), 60 min (bottom left), and 90 min (bottom right) direct Ar/O_2 MW discharge treated Nafion samples.

The 5 min, 30 min, and 90 min samples have a rippled appearance much like the 5 and 15 min VUV photolysis treated samples. The 5 min direct Ar/O_2 MW discharge treated sample contains many lines and rod-shaped bumps. The 90 min sample contains many bumps and ripples.

3.3 Contact Angle Analysis

3.3.1 Untreated Nafion Control

The advancing and receding water contact angles were performed on an untreated Nafion sample to observe the hydrophobic and hydrophilic properties of Nafion. Advancing and receding contact angles along with the size of the water droplets are summarized in Tables 20 and 21, respectively.

Table 20
Advancing water contact angle on untreated Nafion

Advancing Contact Angle (CA)				
	Drop 1	Drop 2	Drop 3	Drop 4
CA (degrees)	90.5	110.9	110.8	115.3
Height of droplet (mm)	1.348	1.881	2.16	2.291
Width of droplet (mm)	2.76	2.83	3.284	3.395

With each increase in size of the drop, the contact angle increases. The added volume of the water droplet causes the fluorocarbon to repel the water more, showing the hydrophobic nature of Nafion.

Table 21
Receding water contact angle on untreated Nafion

Receding Contact Angle (CA)				
	Reduction 1	Reduction 2	Reduction 3	Reduction 4
CA (degrees)	113.4	111.7	78.5	40.3
Height of droplet (mm)	2.243	2.195	1.33	0.521
Width of droplet (mm)	3.484	3.516	3.43	3.147

Reducing the size of the initial drop decreases the contact angle. The receding contact angle demonstrates the hydrophilic properties of Nafion. As water is being taken away, the polar sulfonic acid groups in Nafion favor contact with the water and the angle decreases.

Nafion is both hydrophobic and hydrophilic. When in contact with water, the polymer conforms to bring the hydrophilic sulfonic acid groups toward the droplet of water.

3.3.2 Direct Ar/O_2 MW Discharge Treated Nafion

Table 22 and Fig. 26 show the static water contact angle of Nafion treated with direct Ar/O_2 MW discharge.

Table 22
Static contact angle of direct Ar/O_2 MW discharge treated Nafion

Treatment time	Contact Angle (degrees)
Control	90.5
5 min	85.5
15 min	86.3
30 min	77.2
60 min	66.1
90 min	70.2

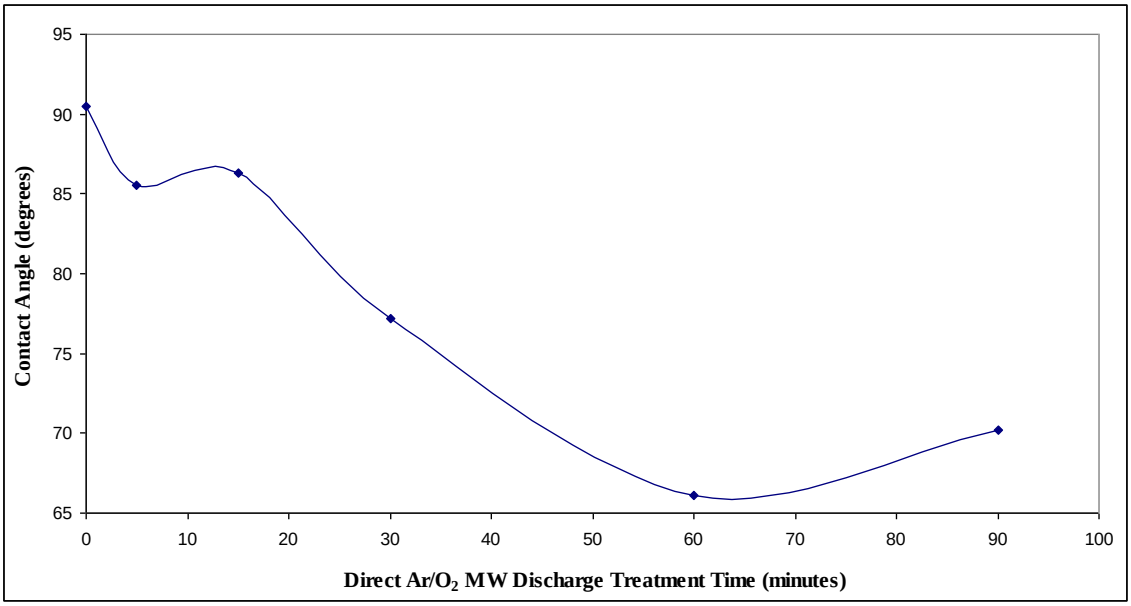

Figure 26. Contact angle of Nafion as a function of direct Ar/O_2 MW discharge treatment time.

The contact angle decreases with treatment time with a minor increase from the 5 min to the 15 min sample and for the 90 min sample. The estimated error for these samples is 0.4 degrees. As seen in Table 5 in section 3.1.2, there is a decrease in the oxygen and

sulfur concentration. However, Table 6 shows an increase in O=C-O groups and a decrease in CF_3 groups that may be the cause of the increase in hydrophilicity.

3.3.3 VUV Photolysis Treated Nafion

The static water contact angle of Nafion treated with VUV photolysis is presented in Table 23 and Fig. 27.

Table 23
Static contact angle of VUV Photolysis Treated Nafion

Treatment time	Contact Angle (degrees)
Control	90.5
5 min	84.3
15 min	78.1
30 min	75.7
60 min	81.8
90 min	82.7

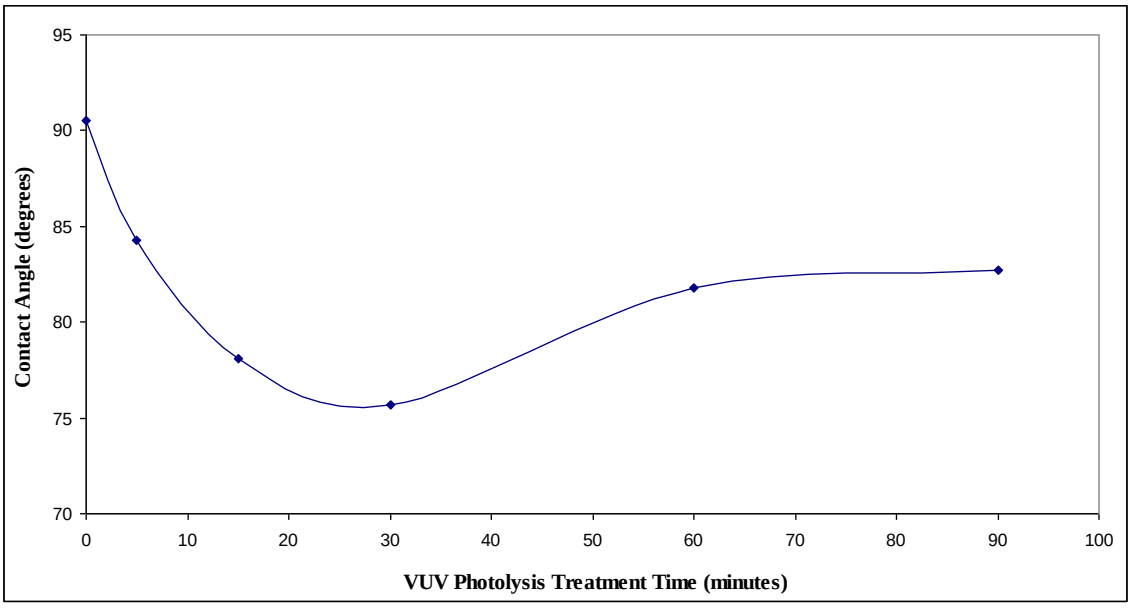

Figure 27. Contact angle of Nafion as a function of VUV photolysis treatment time.

The contact angle of the untreated Nafion control sample is 90.5 degrees, consistent with the value in Table 20. The contact angle decreases with treatment time with the exception of the 60 and 90 min samples, which increase slightly from the 30 min sample, however, they are still lower than the value for the control. The estimated error for these samples is 1 degree with the exception of the 5 minute sample in which values ranged between 10 degrees and the average value was taken as 84.3 degrees.

3.3.4 Poly(acrylic acid) Grafted Nafion and Control Grafted Nafion

The static water contact angle was measured for VUV photolysis treated Nafion exposed to a solution of $FeSO_4 \bullet 7H_2O$ and L-Ascorbic acid without the presence of acrylic acid (control grafted Nafion) (Table 24, Fig. 28) and polyacrylic acid grafted VUV photolysis treated Nafion (Table 25, Fig. 29).

Table 24
Static contact angle of control grafted Nafion

VUV Photolysis Treatment Time	Contact Angle (degrees)
Control	88.6
5 min	66.4
15 min	87.1
30 min	73.8
60 min	79.6
90 min	89.4

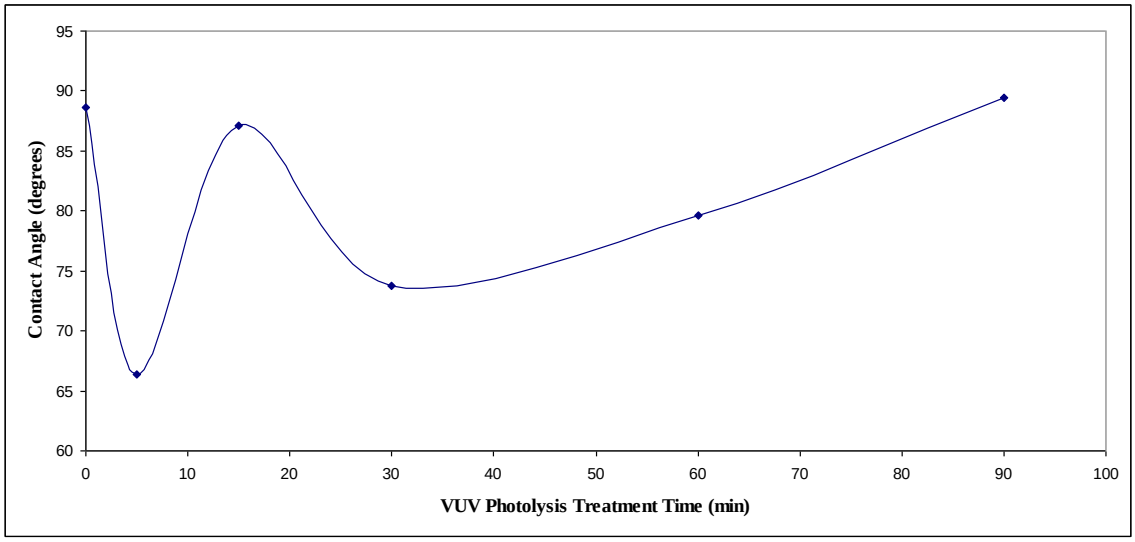

Figure 28. Contact angle of control grafted Nafion as a function of VUV photolysis treatment time.

Table 25
Contact angle of polyacrylic acid grafted VUV photolysis treated Nafion

VUV Photolysis Treatment Time	Contact Angle (degrees)
Control	77.3
5 min	55
15 min	62.9
30 min	68.5
60 min	45.9
90 min	59.8

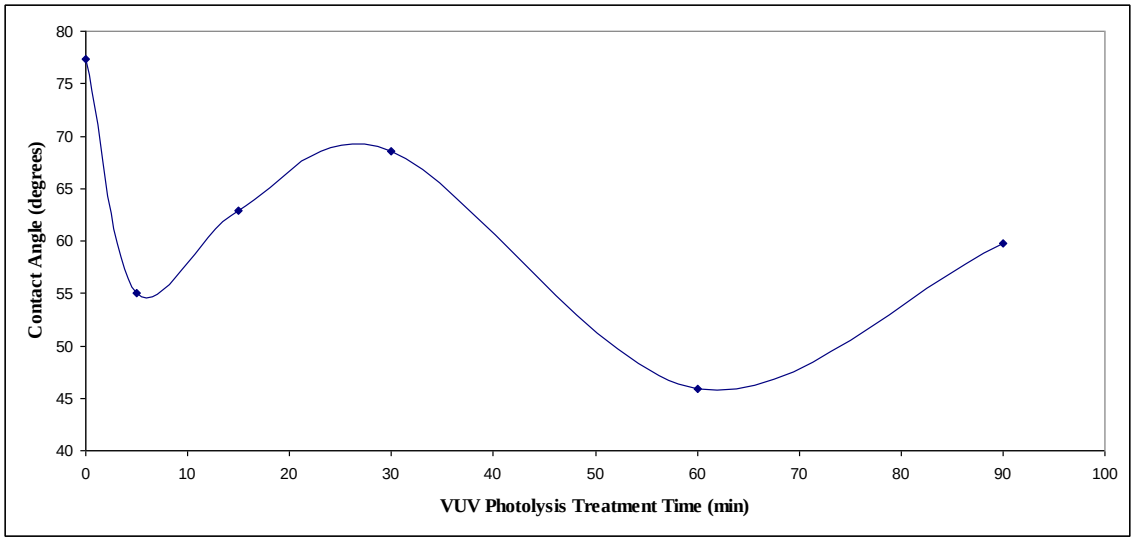

Figure 29. Contact angle of polyacrylic acid grafted Nafion as a function of VUV photolysis treatment time.

The contact angles are smaller for the polyacrylic acid grafted Nafion samples than the control grafted Nafion samples at each treatment time. The polyacrylic acid chains provide an increase in hydrophilicity. There is not a significant difference between the contact angles of VUV photolysis treated Nafion (Table 23) and control grafted Nafion (Table 24).

3.4 Fourier Transform Infrared Spectroscopy

3.4.1 Untreated Nafion Control

An FTIR spectrum of a cleaned, untreated Nafion control sample is presented in Fig. 30 and the identification of peaks is listed in Table 26 [20].

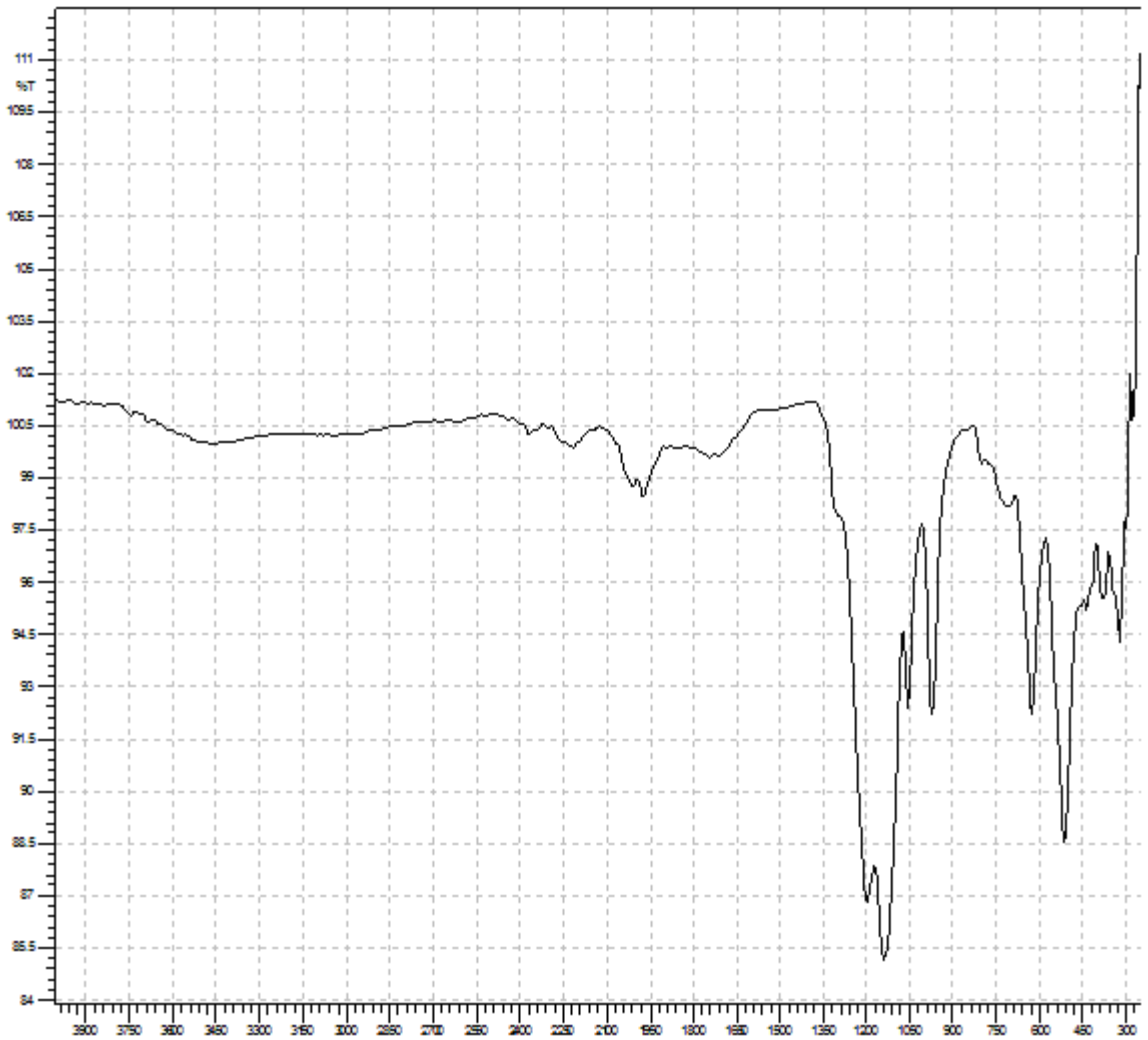

Figure 30. FTIR spectrum of an untreated Nafion control sample.

Table 26
Identification of Nafion peaks in the FTIR spectrum [20]

Wavenumber (cm^{-1})	Identification
972.12	-COC- symmetric stretch
1056.99	$-SO_3-$ symmetric stretch
1141.86, 1195.87	$-CF_2-$ symmetric stretch

The peaks listed in Table 26 are the expected peaks in the untreated Nafion structure.

3.4.2 Control Grafted Nafion Samples

The 0 min sample that was exposed to the initiator solution (Fig. 31) looks similar to the untreated Nafion in Fig. 30.

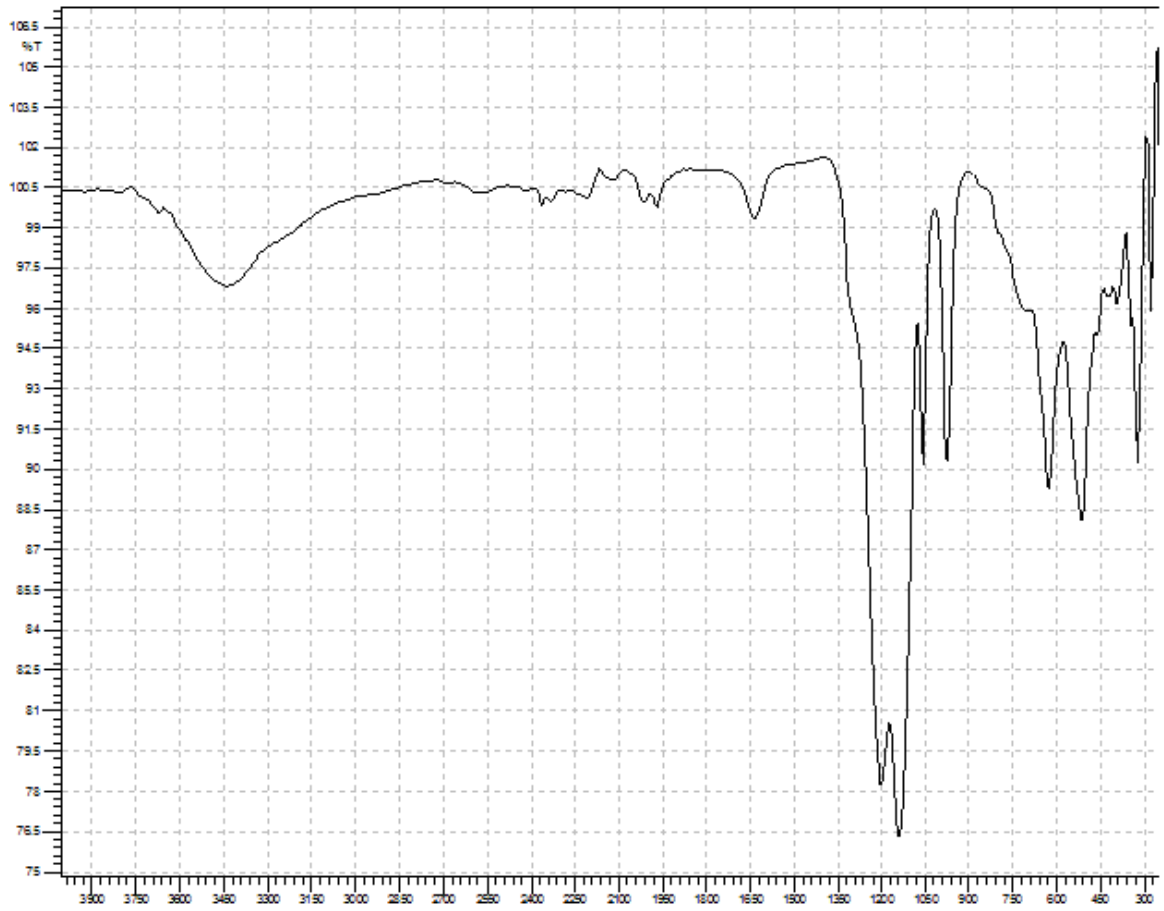

Figure 31. FTIR spectrum for a 0 min VUV photolysis, control grafted Nafion sample.

The peaks around 3450 cm^{-1} and 1640 cm^{-1} could be from water still absorbed within Nafion from the control grafting procedure. The 3450 cm^{-1} corresponding to O-H stretching [65] and the 1640 cm^{-1} corresponding to the O-H bending [71].

Nearly the same spectrum as in Fig. 31 is observed in the 60 min (Fig. 32) and 90 min (Fig. 33) control grafted samples.

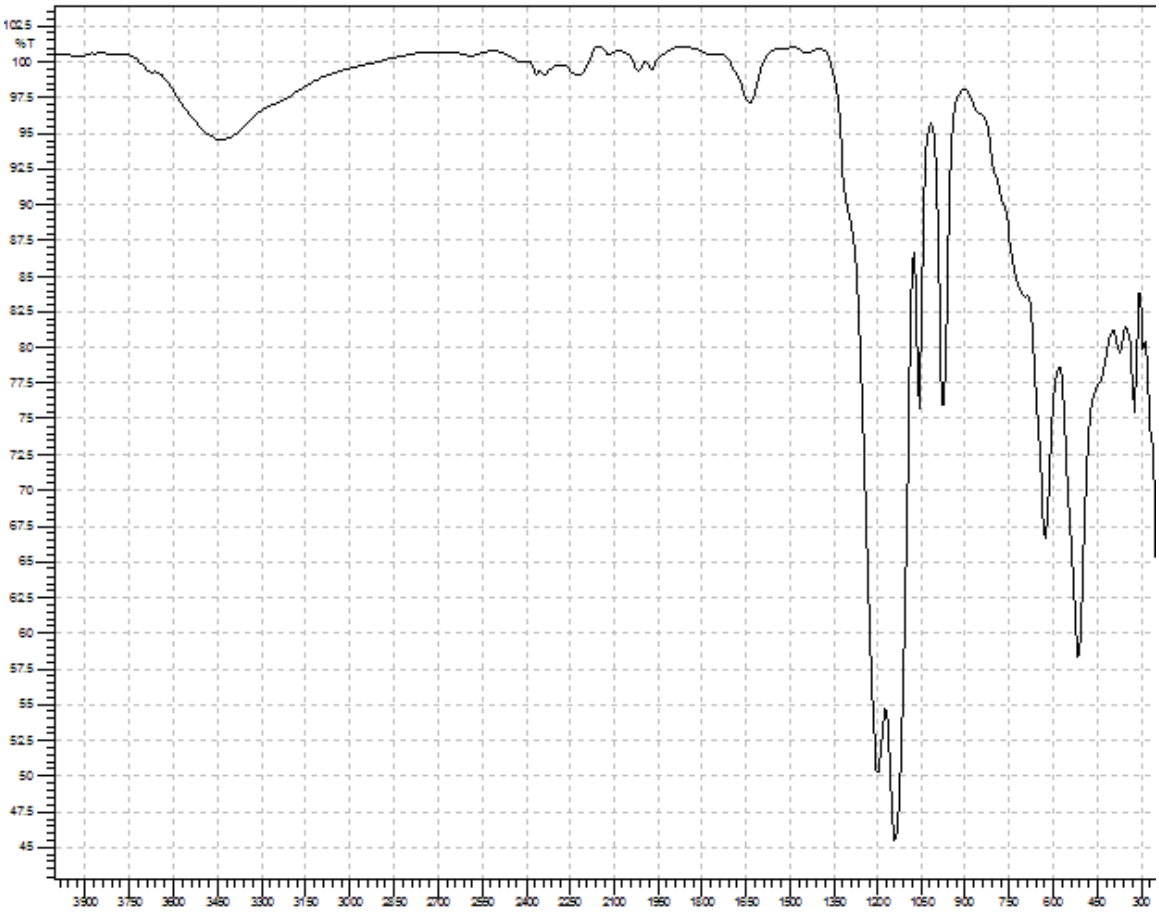

Figure 32. FTIR spectrum for the 60 min VUV photolysis treated control grafted Nafion sample.

Figure 33. FTIR spectrum for the 90 min VUV photolysis control grafted Nafion sample.

3.4.3 Poly(Acrylic Acid) Grafted Nafion Samples

Each of the polyacrylic acid grafted Nafion samples [0 (Fig. 34), 5 (Fig. 35), 15 (Fig. 36), 30 (Fig. 37), 60 (Fig. 38), and 90 (Fig. 39) min VUV photolysis treated] contain a very small peak around 3000 cm^{-1} and a peak in the fingerprint region at 871 cm^{-1} that are not present in the control grafted Nafion samples. The peak at 3000 cm^{-1} indicates C-H stretching [65] and the 871 represents C-H out-of-plane bending [72]. The C-H bond in not present in untreated Nafion and these peaks indicate the addition of polyacrylic acid which contains many C-H bonds.

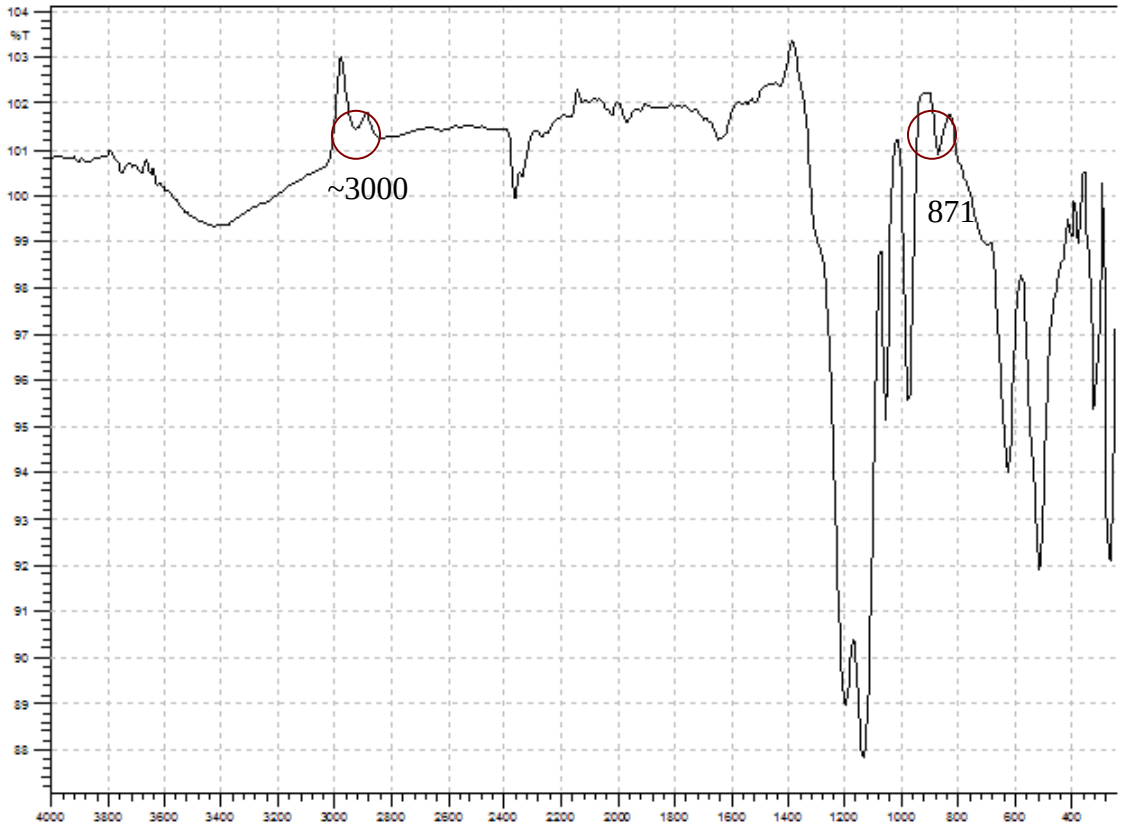

Figure 34. FTIR spectrum for the 0 min VUV photolysis treated polyacrylic acid grafted Nafion sample.

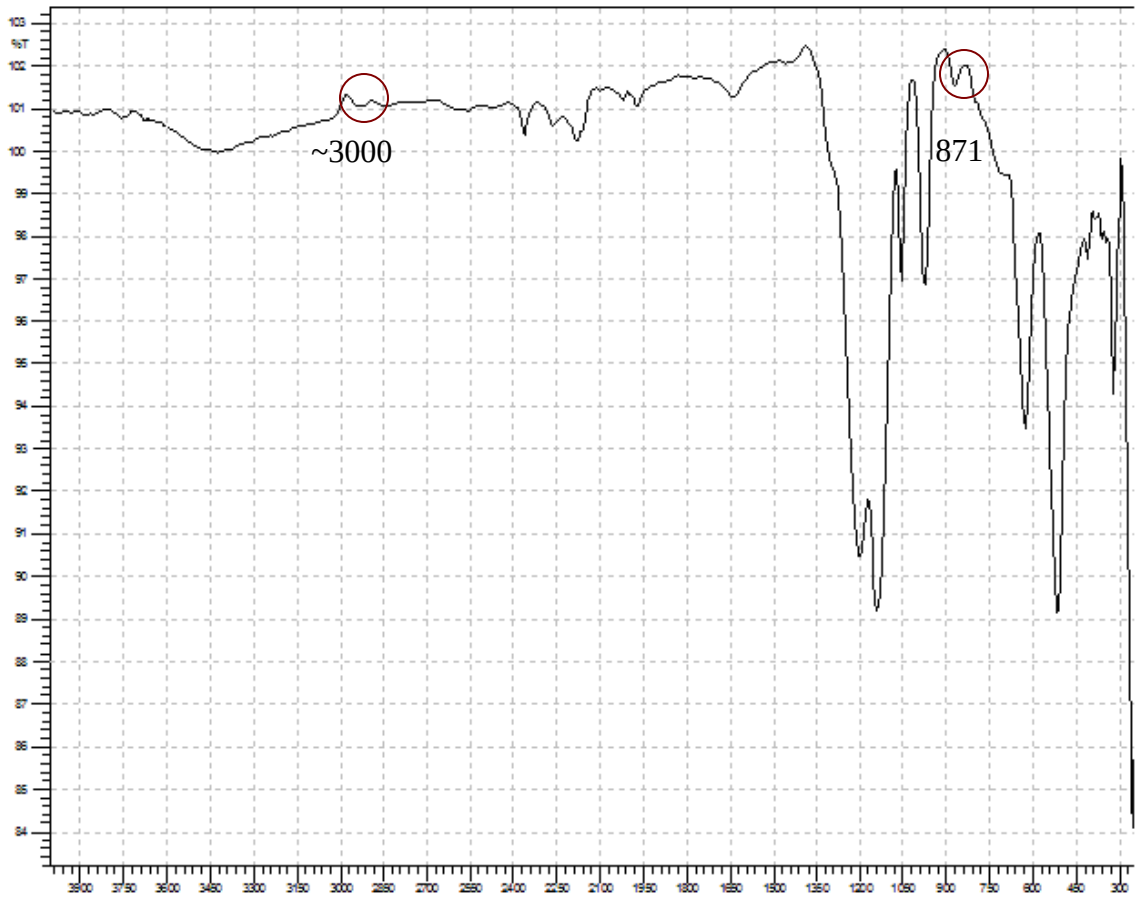

Figure 35. FTIR spectrum for the 5 min VUV photolysis treated polyacrylic acid grafted Nafion sample.

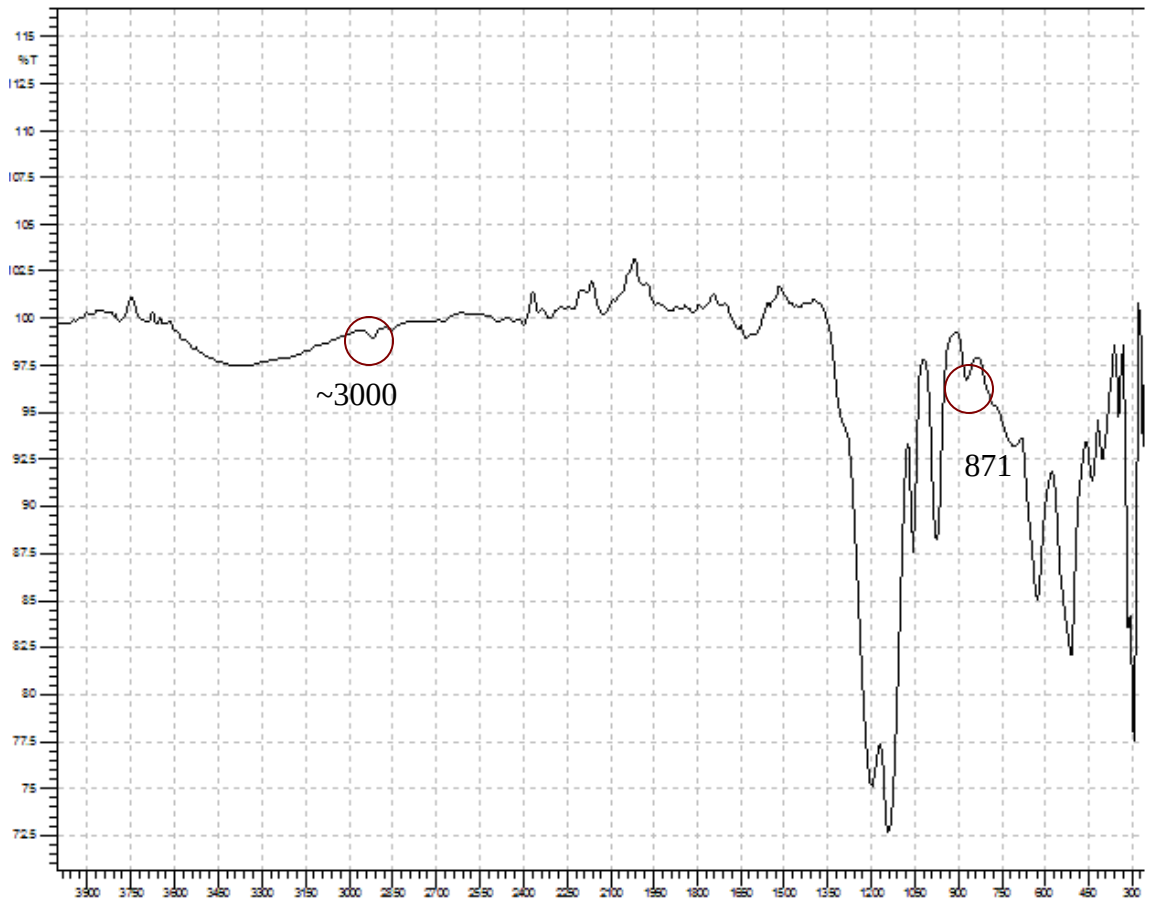

Figure 36. FTIR spectrum for the 15 min VUV photolysis treated polyacrylic acid grafted Nafion sample.

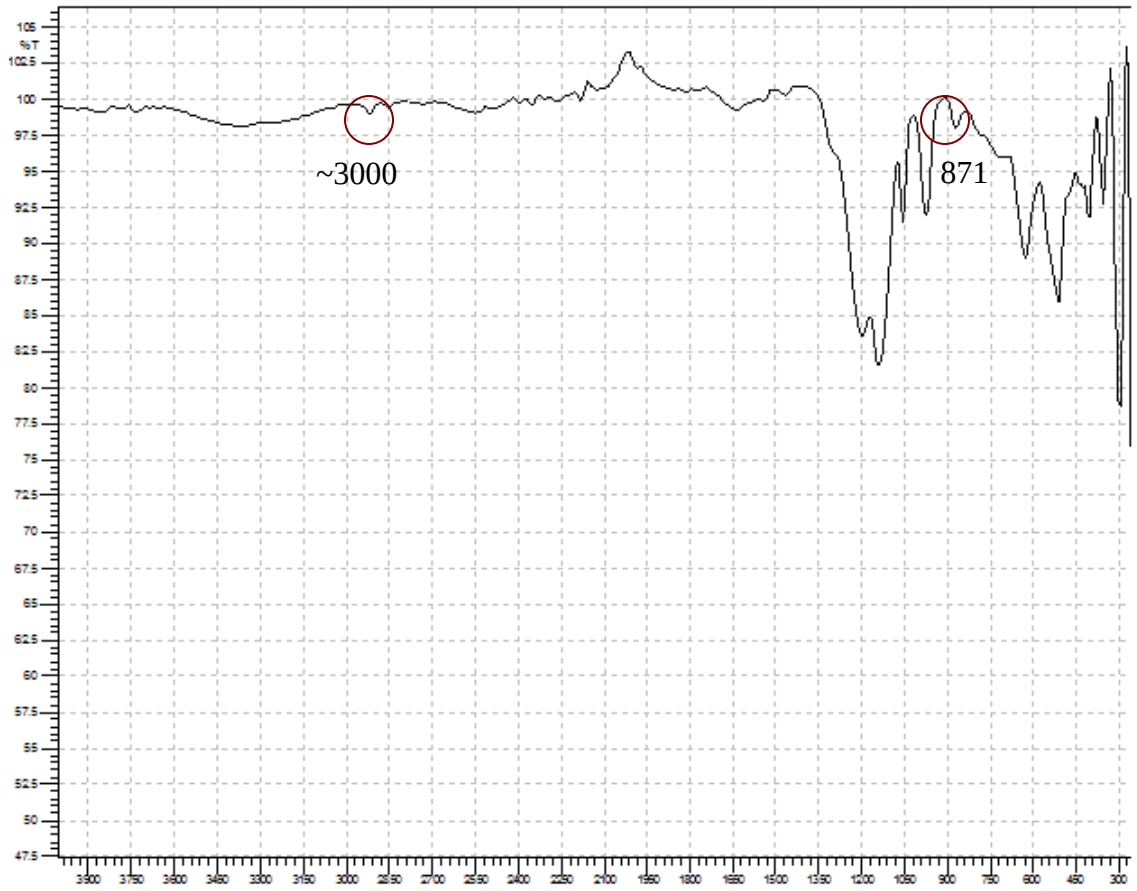

Figure 37. FTIR spectrum for the 30 min VUV photolysis treated polyacrylic acid grafted Nafion sample.

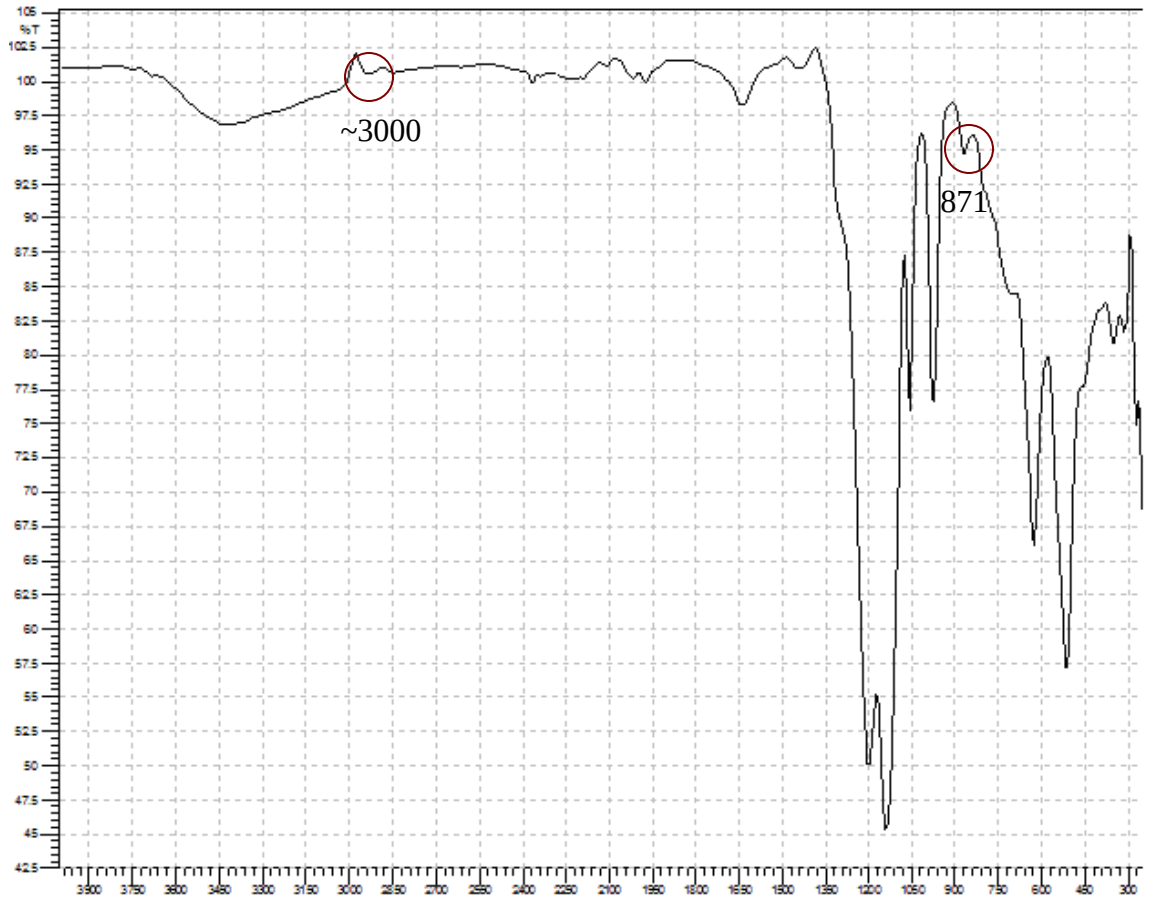

Figure 38. FTIR spectrum for the 60 min VUV photolysis treated polyacrylic acid grafted Nafion sample.

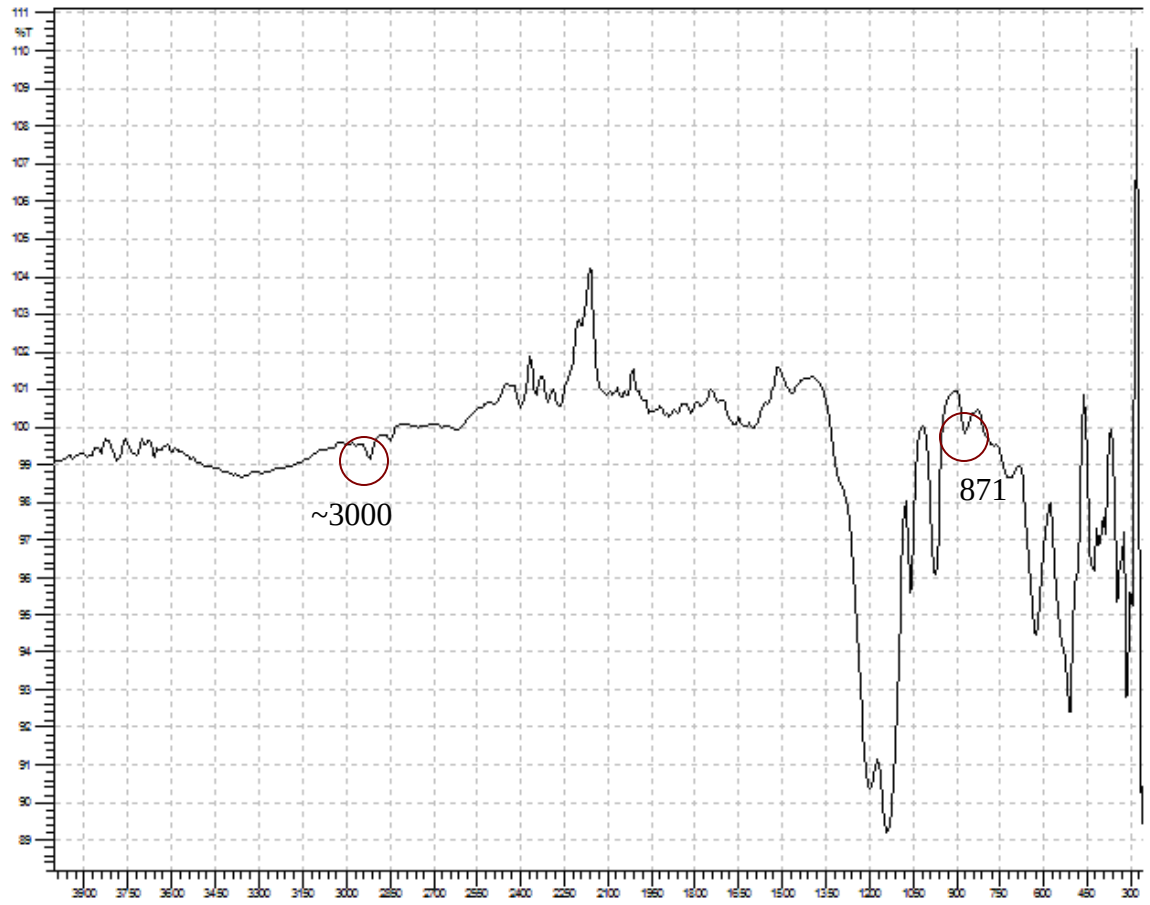

Figure 39. FTIR spectrum for the 90 min VUV photolysis treated polyacrylic acid grafted Nafion sample.

3.5 Hydrogen Storage of Magnesium Hydride

3.5.1. Kinetics of Hydrolysis of Magnesium Hydride with Acetic Acid

The hydrolysis of a 150 mg MgH_2 sample with acetic acid was monitored with a pressure sensor. Pressure increased fairly linearly with reaction time as shown in Fig. 40.

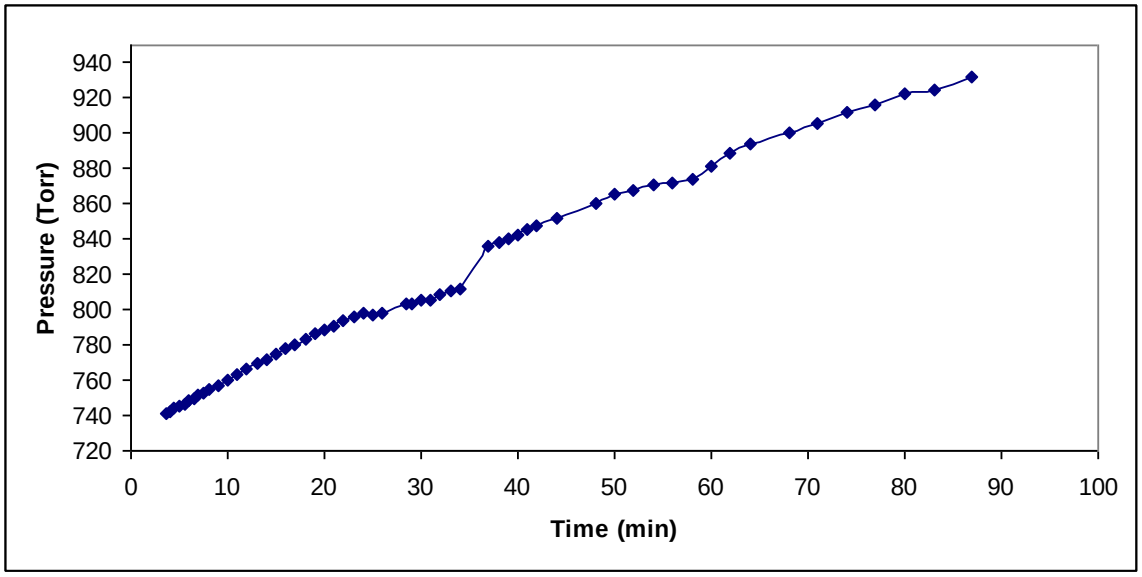

Figure 40. Pressure vs. time of reaction of 149.7 mg MgH_2 in 2 wt% acetic acid.

Using the ideal gas law, the mass and moles of hydrogen produced was calculated. The %mass loss was calculated as follows: $(4.21 \times 10^{-4}$ g hydrogen/0.1497 g $MgH_2) \times 100 =$ 0.28% of the total initial mass of MgH_2 that is attributed to hydrogen release. The average and instantaneous rates of hydrolysis were calculated. The average rates were calculated by (moles hydrogen)/(seconds of reaction) and the instantaneous rates were calculated by drawing a tangent line to each point on a mole vs. time graph and finding the slope of the line. These values are summarized in Table 27.

Table 27
Kinetic measurements for the reaction of 149.7 mg MgH_2 in 2 wt% acetic acid

Time (min)	Moles ($x10^{-4}$)	Mass ($x10^{-4}$ g)	%Mass loss	Average Rate ($x10^{-7}$ mol/sec)	Instantaneous Rate ($x10^{-7}$ mol/sec)
0.00	0.00	0.00	0.00	0.00	0.00
10.0	2.09	4.21	0.28	3.48	3.85
20.0	4.69	9.45	0.63	3.91	3.45
30.0	6.20	12.5	0.84	3.45	4.28
40.0	9.61	19.4	1.30	4.00	5.32
50.0	11.7	23.5	1.57	3.89	2.17
60.0	13.1	26.4	1.76	3.64	2.78
71.0	15.4	31.0	2.07	3.61	3.05
80.0	16.9	34.1	2.27	3.52	2.73

The rate peaks at 40 minutes of hydrolysis which could indicate that at this point in the reaction, the insoluble $Mg(OH)_2$ that forms as a byproduct is being cleared away from the MgH_2 and that the formation of the soluble salt with acetic acid is becoming more prominent allowing more of the MgH_2 to be exposed to the aqueous acetic acid [58].

The %mass loss represents the experimental hydrogen storage capacity of magnesium hydride. At 80 minutes, the %mass loss was 2.27% indicating that the reaction was close to completion at the point at which it was ceased according to the actual hydrogen storage capacity of 3.50% determined from TGA (section 3.5.3). It was calculated that the reaction would need to be carried out for 118 minutes to run to completion.

The hydrolysis of MgH_2 is shown as a first order plot in Fig. 41 with a rate constant 3 x 10^{-5} s^{-1}.

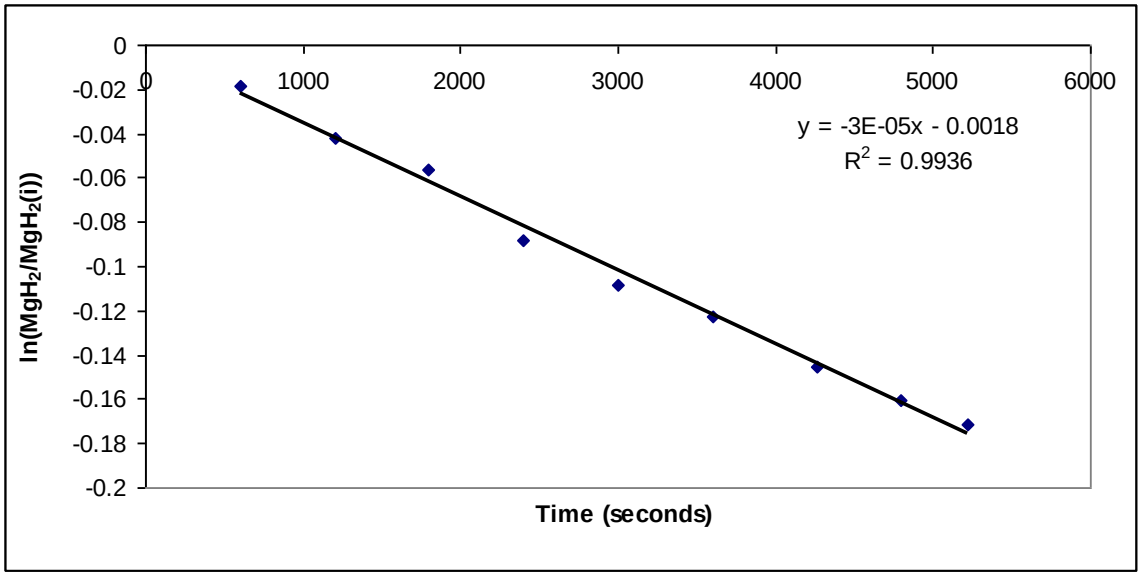

Figure 41. Decomposition of 149.7 mg magnesium hydride in 2 wt% acetic acid.

The use of an acetic acid solution instead of water allows for less of the insoluble $Mg(OH)_2$ to form surrounding the MgH_2. For the hydrolysis using acetic acid, the magnesium from MgH_2 reacts to form both $Mg(OH)_2$ and $Mg(CH_3COO)_2$. Not all of the magnesium reacts to form the insoluble hydroxide as in the hydrolysis using just water. With acetic acid, half of the magnesium reacts to form the soluble acetate salt. Since less of the hydroxide is being produced in this reaction, less of it can block the exposure of MgH_2 to water.

3.5.2. Fuel Cell Consumption of Hydrogen

After the pressure vs. time graph was recorded in section 3.5.1, the pathway to the fuel cell was opened to allow the produced hydrogen to be consumed by the fuel cell. The motor on the measurement box ran for 3 minutes and 5 seconds. The current was initially 0.013A and the voltage was initially 0.73V. The voltage steadily decreased throughout the 3 minutes. After the pathway to the fuel cell was shut off for some time, allowing for a build up in pressure, the pathway was opened again and the motor ran again for 1

minute and 45 seconds. The build up in pressure increases the amount of hydrogen consumed by the fuel cell.

Tables 28 and 29 show the amount of hydrogen consumed by the fuel cell as mass, volume, and percent mass for the hydrolysis of 100 mg of MgH_2 and 150 mg MgH_2, respectively. Since the pathway to the fuel cell from the reaction flask was being shut off at various times to build up pressure and there was not continual hydrogen release to the fuel cell, each calculation had to be done at each step of reaction. For example, for the 100.7 mg MgH_2 experiment, after two minutes of reaction with the clamp closed, the clamp was opened to allow produced hydrogen to reach the fuel cell. At this moment, the time the motor on the measurement box had run, the voltage, and current measurements were recorded. The pathway was shut again until 6.5 minutes of reaction. The pathway was again opened and the same parameters were measured. The mass of hydrogen consumed by the fuel cell was calculated using the equation (7):

$$\text{Mass of hydrogen gas} = (I)(t_{motor})(MM)/nF \quad (7)\ [4]$$

Where I is the current in amps, t_{motor} is the time of the running motor in seconds, MM is the molecular mass of hydrogen (2.016 g/mol), n is number of electrons transferred (2), and F is Faraday's constant (96,485 C/mol).

Table 28
Hydrogen consumption by the fuel cell from the hydrolysis of 100.7 mg magnesium hydride in 2 wt% acetic acid

Time of reaction (minutes)	Mass of hydrogen consumed (x 10^{-5}grams)	Volume of hydrogen consumed (ml)	%Mass loss
2.00	1.22	0.146	0.012
6.50	1.63	0.194	0.016
12.4	1.89	0.225	0.019
26.3	2.98	0.355	0.030
48.7	5.97	0.710	0.060
65.0	10.0	1.20	0.10
78.2	12.5	1.49	0.13

Table 29
Hydrogen consumption by the fuel cell from the hydrolysis of 147.3 mg magnesium hydride in 2 wt% acetic acid

Time of reaction (minutes)	Mass of hydrogen consumed (x 10^{-5}grams)	Volume of hydrogen consumed (ml)	%Mass loss
2.50	1.77	0.210	0.0120
13.0	4.21	0.501	0.0286
19.0	5.84	0.695	0.0397
30.0	8.29	0.986	0.0563
47.0	13.2	1.57	0.0895

The mass of hydrogen consumed reached a value of 12.5 x 10^{-5} grams and a volume of 1.49 ml at 78.2 minutes of reaction in Table 28 and a value of 13.2 x 10^{-5} and 1.57 ml at 47 minutes of reaction in Table 29.

Data for measurements at each step of the two hydrolysis trials are summarized in Tables 30 and 31. The "build up time" column refers to the amount of time that the pinch clamp was shut to build up pressure in the system.

Table 30
Measurements at each step of the hydrolysis for the 100.7 mg MgH_2 trial

Step	Time of reaction (min)	Build up time (sec)	Motor time (sec)	Moles of hydrogen consumed ($x10^{-6}$)	Rate of hydrogen consumed/build-up time ($x10^{-9}$ mol/sec)	Rate of H_2 consumption by fuel cell ($x10^{-8}$ mol/sec)
1	2.00	120	90	6.06	50.5	6.74
2	6.50	180	30	2.02	11.2	6.74
3	26.3	809	80	5.39	6.66	6.74
4	48.7	1260	220	14.8	11.8	6.74
5	65.0	760	300	20.2	26.6	6.74
6	78.2	490	180	12.1	24.7	6.74

Table 31
Measurements at each step of the hydrolysis for the 147.3 mg MgH_2 trial

Step	Time of reaction (min)	Build up time (sec)	Motor time (sec)	Moles of hydrogen consumed ($x10^{-6}$)	Rate of hydrogen consumed/build-up time ($x10^{-9}$ mol/sec)	Rate of H_2 consumption by fuel cell ($x10^{-8}$ mol/sec)
1	2.50	150	130	8.76	58.4	6.74
2	13.0	500	180	12.1	24.3	6.74
3	19.0	180	120	8.09	44.9	6.74
4	30.0	540	180	12.1	22.5	6.74
5	47.0	840	360	24.3	28.9	6.74

On both trials with different masses of magnesium hydride, the average rate of hydrogen consumption by the fuel cell was 6.74 x 10^{-8} mol/sec. This value describes the rate at which the fuel cell takes in hydrogen and uses that hydrogen to run the motor on the measurement box. The rate of H_2 consumption is calculated by moles of hydrogen consumed/motor time. Since the same fuel cell was used for both trials, the value should be constant as represented by the values calculated in Tables 30 and 31.

The rate of hydrogen consumed/build up time is a measure of how the increase in pressure causes more hydrogen to be consumed by the fuel cell. Comparing different

build up times and the moles of hydrogen consumed as well as the time of the motor working can give insight to the rate of hydrolysis. For example, at step 1 and 120 seconds of build up time, for the 100 mg trial in Table 30, the motor worked for 90 seconds, and the fuel cell consumed 6.06×10^{-6} moles of hydrogen. At step 2 and 180 seconds of build up time, the motor only worked for 30 seconds and consequently, the hydrogen consumed dropped to 2.02×10^{-6} moles. This suggests that the rate of hydrolysis is faster initially, and then decreases possibly due to $Mg(OH)_2$ formation. However, comparing steps 3 and 5 of Table 30 which have similar build up times of 809 and 760 seconds respectively, the motor ran for only 80 seconds at step 3 and for 300 seconds at step 5. This now proposes that the rate increased again toward the last 3 steps of the experiment. This is consistent with the increase in rate at 40 minutes of reaction during the kinetic measurements with the pressure sensor in section 3.5.1, Table 27. This part of reaction could be a point at which the $Mg(OH)_2$ begins to clear away after an initial build up. In Table 31, the rate initially is fast as in Table 30. At 19 minutes the rate speeds up again and then decreases. Overall, the rate of hydrolysis at the very start of reaction is fast because there is no $Mg(OH)_2$ formed yet, then decreases as a result of its formation. At some point during the middle of the reaction, the rate speeds up due to the clearing away of the $Mg(OH)_2$ and more prominent acetate salt formation.

The voltage and current measurements at each step were 0.70 V and 0.013 A for a power of 0.0091 W.

3.5.3 Hydrogen Storage Capacity Determination with TGA

The %mass loss in Tables 28 and 29 are the experimental hydrogen capacity of MgH_2 based on the amount of hydrogen that is being supplied to the fuel cell. The value of 0.13% in Table 28 is only about 4% of the actual hydrogen storage capacity of the MgH_2 sample that was used (3.50% from TGA). The TGA plot is shown in Fig. 42. This is due to the fact that the hydrolysis was not run to completion and that not all of the hydrogen produced was able to reach the fuel cell and a portion was left in the flask. There was not enough pressure in the system to push all of the hydrogen out of the flask. Additionally, since there is an area of the flask that is located above the stopcock opening, hydrogen could have become stuck at the top and not pushed out. The %mass loss calculated in Table 27 (2.27%) with the use of a pressure sensor was a more accurate estimation of the experimental hydrogen storage capacity of MgH_2. The pathway to the fuel cell is the limiting factor in powering the cell.

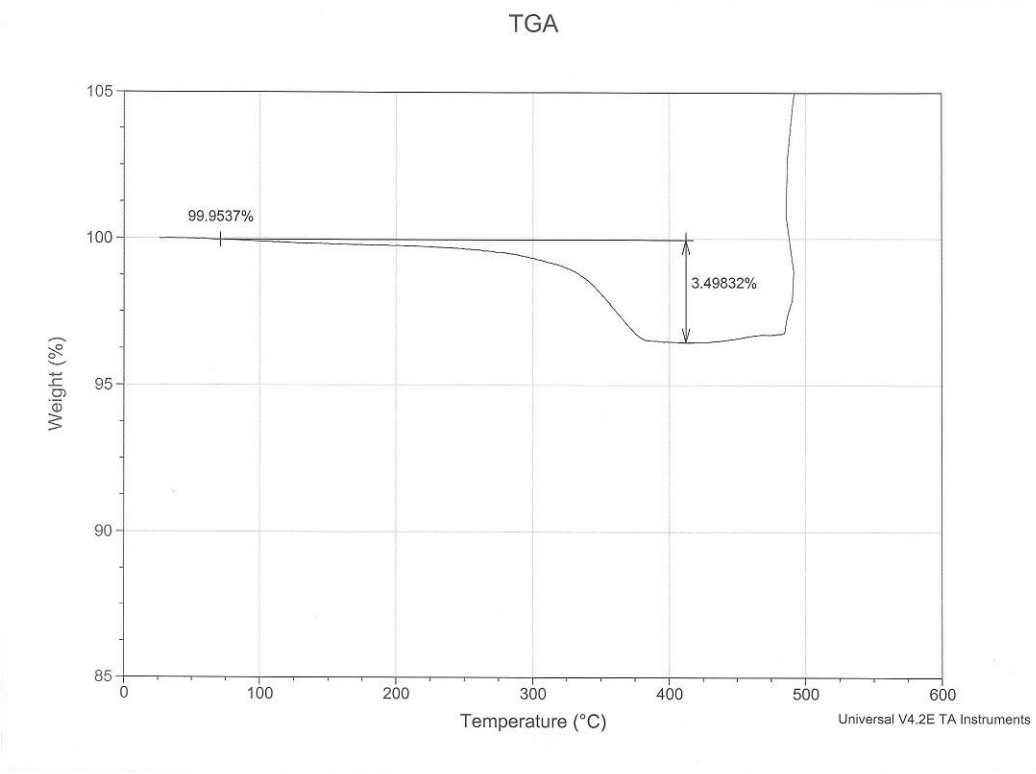

Figure 42. TGA plot showing the percent weight loss due to hydrogen for MgH_2 sample.

Part 4

Discussion

4.1 Surface Modification of Nafion

Three methods were used to modify the surface of Nafion: Indirect Ar/O_2 MW discharge, direct Ar/O_2 MW discharge, and VUV photolysis. The indirect plasmas were not effective at changing the surface chemistry of Nafion. The direct Ar/O_2 MW discharge caused a decrease in the oxygen and sulfur concentrations, however, static contact angle measurements indicated that the surface was more hydrophilic. VUV photolysis was the most effective at surface oxidation and nitrogenation while maintaining sulfonic acid groups.

Fluorine to carbon (F/C), oxygen to carbon (O/C), and sulfur to carbon (S/C) ratios of Nafion are summarized in Table 32 for the direct Ar/O_2 plasma (section 3.1.2) and the VUV photolysis, Trial 1 (section 3.1.3) treatment methods.

Table 32
Fluorine/carbon, oxygen/carbon, and sulfur/carbon ratios for surface modified Nafion

Sample	F/C	O/C	S/C
Control	1.94	0.288	0.0482
5 min direct Ar/O_2	1.92	0.239	0.0220
15 min direct Ar/O_2	1.96	0.218	0.00607
30 min direct Ar/O_2	2.01	0.185	0.00192
60 min direct Ar/O_2	2.03	0.162	0.00192
90 min direct Ar/O_2	2.00	0.161	0.00254
5 min VUV photolysis	1.86	0.235	0.0182
15 min VUV photolysis	1.58	0.344	0.0445
30 min VUV photolysis	1.48	0.390	0.0525
60 min VUV photolysis	1.29	0.353	0.0406
90 min VUV photolysis	0.975	0.346	0.0328

The drastic decrease in sulfur and the decrease in oxygen for the direct Ar/O_2 experiment are shown in the decrease in the S/C and O/C ratios in Table 32. The F/C ratio remained relatively stable for these samples. The F/C ratio decreased, the O/C ratio increased with a slight decrease for the 60 and 90 min samples and overall the S/C ratio remained stable with the exception of the 5 min sample for the VUV photolysis experiment which is supported in quantitative XPS analysis Tables 6a-d in section 3.1.3.

The results from direct Ar/O_2 MW discharge and VUV photolysis can be compared with the results in Table 33, which gives the F/C, O/C, and S/C ratios for VUV photo-oxidized Nafion from previous research [73]

Table 33
Fluorine/carbon, oxygen/carbon, and sulfur/carbon ratios for VUV photo-oxidized Nafion [73]

Sample	F/C	O/C	S/C
Control	1.92	0.267	0.0289
15 min	1.58	0.226	0.0113
30 min	1.56	0.249	0.0169
60 min	1.73	0.392	0.0637

VUV photolysis caused a greater significance in defluorination of Nafion than VUV photo-oxidation in the treatment times displayed as shown in the F/C ratios in Tables 32 and 33. Overall, there was more oxidation in VUV photolysis as seen in the O/C ratios with the exception of the 60 min treatment time. The S/C ratios were lower for the 15 and 30 min samples for the VUV photo-oxidation than for the VUV photolysis treatments, possibly due to a similar reason as in the direct Ar/O_2 plasma experiments: at lower treatment times the photons break C-S bonds before C-C, C-O, and C-F. The longer 60 min time may allow for reformation of the C-S bonds. The VUV photolysis also showed an increase in nitrogen concentration in Tables 6a-d (section 3.1.3) and an increase in nitrogen is not recorded for the VUV photo-oxidation treatment.

Fig. 43 shows the contact angle for VUV photolysis treated and direct Ar/O_2 treated Nafion.

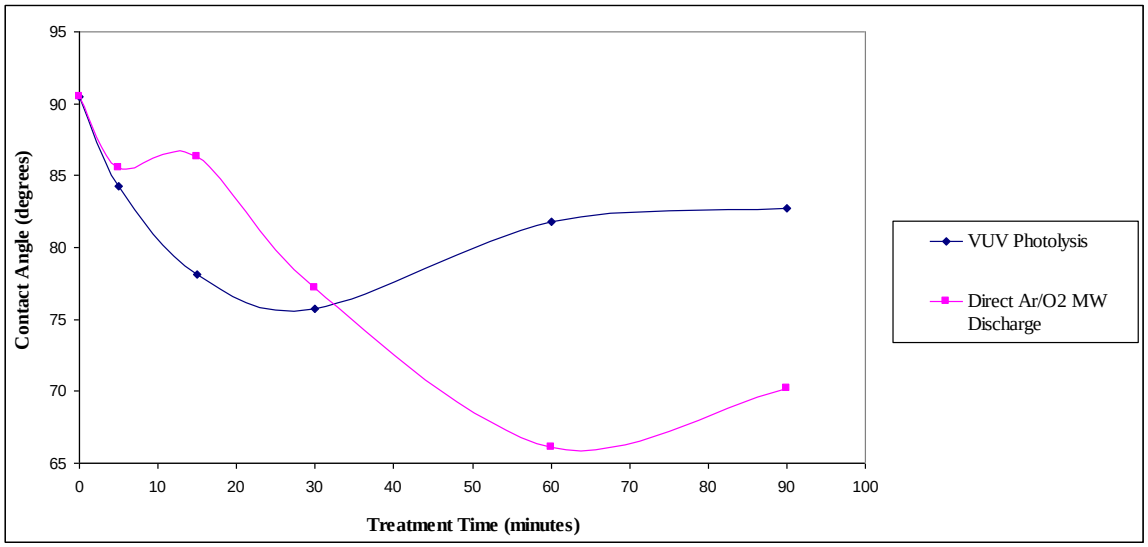

Figure 43. Comparison of the contact angle of VUV photolysis and direct Ar/O_2 MW discharge treated Nafion.

The 5, 15, and 30 min VUV photolysis samples had a smaller contact angle than the direct Ar/O_2 samples and the 60 and 90 min direct Ar/O_2 samples had a smaller contact angle than the VUV photolysis samples. A decrease in contact angle indicating an increase in hydrophilicity is expected for VUV photolysis treated samples because XPS analysis determined there to be an increase in oxygen percentage (Tables 6a-d, section 3.1.3). The increase in the contact angle for the 60 and 90 min VUV photolysis samples and the 90 min direct Ar/O_2 sample could be attributed to the surface modification not being uniform. There may be more modification in one part of the sample than in another.

From XPS analysis and the atomic ratios in Table 32, the VUV photolysis treated samples would be expected to be more hydrophilic than the direct Ar/O_2 samples however, this is not the case. Another research group [20] that found a decrease in sulfur percentage on Nafion when exposed to an argon plasma determined that the contact angles after 25 minutes of the placement of the drop on the treated samples were larger than the contact angle of the untreated Nafion sample at 25 minutes. Since the polymer had time to rearrange and had less sulfonic acid groups, it was overall more hydrophobic. The contact angles of samples exposed to an argon plasma for 300 seconds with different powers are shown in Fig. 44 from this research study [20].

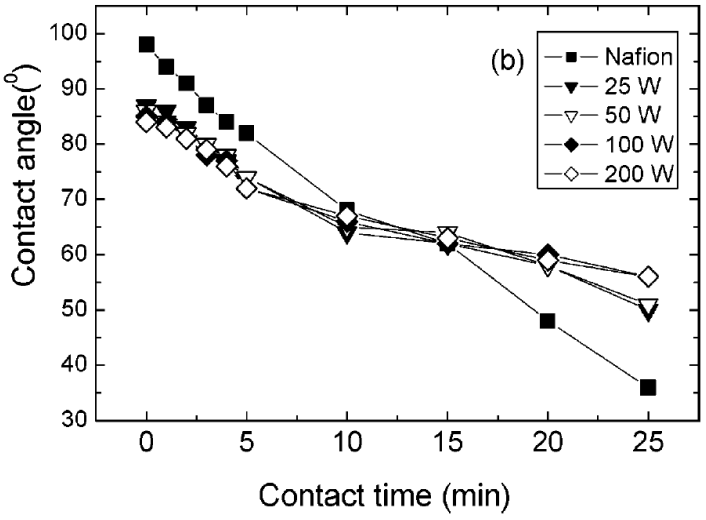

Figure 44. Contact angle vs. contact time for Nafion samples exposed to 300 seconds of argon plasma at varying power [20].

In this thesis, the contact angles were measured soon after the placement of the drop. Future work may include time dependent contact angle analysis, as done in reference 20, for the direct Ar/O_2 MW discharge treated samples.

4.2 Grafting of Surface Modified Materials with Poly(Acrylic Acid)

4.2.1 Grafting of VUV Photolysis Treated Nafion

Polyacrylic acid was grafted to Nafion treated with VUV photolysis. Previous research grafted polyacrylic acid to VUV photo-oxidized Nafion [63, 73]. A comparison of the quantitative XPS analysis for both grafting experiments is shown in Fig. 45.

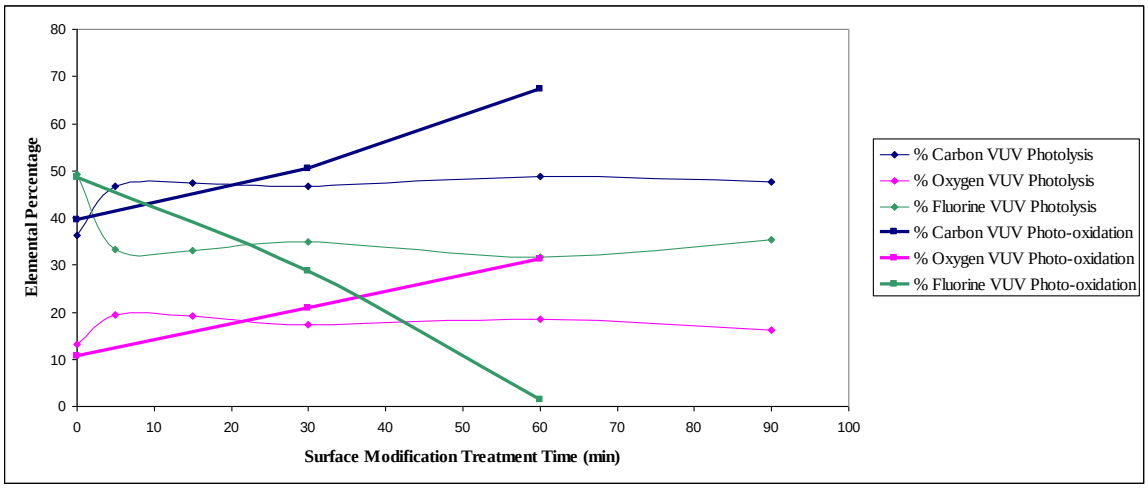

Figure 45. Quantitative XPS analysis for VUV photolysis treated and VUV photo-oxidized Nafion grafted with polyacrylic acid.

A more drastic change in elemental concentration is observed for the grafted samples pre-treated with VUV photo-oxidation than grafted samples pre-treated with VUV photolysis. The change in percentage of carbon, oxygen, and fluorine shown in Fig. 45 indicate that VUV photo-oxidation may be a better pre-treatment to activate the surface of Nafion for grafting with polyacrylic acid.

A comparison of the water contact angle (Fig. 46) between the VUV photolysis treated, control grafted, and polyacrylic acid grafted Nafion indicates the hydrophilicity of each sample.

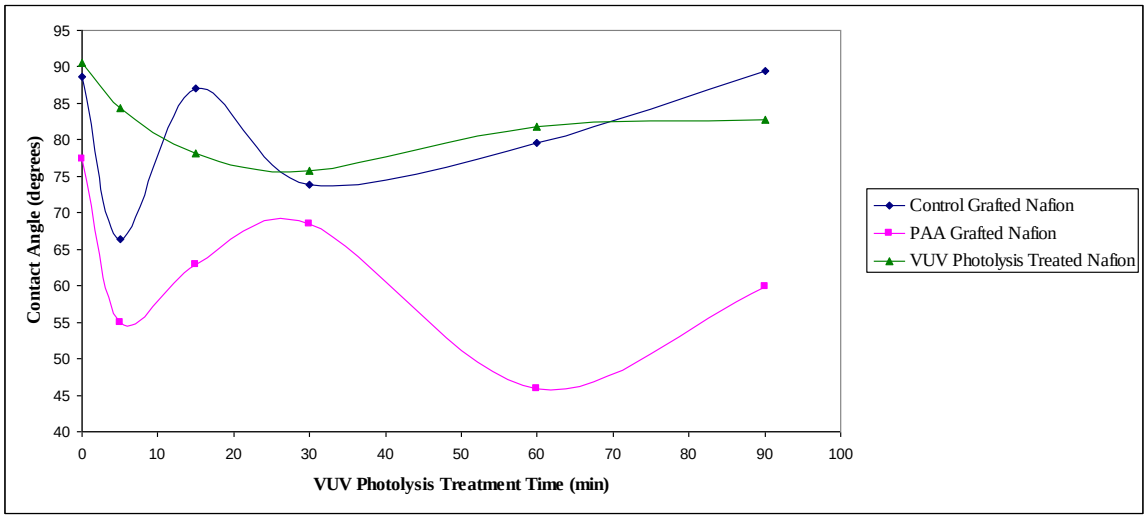

Figure 46. Water contact of VUV photolysis treated, control grafted, and polyacrylic acid grafted Nafion.

The contact angles of the polyacrylic acid grafted Nafion samples were substantially lower than the contact angles of the other two treatments, indicating grafting takes place.

4.2.2 Grafting of VUV Photo-oxidized Single-Walled Carbon Nanotubes

The grafting of VUV photo-oxidized single-walled carbon nanotubes was done in two trials and a control grafting experiment was performed in the absence of acrylic acid. The factor giving the most evidence of successful polyacrylic acid grafting was the larger presence of sp^3 hybridized C-C bonds in the polyacrylic acid grafted samples than the control grafted and the VUV photo-oxidized samples. Sp^3 hybridized C-C bonds correspond to a peak at 285.2 eV in the C 1s curve fittings as was shown in Table 13 in

section 3.1.5. Fig. 47 compares the amounts of sp^3 hybridized C-C bonds in each experiment by area under the 285.2 eV peak vs. VUV photo-oxidation treatment time.

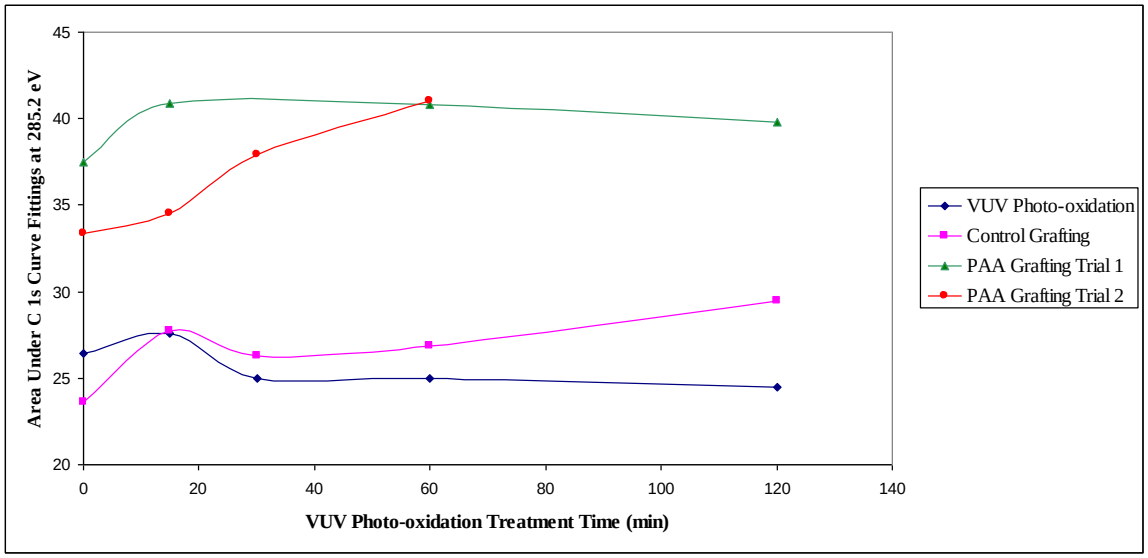

Figure 47. Sp^3 hybridized C-C bonds for VUV photo-oxidized, control grafted, and polyacrylic acid grafted SWNT samples as function of VUV photo-oxidation treatment time.

The polyacrylic acid grafted samples contain the most sp^3 hybridized C-C bonds indicating successful grafting by giving evidence of an added polymer chain.

4.3 Hydrogen Storage of Magnesium Hydride

The kinetics of the hydrolysis of magnesium hydride in 2 wt% acetic acid was monitored and the hydrogen produced was consumed by a fuel cell. The average rate of hydrogen production using our system ranged from 3.45 to 4.00 x 10^{-7} mol/s and the rate of hydrogen consumption by the fuel cell was 6.74 x 10^{-8} mol/s. Not all of the hydrogen produced was able to reach the fuel cell as it could not overcome the atmospheric

pressure to travel the path. Building up pressure with the use of a pinch clamp increased the pressure and enhanced the amount of hydrogen reaching the fuel cell. The initial rate of hydrogen consumed/build up time in Tables 30 and 31 (section 3.5.2) is fast because the acetic acid can react with pure MgH_2. Once insoluble $Mg(OH)_2$ forms, the rate slows down. At some point during the middle of the reaction, the rate speeds up again as shown in Table 27 at 40 min, Table 30 at 65 min, and Table 31 at 19 min in sections 3.5.1 and 3.5.2. At this point, some of the $Mg(OH)_2$ may begin to be cleared away from the MgH_2. If fresh MgH_2 is present that has not yet been exposed to the solution, the hydrolysis will occur more readily than if MgH_2 is covered by a layer of $Mg(OH)_2$ as described by Hu et al.[58].

This research was modified and used as an undergraduate laboratory assignment for a course on clean energy. Students run the hydrolysis of MgH_2 in 2 wt% acetic acid with a connected pressure and temperature sensor and ideal gas law syringe shown in Fig. 10 in section 2.8.1. Pressure changes are monitored and a pressure vs. time graph is constructed. Using the pressure vs. time graph, students calculate the mass of hydrogen that is released from the hydrolysis. After the hydrolysis is stopped, the pathway to the fuel cell is opened and students observe the working motor on the measurement box and record the current, voltage, and motor time. Students then calculate the total mass of hydrogen consumed by the fuel cell using equation (6) in section 3.5.2.

Part 5

Conclusions

Plasma modification treatments were successful in altering the chemistry of the surface of Nafion. The indirect Ar/O_2 plasma treatment showed minimal changes indicating that the oxygen atoms are not energetic enough to break the bonds of Nafion. Sulfur and oxygen atoms were removed from the direct Ar/O_2 plasma treated samples, however, O=C-O groups increased as shown in the results of the curve fittings. Surface oxidation and nitrogenation of Nafion occurred from the VUV photolysis treatment. The increase in oxygen-containing functional groups in both the direct Ar/O_2 and VUV photolysis treated samples caused the hydrophilicity to increase for the samples treated by both methods. An increase in the hydrophilicity of Nafion may improve its absorption of water which could enhance proton conductivity in a fuel cell.

The physical characteristics were not significantly changed in either treatment method as shown by the SEM images. Some of the samples that were reported to have a decrease in sulfur concentration showed a slightly more rippled appearance than samples that did not have a decrease in sulfur.

Grafting of VUV photolysis treated Nafion samples and VUV photo-oxidized single-walled carbon nanotube paper with polyacrylic acid were shown to be successful by XPS analysis for both materials and FTIR and contact angle analysis for Nafion. The added bulk of the polymer grafted to Nafion could reduce methanol permeation in a direct

methanol fuel cell [34]. The presence of polyacrylic acid also increases hydrophilicity of the membrane.

The hydrolysis of MgH_2 in 2 wt% acetic acid producing hydrogen for fuel cell consumption was examined. The kinetics were analyzed with the use of ideal gas law equipment and the hydrogen produced directly powered a fuel cell. About 2 hours were required for the magnesium hydride (150 mg) to release all of its hydrogen with a rate ranging from about 3.4 to 4.0 x 10^{-7} mol/s and a hydrogen storage capacity of 3.50%.

The fuel cell consumed approximately 1.5 ml hydrogen from 100.7 mg MgH_2 in 78 minutes and about 1.6 ml hydrogen from 147.3 mg MgH_2 in 47 minutes which were enough hydrogen to run the motor on the measurement box for a total time of 15.4 minutes and 16.2 minutes, respectively. From calculations of the hydrogen storage capacity and from values of hydrogen consumed by the fuel cell, it is evident that there are obstacles to overcome that prevent the majority of the hydrogen from reaching the fuel cell in this system which need to be improved for more efficient consumption. The hydrogen produced from the hydrolysis was, however, effective enough to power the fuel cell for a considerable amount of time as demonstrated by a working motor on a measurement box.

Part 6

Future Work

Further research can supplement the work in this thesis. Some future work may include:

1) Grafting of direct Ar/O_2 MW discharge treated Nafion with polyacrylic acid.

2) N 1s XPS studies to examine nitrogen-containing functional groups present in VUV photolysis treated Nafion samples.

3) Additional FTIR experiments to add to the evidence for polyacrylic acid grafting to single-walled carbon nanotubes and Nafion.

4) Methanol permeation testing of grafted and non-grafted Nafion.

5) Time dependent contact angle analysis for direct Ar/O_2 MW discharge and VUV photolysis treated Nafion.

6) Proton conductivity measurements to observe how surface modification alters proton transport.

7) Hydrolysis of magnesium hydride altering the concentration of acetic acid and observe any changes in kinetics.

8) Increase the pressure of hydrogen in the pathway from the hydrolysis of MgH_2 to the fuel cell.

Part 7

References

[1] http://drivesteady.com/the-epa-and-emissions-standards. Accessed August 16, 2011.

[2] http://www.greenlivingtips.com/articles/269/1/Car-exhaust-chemicals.html. October 17, 2008.

[3] http://www.hydrogen.energy.gov/pdfs/doe_h2_fuelcell_factsheet.pdf. Accessed October 2006.

[4] R.J. Press, K.S.V. Santhanam, M.J. Miri, A.V. Bailey, G.A. Takacs, Introduction to Hydrogen Technology., John Wiley & Sons, Inc., Hoboken, New Jersey, 2009.

[5] http://americanhistory.si.edu/fuelcells/basics.htm#q4. 2008.

[6] G. Alberti, M. Casciola, Comprehensive Membrane Science and Engineering 2 (2010) 431-465.

[7] http://www.permapure.com.

[8] http://pslc.ws/macrog/ionomer.htm. 2005. Greg Brust.

[9] M. Miri, Exp. 4 – Properties of Proton Exchange Membranes Used in Fuel Cells (Personal communication) 1-11.

[10] N. Bhatnagar, S. Jha, S. Bhowmik, Adv. Mat. Lett. 2 (2011) 52-57.

[11] F.-E. Truica-Marasescu, M.R. Wertheimer, Macromol. Chem. Phys. 206 (2005) 744-757.

[12] M. Naddaf, S. Saloum, B. Alkhaled, Vacuum. 85 (2010) 421-428.

[13] L. Hongxia, L. Yun, Plasma Sci. Technol. 14 (2012) 728-734.

[14] J.R. Hollahan, B.B. Stafford, J. Appl. Polym. Sci. 13 (1969) 807-816.

[15] N. Inagaki, S. Tasaka, H. Kawai, J. Adhesion Sci. Technol. 3 (1989) 637-649.

[16] M.A. Golub, T. Wydeven, R.D. Cormia, Langmuir 7 (1991) 1026-1028.

[17] M.A. Golub, E.S. Lopata, L.S. Finney, Langmuir 9 (1993) 2240-2242

[18] Y. Momose, Y. Tamura, M. Ogino, S. Okazaki, M. Hirayama, J. Vac. Sci. Technol. A 10 (1992) 229-238.

[19] J.P. Badey, E. Urbaczewski-Espuche, Y. Jugnet, D. Sage, T.M. Duc, B. Chabert, Polymer 35 (1994) 2472-2479.

[20] B. Bae, D. Kim, H.-J. Kim, T.-H. Lim, I.-H. Oh, H.Y. Ha, J. Phys. Chem. B 110 (2006) 4240-4246.

[21] J.H. Kim, J. Sohn, J.H. Cho, M.Y. Choi, I.G. Koo, W.M. Lee, Plasma Process. Polym. 5 (2008) 377-385.

[22] S.A Cho, E.A. Cho, I.-H. Oh, H.-J. Kim, H.Y. Ha, S.-A. Song, J.B. Ju, J. Power Sources 155 (2006) 286-290.

[23] Y.-H. Cho, J.W. Bae, Y.-H. Cho, J.W. Lim, M. Ahn, W.-S. Yoon, N.-H. Kwon, J.Y. Jho, Y.-E. Sung, Int. J. Hydrogen Energy 25 (2010) 10452-10456.

[24] D. Ramdutt, C. Charles, J. Hudspeth, B. Ladewig, T. Gengenbach, R. Boswell, A. Dicks, P. Brault, J. Power Sources 165 (2007) 41-48.

[25] S.R. Yoon, G.H. Hwang, W.I. Cho, I.-H. Oh, S.-A. Hong, H.Y. Ha, J. Power Sources 106 (2002) 215-223.

[26] W.C. Choi, J.D. Kim, S.I. Woo, J. Power Sources 96 (2001) 411-414.

[27] R. O'Hayre, S.-J. Lee, S.-W. Cha, F.B. Prinz, J. Power Sources 109 (2002) 483-493.

[28] A.T. Haug, R.E. White, J.W. Weidner, W. Huang, S. Shi, T. Stoner, N. Rana, J. Electrochem. Soc.149 (2002) A280-A287.

[29] Z. Ogumi, Y. Uchimoto, M. Tsujikawa, Z. Takehara, J. Electrochem. Soc. 137 (1990) 1430-1435.

[30] Z. Ogumi, Y. Uchimoto, M. Tsujikawa, Z. Takehara, J. Electrochem. 136 (1989) 1247-1248.

[31] R. Zeng, Z. Pang, H. Zhu, J. Electroanal. Chem. 490 (200) 102-106.

[32] M. Walker, K.-M. Baumgärtner, M. Kaiser, J. Kerres, A. Ullrich, E. Räuchle. J. Appl. Polym. Sci. 74 (1999) 67-73.

[33] J. Feichtinger, J. Kerres, A. Schulz, M. Walker, U. Schumacher. J. New. Mat. Electrochem. Systems 5 (2002) 155-162.

[34] M.S. Mohy Eldin, A.A. Elzatahry, K.M. El-Khatib, E.A. Hassan, M.M.-El Sabbah, M.A. Abu-Saied, J. Appl. Polym. Sci. 119 (2011) 120-133.

[35] Q.M. Huang, Q.L. Zhang, H.L. Huang, W.S. Li, Y.J. Huang, J.L Luo, J. Power Sources 184 (2008) 338-343.

[36] M.A. Smit, A.L. Ocampo, M.A. Espinosa-Medina, P.J. Sebastián, J. Power Sources 124 (2003) 59-64.

[37] D.H. Kang, D. Kim, Korean J. Chem. Eng. 24 (2007) 1101-1105.

[38] S. Iijima, Nature 354 (1991) 56-58.

[39] S. Iijima, T. Ichihashi, Nature 363 (1993) 603-605.

[40] S. Niyogi, M.A. Hamon, H. Hu, B. Zhao, P. Bhowmik, R. Sen, M.E. Itkis, R.C. Haddon, Acc. Chem. Res. 35 (2002) 1105-1113.

[41] R. Kannan, V.K. Pillai, J. Indian Inst. Sci. 89:4 (2009) 425-436.

[42] P.S. Fernández, E.B. Castro, S.G. Real, M.E. Martins, Int. J. Hydrogen Energy 34 (2009) 8115-8126.

[43] P. Li, H. Liu, Y. Ding, Y. Wang, Y. Chen, Y. Zhou, Y. Tang, H. Wei, C. Cai, T. Lu, J. Mater. Chem. 22 (2012) 15370-15378.

[44] L. Song, G. Toth, R. Vajtai, M. Endo, P.M. Ajayan, Carbon 50 (2012) 5521-5524.

[45] U. Dettlaff-Weglikowska, J. Yoshida, N. Sato, S. Roth, ESC Transactions 25 (2010) 211-217.

[46] J. Ma, F. Yu, J. N. Wang, J. Mater. Chem. 20 (2010) 5742-5747.

[47] H.-X. Wu, R. Tong, X.-Q. Qiu, H.-F. Yang, Y.-H. Lin, R.-F. Cai, S.-X. Qian, Carbon 45 (2007) 152-159.

[48] S. Chen, G. Wu, y. Liu, D. Long, Macromolecules 39 (2006) 330-334.

[49] D. Yang, J. Hu, C. Wang, Cabon 44 (2006) 3161-3167.

[50] D.-S. Yang, D.-J. Jung, S.-H. Choi, Radiat. Phys. Chem. 79 (2010) 434-440.

[51] Z. Yang, X.-H. Chen, S.-Z. Xia, Y.-X. Pu, H.-Y. Xu, W.-H. Li, L.-S. Xu, B. Yi, W.-Y. Pan, J. Mater. Sci. 42 (2007) 9447-9452.

[52] B. Sakintuna, F. Lamari-Darkrim, M. Hirscher, Int. J. Hydrogen Energy 32 (2007) 1121-1140.

[53] Y. Kojima, K.-I. Suzuki, Y. Kawai, J. Mater. Sci. 39 (2004) 2227-2229.

[54] R. Schulz, J. Huot, G. Liang, S. Boily, G. Lalande, M.C. Denis, J. P. Dodelet, Mater. Sci. Eng. A267 (1999) 240-245.

[55] V. Bhat, A. Rougier, L. Aymard, G.-A. Nazri, J.-M. Tarascon, Int. J. Hydrogen Energy 32 (2007) 4900-4906.

[56] R. Gosalawit-Utke, T.K. Nielsen, I. Saldan, D. Laipple, Y. Cerenius, T. R. Jensen, T. Klassen, M. Dornheim, J. Phys. Chem. C 115 (2011) 10903-10910.

[57] L. Baum, M. Meyer, L. Mendoza-Zélis, Physica B 389 (2007) 189-192.

[58] H. Lian-xi, W. Er-de, Trans. Nonferrous Met. Soc. China 15 (2005) 965-970.

[59] S. Hiroi, S. Hosokai, T. Akiyama, Int. J. Hydrogen Energy 36 (2011) 1442-1447.

[60] S.D. Kushch, N.S. Kuyunko, R.S. Nazarov, B.P. Tarasov, Int. J. Hydrogen Energy 36 (2011) 1321-1325.

[61] M.-H. Grosjean, M. Zidoune, L. Roué, J.-Y. Huot, Int. J. Hydrogen Energy 31 (2006) 109-119.

[62] M.-H. Grosjean, L. Roué, J. Alloy. Compd. 416 (2006) 296-302.

[63] A. Bailey, F. Lu, A. Khot, S. Hussain, K.W. Rugg, G.J. Leong, T. Debies, G.A. Takacs, Mater. Res. Soc. Symp. Proc. 1269 (2010).

[64] F. Lu, MS Thesis, Rochester Institute of Technology (2010).

[65] G.M. Lampman, D.L. Pavia, G.S. Kriz, J.R. Vyvyan, Spectroscopy, fourth ed., Brooks/Cole, Belmont, CA, 2010.

[66] M. Mehan, XPS Analysis of VUV Treated Nafion Films (Unpublished results) (2013) 1-7.

[67] M. Mehan, Surface Analysis of Single Walled Carbon Nanotubes Paper Exposed to Oxygen and VUV Radiation and PAA Grafting (Unpublished results) (2012) 1-7.

[68] D.A. Skoog, F.J. Holler, S.R. Crouch, Principles of Instrumental Analysis, sixth ed., Brooks/Cole, Belmont, CA 2007.

[69] G. Thompson, SEM Analysis of Modified Nafion Samples (Unpublished results) (2012) 1-2.

[70] M. Mehan, Surface Analysis of Single Walled Carbon Nanotubes Paper Exposed to VUV Photo-Oxidation (Unpublished results) (2013) 1-6.

[71] S.E. Lappi, B. Smith, S. Franzen, Spectrochimica Acta Part A 60 (2004) 2611-2619.

[72] S.G. Prasad, A. De, U. De, Int. J. Specrosc. 2011 (2011) 1-7.

[73] A. Khot, MS Thesis, Rochester Institute of Technology (2012).